Nonlinear methods for spatial and temporal noise reduction in ultrashort pulse optical systems

PhD Thesis

Zoltán Bakonyi

Supervisors:
Dr. Sándor Szatmári
Dr.George Onishchukov

University of Szeged
Department of Experimental Physics
Szeged
2000

Acknowledgments:

It is a pleasure to acknowledge all my present and former colleagues for they help and encouragement. I am particularly grateful to *Dr. István Földes, Dr. Gábor Kocsis, Dr. Gábor Veres, Dr. Miklós Kedves* at the KFKI-Research Institute for Particle and Nuclear Physics and to *Dr. Ian Ross* at the Rutherford Appleton Laboratory.

I owe a great debt of thanks to *Dr. Tamás Nagy* for the stimulating discussions and for his useful suggestions. I am grateful for the assistance in my daily experimental work to *Dr. Andrew Okhrimchuk, Dr. Arkady Shipulin* and to *Dr. Peter Riedel.*

I would like to thank for the many contributions and invaluable help of *Dr. Michael Gölles, Christian Knöll* and *Dr. Dirk Michaelis* at the Institute of Solid-State Theory and Theoretical Optics of the Friedrich-Schiller-University, Jena and to *Enno Hilliger* at the Heinrich-Hertz-Institut, Berlin.

I am especially indebted to *Prof. Imre Hevesi* for his support and for his suggestions, which greatly improved the presentation of the hungarian language extract.

I am grateful for the support and for the stimulating discussions to *Prof. Falk Lederer* and to *Prof. Andreas Tünnermann.*

Finally I would like to thank my supervisors: *Dr. George Onishchukov* for introducing me to the world of fiber optics and fiber communication technology and *Prof. Sándor Szatmári* how had a significant impact on my view of photonics. I am grateful for they encouragement, for the fascinating scientific discussions and for helping me on all possible means.

Contents

Preface

In the last thirty years the rapid progress is the generation of ultrashort pulses opened new territories for the application of optical systems. Probably the two largest beneficiaries are the telecommunication industry and high-energy physics. But simultaneously with the spread of short pulse optical laser technology the applications set up even more stringent requirements, making the effective control of optical noise necessary.

Information transmission in optical fibers has become wide spread during the decade of the 1980s. Since this technology complies well with the requirements of the emerging new media like the internet or digital broadcasting it is very likely that the informational revolution of the next century will go hand in hand with the development of fiber optics communication technology.

In an optical fiber transmission line the losses have to be compensated. In the past optoelectronic repeaters were used for that purpose. The optical signal was converted to electric one, then amplified and converted back to the optical domain. Such a device has a limited bandwidth and it is not only costly, but especially in Wavelength-Division-Multyplexing (WDM) systems with the number of channels up to 100 and more, the use of such a large number of optoelectronic repeaters is simply impossible. Presently, in all practical optical fiber transmission systems in-line optical amplifiers are applied. Due to the fundamental physical properties of the fused silica telecommunication fiber, two distinct spectral regions are used for transmitting information: the 1.5μm telecommunication window and the 1.3μm window. The first claims lower absorption and the later has low group velocity dispersion in standard communication fibers. Usually the amplifier of choice at 1.5μm is the Erbium Doped Fiber Amplifier (EDFA) because of its high gain, low noise and very long gain recovery time (compared to the bit rate). However in the 1.3μm region the fiber amplifier technology is rather immature and expensive.

Semiconductor optical amplifiers (SOA) could be a very appealing choice for in-line amplification because of their efficiency, low cost and compactness. Moreover, SOA

can be manufactured for any communication wavelength. Though, the performance of semiconductor amplifiers is limited by several factors like bit rate comparable gain recovery time, low saturation energy, large linewidth enhancement factor, comparatively high noise figure, but the most important limitation is the fast growth of amplified spontaneous emission (ASE) in the transmission line. SOA can be a challenging, very cost-effective solution for high bit-rate communication systems provided that the growth of ASE can be controlled.

There are two possible ways to avoid this problem one is to apply phase shift keying (PSK) modulation format resulting in a quasy-CW optical signal or to utilise saturable absorption in amplitude shift keying (ASK) transmission mode. It will be demonstrated that in PSK transmission not only the very strong phase noise of SOAs but a novel type of modulation instability phenomenon originating in the interplay of the SOA nonlinearity and the applied in-line optical filter is introducing severe limitations on the system performance. Leaving saturable absorption as probably the only effective tool to address the problem. Moreover, saturable absorbers (SA) can be easily integrated with SOAs (multiple section SOA, ion implantation).

The main objective of my thesis is to reveal the most important features of such combined SOA-SA based transmission lines and to demonstrate that they could be competitive alternatives for fiber amplifier based systems.

Nonlinear components can alter not only the temporal properties of ultrashort light pulses but their spatial distribution can be improved as well. In high intensity laser experiments the uniform spatial intensity profile of the beam is of key importance, since any inhomogeneity could lead to a larger focal spot i.e. lower focused intensity (which is one of the most important figures of merit of such laser systems). Additionally, random fluctuations of the intensity profile could deteriorate the reproducibility of the experiments. Since the late 1960s, several effective beam filtering methods have been developed. Nevertheless, it is still very difficult to apply them in short pulse, high power laser systems. Some of the methods cause temporal broadening of the laser pulse, others are very sensitive to the direction of the input beam. Large, complex laser systems have inherently limited pointing stability i.e. the direction of the beam is slightly changing from shot to shot. For such systems a novel nonlinear optical component based beam

filtering method is presented, which can not only improve the spatial distribution of limited pointing stability laser beams but enhances the temporal contrast as well.

In the first part of this work the basic physical principles determining the operation of all optical telecommunication networks are introduced with special emphasis on the Semiconductor Optical Amplifier (SOA) based systems operating at the 1.3μm communication window. The influence of the different modulation formats on the performance for such systems are going to be discussed. Then the theoretical predictions for a novel modulation instability phenomena originating from the interplay between SOA nonlinearity and the in-line optical bandpass filter are discussed and experimental proof is presented for the existence of such a modulation instability phenomenon. Such an effect, beside the phase noise is one of the most important limitations in phase-shift keying transmission mode. Then the feasibility of extending the system performance in amplitude-shift keying mode by combining semiconductor optical amplifiers and saturable absorbers is studied theoretically and a dramatic improvement in the system performance is demonstrated experimentally. In the last chapter of this work it is shown that not only the temporal properties of ultrashort optical pulses but also the spatial intensity distribution of the laser beams can be improved through nonlinear optical interactions.

The research connected to fiber optical transmission lines has been carried out at the Institute of Applied Physics of the Friedrich Schiller University, Jena. The free air optics experiments were done at the Department of Experimental Physics at the University of Szeged.

I. Introduction

I.1. Optical fibers

I.1.1. Feasibility of lightwave communication

Because of the very high (several hundred THz) frequency of light in principle optical waves are ideal for broad band, high-speed information transmission. However for the practical realisation of such optical communication network it is essential to have reliable, efficient, high power light sources and a suitable transmission medium.

At the early 1960s with the discovery of lasers such light sources emerged on the horizon. But since light suffers strong random distortion and considerable attenuation during propagation in the atmosphere, only at the 1970s with the advent of high performance optical fibers, optical data transmission became a feasible alternative.

Optical fibers utilise the principle of total internal refraction for guiding light. The two most important parameters to characterise an optical fiber from the point of data transmission are the fiber attenuation and the degree it temporally broadens an optical pulse. At the early stages of optical fiber technology, optical fibers had extremely high

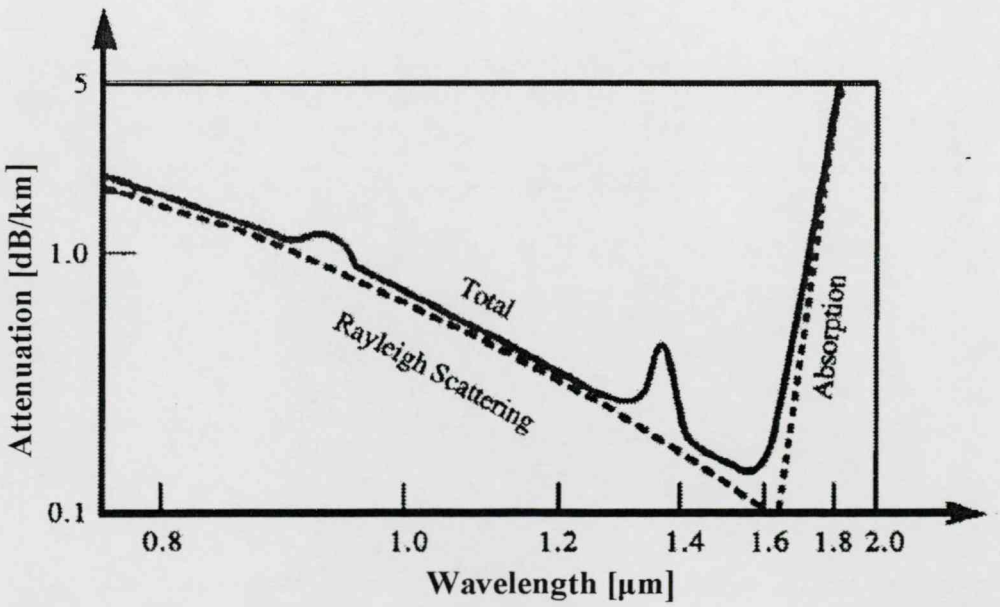

Fig.I.1.1: Attenuation of silica fiber versus wavelength. At short wavelengths fiber losses are determined by Rayleigh scattering, at longer wavelengths there is a sharp cut off due to absorption of the silica. The two parasitic peaks are due to residual contaminants.

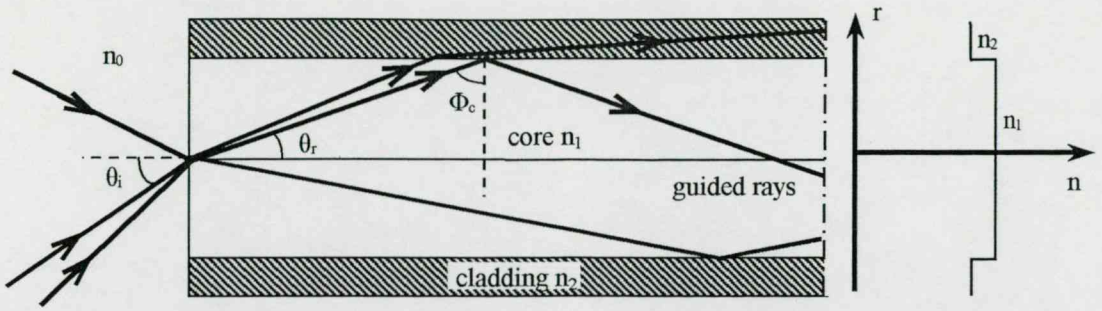

Fig. I.1.2: Ray traces and the refractive index profile in a step index fiber. θ_i is the largest angle of incidence resulting in the confinement of ray. Φ_c is the critical angle of incidence at the core-cladding interface .

losses (~1000dB/km) and they were only used in some medical imaging applications. The attenuation of fibers was reduced to 20dB/km during the 1970s [1,2] and at the early 1980s losses were further decreased to the range of 0.2dB/km [3]. Fig.I.1.1 shows the wavelength dependent attenuation of a typical modern silica fiber. It is worth to mention here that recently a fiber without an absorbtion peak at the 1340nm region was developed.

To discuss the temporal broadening in optical fibers the three most common type of optical fibers has to be described.

I.1.2 Multimode step index fiber

In a step-index fiber the fiber core has a refractive index of n_1 and the surrounding cladding has a somewhat lower refractive index of n_2. Fig.I.1.2. shows the cross section and the refractive index profile of a step index fiber. If a ray hits the core in an angle less then a critical angle (Φ_c), the ray suffers total internal refraction and it is confined to the core of the fiber (Fig.I.1.2). Following Snell´s law, the critical angle can be calculated as: $\sin(\Phi_c)=n_2/n_1$ and the largest angle of incidence (θ_i) resulting in the confinement of the incident ray can be expressed as:

$$n_0 \sin(\theta_i) = n_1 \cos(\Phi_c) = \sqrt{n_1^2 - n_2^2}\,. \qquad \text{(I.1.1)}$$

Similarly to lenses, $n_0\sin(\theta_i)$ is called the numerical aperture of the fiber (NA) and it represents its light gathering capability. Presuming that $n_1 \approx n_2$, the numerical aperture can be approximated as:

$$NA = n_1 (2\Delta)^{1/2}, \text{ where} \qquad \Delta = (n_1 - n_2)/n_1\,. \qquad \text{(I.1.2)}$$

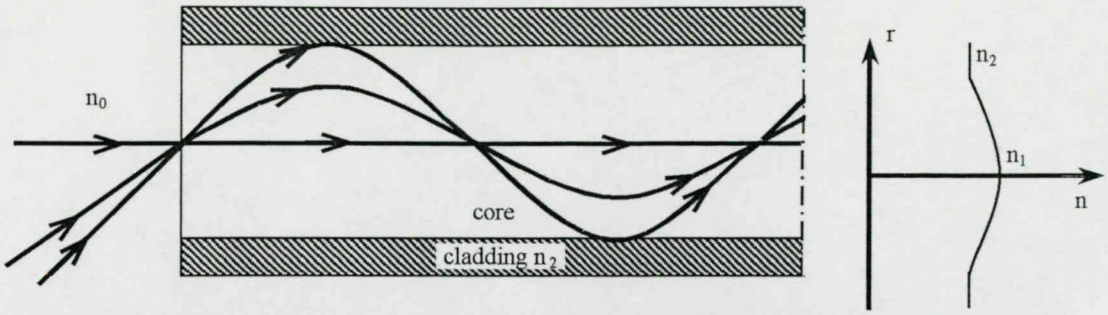

Fig.I.1.3: Ray traces and the refractive index profile in a graded index fiber.

Δ is called the fractional index change at the core-cladding interface.

Now consider the different possible ray paths along the fiber. Obviously the shortest path is parallel with the fiber and the longest ray path belongs to the critical angle (Φ_c). If the fiber length is L, the path difference can be expressed as:

$L/\sin(\Phi_c)$-L and the resulting temporal delay between the two rays is:

$$\Delta T = \frac{\Delta}{c}\frac{n_1^2}{n_2}L, \qquad \text{(I.1.3)}$$

where c is the speed of light in vacuum. This phenomenon is called multipath dispersion or intermodal dispersion. It is easy to see that for information transmission in such fibers the bit slot T_B (the time interval preserved for one bit) have to be larger than the temporal broadening caused by intermodal dispersion $T_B < \Delta T$. Using (eq.I.1.3) we get:

$$BL < \frac{n_2}{n_1^2}\frac{c}{\Delta}, \qquad \text{(I.1.4)}$$

where $B=1/T_B$ is the bit rate. As an example let us consider a fiber with $n_1=1.5$, $n_2=1.485$ and $\Delta=0.01$. It has a BL product of less than <20(Mb/s)*km. Such a fiber can only satisfy the requirements of some local area networks.

I.1.3. Multimode graded index fiber

In a graded index fiber (Fig.I.1.3) the refractive index of the fiber core is gradually reduced with the core radius. In Fig.I.1.3 one can see that the longer ray paths corresponding to larger angle of incidence (θ_i) goes through the lower refractive index regime of the fiber. Thus the average speed of light on the longer paths is larger. Using a

paraxial approximation it can be shown that the intermodal dispersion is eliminated all together [4] in the case of a parabolic index profile:

$$n(\rho)= \begin{cases} n_1[1-\Delta(\rho/a)^{\alpha}] & : \rho<a, \\ n_1[1-\Delta]=n_2 & : \rho\geq a, \end{cases} \qquad \text{(I.1.5)}$$

where a is the core radius and $\alpha=2$. Unfortunately, this approximation does not stand for the practice. More accurate considerations based on wave propagation techniques show that the minimum of the intermodal dispersion ($\Delta T/L$) occurs at $\alpha=2(1-\Delta)$ [5] and its minimum value is:

$$\frac{\Delta T}{L} = n_1\Delta^2/8c. \qquad \text{(I.1.6)}$$

That gives a limitation for the bit rate-length product:

$$BL < 8c/n_1\Delta^2. \qquad \text{(I.1.7)}$$

Although such fibers still can not be used for long haul fiber links, recently graded index plastic fibers has attracted considerable attention. The large core area and the large numerical aperture make them cheap and easy to handle alternatives in every day applications such as data links between home appliances or in vehicles. The typical value of the BL product in such fibers exceeds 2Gb/s*km.

I.1.4. Single mode fiber

By studying the propagation of electromagnetic waves in a step index fiber [5] one can find that the fiber supports only a single mode, if the

$$\frac{2\pi}{\lambda} aNA < 2.405 \qquad \text{(I.1.8)}$$

condition is satisfied. Where λ, a, NA, are the wavelength in vacuum, the core radius, and the numerical aperture of the fiber, respectively. Single mode fibers have essentially smaller numerical aperture and core radius. For example, a standard single mode telecommunication fiber used in the λ=1.3-1.6μm range has typically a=4.5μm core radius and a numerical aperture of NA=0.1.

Since in a single mode fiber there is no intermodal dispersion, there the chromatic dispersion plays an important role. Let's consider a pulse with a centre wavelength λ and

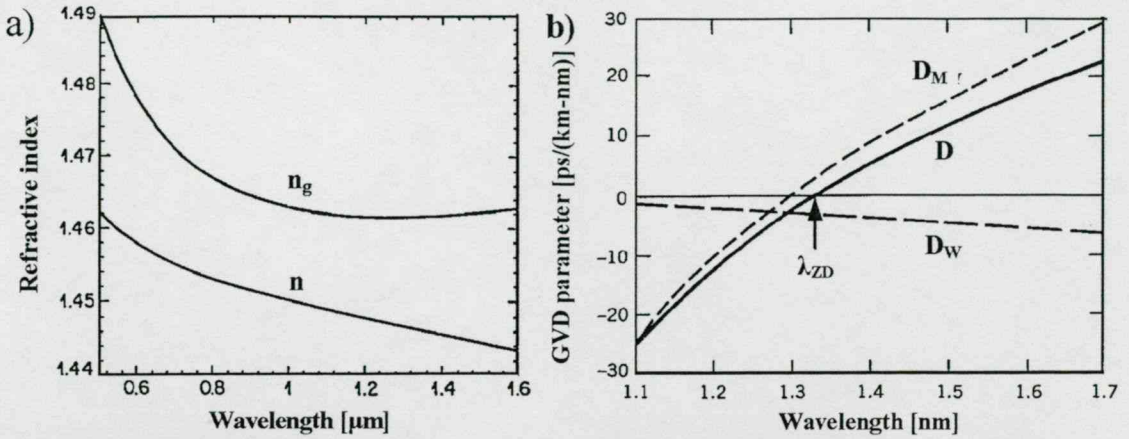

Fig.I.1.4: a) The dependence of the refraction index n and the group index n_g on the wavelength in fused silica. b) The wavelength dependence of the GVD parameter (D) and the contribution of the material GVD (D_M) and the weavguide introduced GVD (D_W) in a standard telecommunication fiber. The wavelength where the GVD parameter is zero is called the zero dispersion wavelength λ_{zd}.

$\Delta\lambda$ bandwidth. The time it takes the pulse to travel through a dispersive medium is $T=L/v_g$ where v_g is the group velocity. The group velocity is defined as:

$$v_g = \frac{c}{n - \lambda \dfrac{dn}{d\lambda}}, \tag{I.1.9}$$

where n is the refractive index of the material and $dn/d\lambda$ is generally referred as the linear dispersion coefficient. The denominator of eq.I.1.9 is called the group index (n_g). Fig.I.1.4a shows the wavelength dependence of the refractive index and that of the group index in fused silica.

The temporal broadening of a pulse is given by:

$$\Delta T = \frac{dT}{d\lambda}\Delta\lambda = -L\frac{\lambda}{c}\frac{d^2n}{d\lambda^2}\Delta\lambda = DL\Delta\lambda\,. \tag{I.1.10}$$

D is called the group velocity dispersion (GVD) parameter witch give the temporal broadening for a unit bandwidth as the pulse travels through a unit length in the medium. The GVD parameter of a fiber is determined by two terms: the GVD introduced by the fiber material and the GVD introduced by the waveguide structure itself: $D=D_{mat}+D_{waveg}$. Fig.I.1.4b shows the wavelength dependence of the GVD parameter and the contribution of the material and the fiber GVD parameter in a standard single mode fused silica telecommunication fiber. The wavelength where the GVD parameter is zero is called the zero dispersion wavelength λ_{zd}. Since any optical signal has a finite bandwidth as a result

of the GVD the pulses are broadening during the propagation. The limitation imposed by GVD to an optical transmission system can be expressed as:

$$BL|D|\Delta\lambda < 1. \qquad \text{(I.1.11)}$$

As it is seen in Fig.I.1.4b) the dispersion parameter is very close to zero for standard single mode fused silica telecommunication fibers around 1.3μm. At the vicinity of the zero group velocity dispersion wavelength the third order dispersion plays an important role. Usually, there the dispersion is characterised by a parameter called the differential dispersion parameter or dispersion slope: $S=dD/d\lambda$. If the light source is tuned to the zero group velocity dispersion wavelength, the temporal broadening of a pulse with the spectral width $\Delta\lambda$ can be expressed as:

$$\Delta T = \frac{1}{2} SL(\Delta\lambda)^2. \qquad \text{(I.1.12)}$$

There a typical value for S is 0.09 ps/(km*nm^2). And the limitation imposed for the BL product is given by:

$$BLS(\Delta\lambda)^2 < 2. \qquad \text{(I.1.13)}$$

It is easy to see that the system has the best performance if transform limited pulses are applied. Though it is necessary to mention that the limitations introduced by chromatic dispersion can be softened in the practice by dispersion compensation or by the compensating effect of the optical fiber Kerr-nonlinearity in the soliton transmission case. Generally, the most important reason for the signal degradation in single mode fiber links is the noise introduced during the re-amplifications made necessary by distribution and fiber losses. In the next chapters the limitations introduced by optical amplifiers will be discussed in detail.

1.2. Optical amplifiers

I.2.1 Semiconductor optical amplifier concept

The heart of a semiconductor optical amplifier is a p-n junction well-known from other semiconductor devices like diodes. Semiconductor laser action relies on the generation of photons during the interband recombination process of charge carriers (electrons and holes). By applying a forward bias current on a p-n junction the holes and the electrons are drifting and diffusing across the junction. In a narrow depletion region the electron-hole pairs are recombined either non-radiatively or radiatively. Electrons and

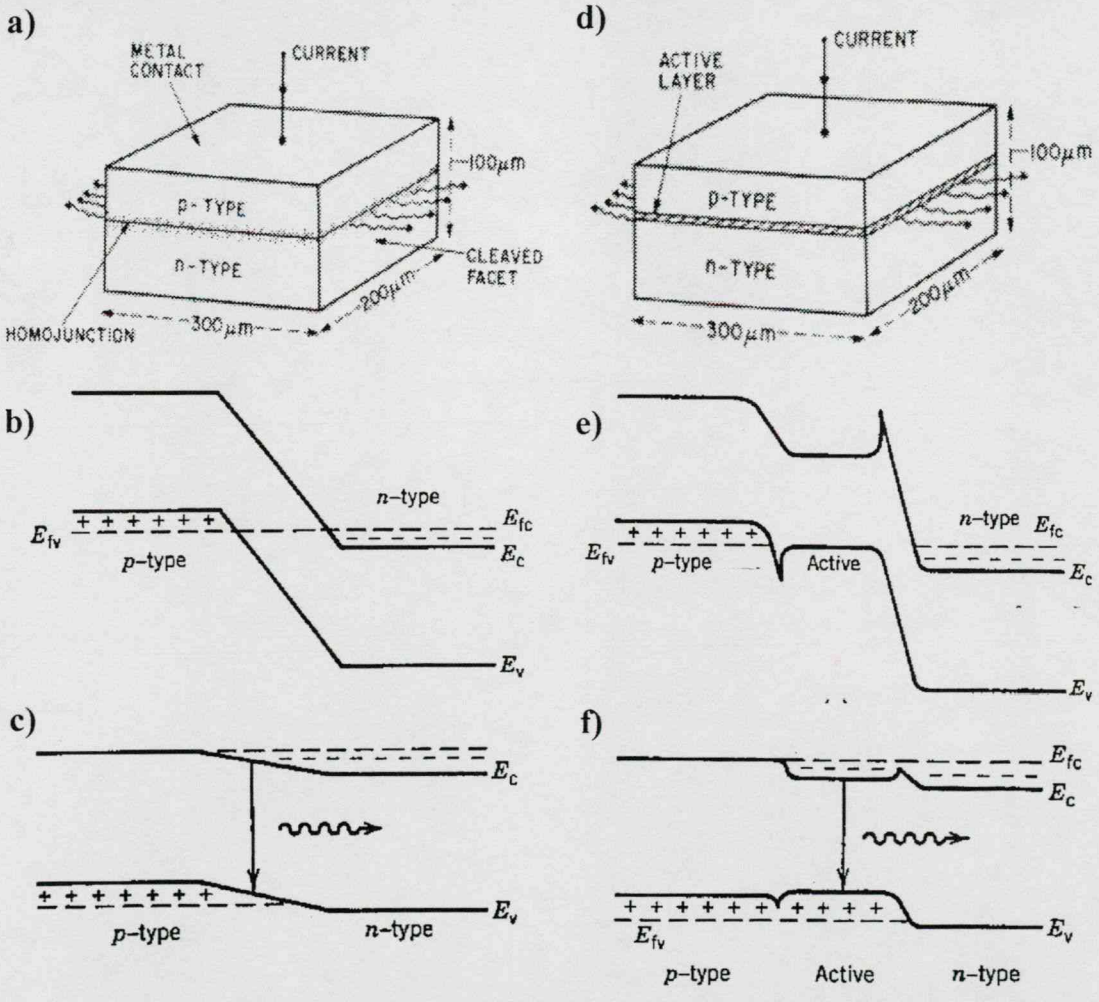

Fig. I.2.1: Schematic illustration of a homojunction semiconductor laser with the typical dimensions a), energy-band diagram of a p-n junction at zero bias b), at forward bias c). Schematic of a double heterostructure laser d), the energy-band diagram of a double heterostructure p-n junction at zero bias e) and at forward bias current f).

holes can also absorb radiation. If the current through the junction exceeds a critical value, population inversion is achieved and the rate of photon emission exceeds the rate of absorption.

Semiconductor laser structures can be classified as surface and edge emitters. Here we focus on the latter one since semiconductor laser amplifiers are exclusively edge emitter structures. Semiconductor lasers and laser amplifiers can be divided into two groups according to the structure of the p-n junction: homojunction (p-n), and heterojunction devices (Fig I.2.1).

Although a homojunction device is able to amplify electromagnetic radiation the thickness of the region where the optical gain is sufficiently large is very small. This is because there is no mechanism to confine carriers. To the author's knowledge no homojunction laser operating on room temperature have been reported yet.

Heterojunction structures are usually classified into two further groups called as single or double-heterostructure devices depending on whether the active region where lasing occurs is surrounded by a cladding layer of higher bandgap on one or both sides. In a double heterostructure the material of the active region has got a smaller energy gap than both the surrounding p-type and the n-type material. In such a case, as it is shown in Fig.I.2.1.f), both the electrons and the holes driven into the middle region by the forward current are trapped.

Another way to categorise a laser structure is according to the type of the active layer into bulk, quantum well and multiple quantum well structures. In the late 1980s the growth of extremely thin layers of semiconductor materials became possible and it allowed the fabrication of the so-called quantum well (QW) structures. In a QW laser the thickness of the active layer is reduced to 2-10 nm. Since the thickness of the structure is at the range of the de Broglie wavelength of electrons in the semiconductor, quantum size effects arise from the confinement of carriers to the potential wells. The energy of electrons and holes moving in the direction of confinement is quantised into discrete

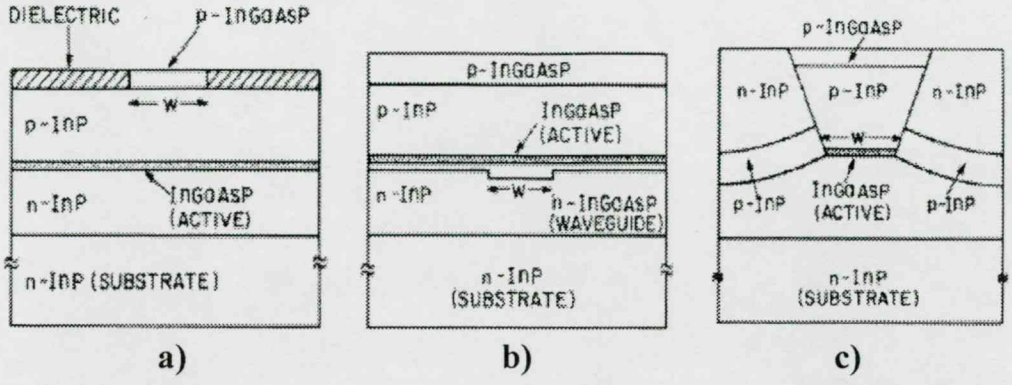

Fig.1.2.2: Schematic layout of a gain guided a) weakly index guided b) and a strongly index guided c) laser structure.

energy levels. This one-direction confinement means that the density of states is similar to that of a two dimensional system and not of a three dimensional one (like in bulk structures). QW lasers usually have higher differential gain, lower threshold current density, and improved temperature performance [6,7]. Since early 1990s multiple quantum well structure (MQW) based laser amplifiers become commercially available. It is interesting to note that recently quantum dot laser structures are also emerging on the horizon offering very low linewith enhancement factor and short gain recovery time.

Another way to classify semiconductor laser structures is based on the way how the guidance of light is accomplished. The vertical confinement of light is not a problem due to gain guiding. Moreover in double heterojunction structures the lower bandgap layer has inherently larger index of refraction leading to index guiding. For horizontal confinement three basic solution are known: gain guiding, weak index guiding and strong index guiding.

In a gain-guided laser the flow of current is limited to a narrow area by two lateral stripes of insulators (Fig.I.2.2a). The optical field confinement here is due to the optical gain.

In weakly guided structures the cladding layer thickness is varied leading to an additional index guiding (Fig.I.2.2b). The introduced effective index step is at the 10^{-2} range.

In a strongly indexed guided structure there is a lateral index step along the junction. The index step is ~0.2. These structures are often noted as buried heterostructures (Fig.I.2.2c).

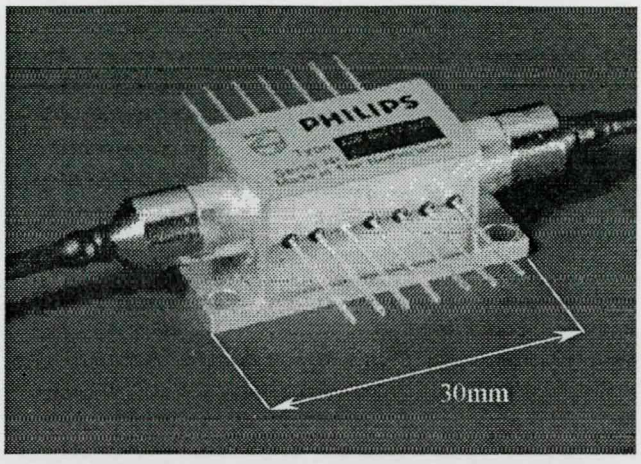

Fig. I.2.3: A picture of a Philips semiconductor optical amplifier (SOA) module.

For a practical realisation of a semiconductor travelling wave optical amplifier it is not only necessary to provide optical gain but to eliminate optical feedback. This mostly originates from the reflection on the cleaved facets of the device. The easiest way to reduce reflection is to cover the facets with antireflection coatings. Since it is very difficult to fabricate antireflection coatings having reflections lower than 10^{-3} for high gain amplifiers additional techniques are needed, such as angled facet or (and) buried-facet window structures [8,9]. With such techniques the back reflections can be reduced well under 10^{-4}.

Commercially available optical amplifiers are usually packaged. Such a package contains the input and output coupling to a fiber pigtail, a Peltier cooler and a thermistor to control the operating temperature. It is worth noting that presently the coupling losses at both sides are usually in the 2-3dB range. Recently strong reduction of the coupling losses (<0.5dB) was reported, which could lead to a significant improvement on SOA performance [10]. As a typical example for a SOA Fig.I.2.3 shows a Philips (*JDS UNIPHASE*) TW-SOA module.

I.2.2 Pulse amplification in semiconductor optical amplifiers.

The Agrawal-Olsson model is very commonly used [11] to describe the behaviour of the semiconductor optical amplifiers. In this model the response of the medium to the optical field is described by the following rate equations:

$$\frac{\partial P}{\partial z} = (g(N) - \alpha_{\text{int}})P, \tag{I.2.1}$$

$$\frac{\partial \Phi}{\partial z} = -\frac{1}{2}\alpha g(N), \tag{I.2.2}$$

$$\frac{\partial N}{\partial \tau} = \frac{I}{qV} - \frac{N}{\tau_c} - \frac{g(N)}{\hbar\omega_0}P, \tag{I.2.3}$$

where z is the spatial coordinate, parallel with the device axes; $\tau=t-z/v_g$ is the reduced time, $P(z,\tau)$ is the optical power, $\Phi(z,\tau)$ is the phase, α_{int} is the linear absorption coefficient of the device, α is the so-called linewidth enhancement factor, g is the gain coefficient, g_0 is the small signal gain coefficient, N is the carrier density, I is the injection current, q is the electron charge, V is the active volume, τ_c is the carrier lifetime, $\hbar\omega_0$ is the photon energy. The gain coefficient is defined as:

$$g(N) = \Gamma a(N - N_0), \tag{I.2.4}$$

where Γ is the confinement factor, a is the differential gain , N_0 is the carrier density required for transparency. From eq.I.2.1 and eq.I.2.3 the gain coefficient of the device can be expressed as:

$$\frac{\partial g}{\partial \tau} = \frac{g_o - g}{\tau_c} - \frac{g}{\varepsilon_{sat}}P \tag{I.2.5}$$

where $\varepsilon_{sat} = \dfrac{\hbar\omega\sigma_{\text{mod}}}{a}$ is the saturation energy and $\sigma_{\text{mod}}=wd/\Gamma$ is the mode cross section. The small signal gain coefficient is defined as: $g_0 = \Gamma a N_0(I/I_0 - 1)$ and the current required for transparency is $I_0=qVN_0/\tau_c$. Solving the equations for the case, when the duration of the optical pulse is much shorter than the recovery time and $\alpha_{\text{int}} \ll g$:

$$E_{out} = \varepsilon_{sat} \ln\left\{1 + \left[\exp\left(\frac{E_{in}}{\varepsilon_{sat}}\right) - 1\right]\exp(g_0 z_a)\right\} \tag{I.2.6}$$

is obtained for the output energy [12,13,14]. Where E_{in} is the input energy and z_a is the length of the active region.

During amplification not only the pulse energy but the pulse spectrum is modified since the depletion of the carrier density by the pulse results in a change of the refractive index (eq.I.2.2). This effect is called slow self-phase modulation (SSPM) and can be expressed by:

$$\Delta\nu_c(\tau) = -\frac{1}{2\pi}\frac{d\phi}{d\tau} = -\frac{\alpha}{4\pi}\frac{d}{d\tau}\left[\int_0^{z_a} g(z,\tau)dz\right]. \qquad \text{(I.2.7)}$$

The chirp is generally larger for more energetic pulses while the exact shape of the introduced chirp is strongly dependent on the pulse shape. The spectrum of the amplified pulse becomes considerably broad and could contain several peaks of different amplitude. Since the linewidth enhancement factor of semiconductor structures is generally positive, the peak of the spectrum is shifted to the red during amplification of short pulses and to the blue if the structure is used as a saturable absorber.

It is worth noting that in this model the differential gain (a) is presumed to be independent of the carrier density. In practice it is not the case. More detailed calculations [15,16,17] show that a could significantly depend on the carrier concentration. As a result a can be substantially higher at low carrier densities, especially under the transparency point (N_0), when the device works as a saturable absorber. This means that the saturation energy of such a device operating as a saturable absorber could be much lower than that in amplifier mode [17].

Another uncertainty of the model is that the recovery time of the device is considered by a single constant, though it is strongly carrier density dependent:

$$\frac{1}{\tau_c} = \frac{N}{A_{nr}N + BN^2 + CN^3 + \frac{n_g}{c}g(N)N_{phot}}, \qquad \text{(I.2.8)}$$

where A_{nr} is the non-radiative recombination coefficient; the BN^2 - quadratic term stands for the spontaneous radiative recombination and the CN^3 term is referred to as Auger recombination term. The last term of the formula describes the carrier recombination due to the stimulated emission (n_g is the group index of the material, c is the speed of light, and N_{phot} is the photon density). The typical literature values for the coefficients are

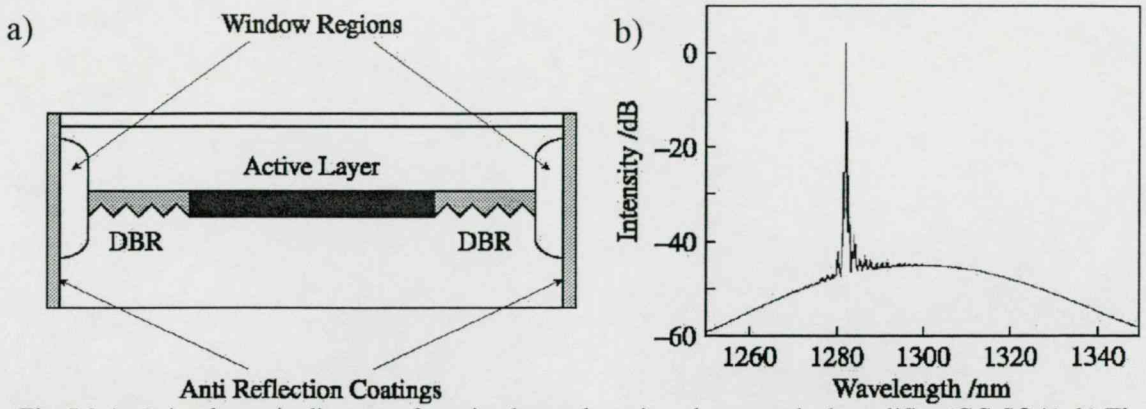

Fig. I.2.4: a) A schematic diagram of a gain clamped semiconductor optical amplifier (GC-SOA). b) The spectrum of the GC SOA if no signal is present.

A=5*10^{7}s^{-1}, B=10^{-16}m^{3}/s, C=4*10^{-41}m^{6}/s and a typical value for the initial carrier density is N=2*10^{24}m^{-3} [18,19,20]. These values give an estimate for the carrier recombination time to be around ~3ns, which is an order of magnitude larger than the usually measured values. This clearly shows the importance of the stimulated emission term. In [21] it was shown that the recovery time of long amplifiers could be significantly shorter because of the large contribution of the stimulated recombination rate. For the same chip structure of 500μm and of 1500μm length, 250ps and 100ps recovery times were measured, respectively. However long chips are still unpractical in optical transmission lines because of their stronger noise.

I.2.4 Gain clamping

A promising way to improve the recovery and the saturation characteristics of SOA is gain clamping. The concept for gain-clamped SOA (GC-SOA) was first described by Simon in 1994 [22]. In a gain clamped amplifier the active medium is surrounded by two Bragg reflectors introducing wavelength sensitive feedback (Fig.I.2.4). The device lases at the corresponding wavelength as soon as the roundtrip gain (gain times mirror losses) equals to unity. At this point the carrier concentration is fixed by the lasing [23]. Thus the optical gain for a signal coming at a different wavelength is also clamped as long as the output signal power is not comparable to the power of the lasing mode. The gain curve of such an amplifier is quite flat and saturates abruptly (Fig.I.2.5). One of the most promising applications of GC-SOA are in optical switching blocks, where the performance of common SOA is limited by the reduction of

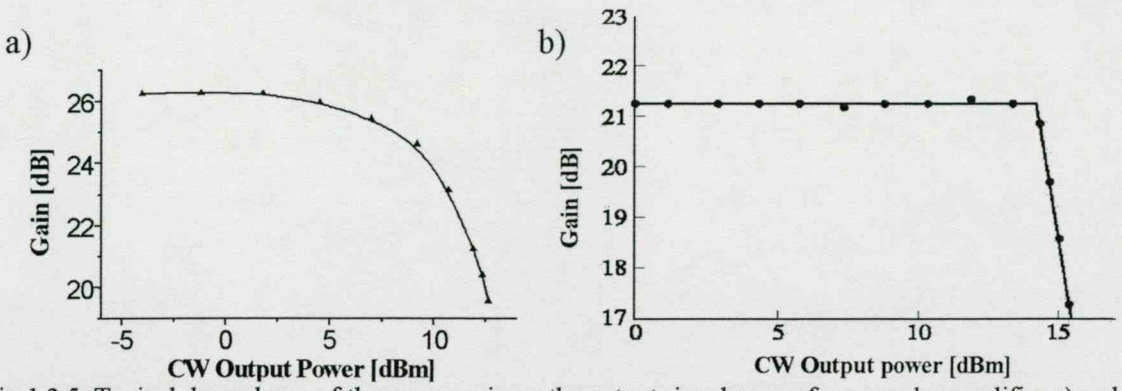

Fig 1.2.5: Typical dependence of the power gain on the output signal power for a regular amplifier a) and for a gain-clamped device b).

extinction ratio due to gain saturation [24,25]. Because of its linearity such amplifiers can even be used in analogue applications like cable television (CATV). It is worth to mention here that the relaxation oscillations of the clamping laser could significantly influence the high bit rate performance of such amplifiers [26,27].

I.2.5 Comparison of the Semiconductor Optical Amplifier with the Erbium Doped Fiber Amplifier

	SOA	EDFA
Gain:	15-30dB	20-40dB
Saturation power:	10-15dBm	15-20dBm
Recovery time:	~200ps	1ms
Noise figure:	6-8dB	4-6dB
Operating wavelength:	available in broad range	1.55μm
Gain bandwidth:	~50-80nm	~20-30nm
Pumping:	electrical	optical
Switchable:	yes	no
Dimensions:	single chip	rack design
Cost :	~2500$	~15000$

Table I.2.1: The comparison of the main SOA and EDFA characteristics

At present, the choice of in-line optical amplifier is almost exclusively the Erbium-doped fiber amplifier (EDFA) in the 1.5μm communication window. In such an amplifier an erbium doped fiber is optically pumped usually with one or more laser diodes operating at 0.98μm or 1.48μm. In Table I.2.1 the comparison of the most important characteristics of the SOA and the EDFA are given. Probably the main advantage of the EDFA is the long gain recovery time. As a result of that the amplifier is saturated by the average signal power rather than by the individual signal pulses. For this reason no patterning occurs. Unfortunately, EDFAs can only be used in lightwave systems operating at the 1.55 μm range. However the worldwide communication network contains more than 50 million kilometers of standard telecommunication fiber whose performance is optimised for 1.3μm operation. Since no doped fiber amplifier is capable to satisfy the practical needs of a 1.3 μm communication network (Pryaseodymium-doped fiber amplifiers are expensive, inefficient and unreliable), SOA is the exclusive choice for the 1.3 μm communication window. In future systems the simultaneous use of

both communication windows will also be of great interest. Moreover, SOA is more compact, reliable, much cheaper than EDFA and it has got a potential to be integrated on plano lightwave circuits (PLC).

I.3. Amplifier noise

In the following section the characteristics of the noise propagating together with the signal in optical transmission lines will be discussed. This problem recently attracted considerable attention and three fundamentally different approaches applied 1) quantum-mechanical field operator 2) rate equations and 3) a semiclassical approach based on field beating. Here the third approach is going to be used as it was first described by Olsson [28].

It is known from the rigorous quantum mechanical treatment [29] that any type of phase insensitive amplification process degrades the signal-to-noise ratio (SNR). The deterioration of the SNR is usually quantified by a parameter called noise figure:

$$F_n = \frac{(SNR)_{in}}{(SNR)_{out}}, \tag{I.3.1}$$

where the SNR refers to the electrical power generated, when the signal is converted to electrical current in the photo-detector. The fundamental limit for the noise figure is 2 (3dB), i.e.: the SNR is at least a factor of two lower after any laser amplifier than it was before. To obtain the noise figure of an amplifier let us presume that the signal is amplified by a factor G ($P_{out}=GP_{in}$) and the SNR at the input is:

$$SNR_{in} = \frac{< I >^2}{\sigma_s^2} = \frac{(RP_{in})^2}{2q(RP_{in})\Delta f} = \frac{P_{in}}{2h\nu\Delta f}, \tag{I.3.2}$$

where $<I>=RP_{in}$ is the average photo current, $R=q/h\nu$ is the responsivity of an ideal photodetector, q is the fundamental charge, $h\nu$ is the photon energy, Δf is the detector bandwidth and

$$\sigma_s^2 = 2q(RP_{in})\Delta f \tag{I.3.3}$$

is the shot noise at the detector. The signal-to-noise-ratio is deteriorated by additional noise terms at the output. These terms are originating from the beating between the signal and the ASE field, from the beating between the different frequency components of the

ASE field and from the shot noise induced by the ASE at the detector. It turns out that if the input power is sufficiently large compared to the generated noise power, the term corresponding to the signal-ASE beating at the detector is the dominant one.

The amplified spontaneous emission induced optical noise power that is generated in a band Δf centered at the optical carrier frequency at the output is given as:

$$F_0(\nu) = (G-1)n_{sp}h\nu\Delta f = S_{sp}\Delta f, \tag{I.3.4}$$

where S_{sp} is the spectral density of the ASE noise, n_{sp} is the inversion factor defined as:

$$n_{sp} = \frac{N}{N_1 - N_0}. \tag{I.3.5}$$

Here N is the carrier density and N_0 is the carrier density required for transparency.
The signal-ASE beat term can be written as:

$$\langle i^2 \rangle_{sig-ASE} = 4(GRP_{in})(RS_{sp})\Delta f \tag{I.3.6}$$

and the SNR at the output can be expressed as:

$$(SNR)_{out} = \frac{< I >^2}{\sigma_s^2 + \langle i^2 \rangle_{sig-ASE}} = \frac{(GP_{in}R)^2}{2q(RGP_{in})\Delta f + 4GR^2P_{in}S_{sp}\Delta f} \approx \frac{GP_{in}}{4S_{sp}\Delta f}. \tag{I.3.7}$$

The last simplification was obtained by neglecting the shot term and it is valid as long as $G>>1$. From here the noise figure of a semiconductor optical amplifier can be given as:

$$\mathrm{F}_n = 2\frac{N}{N-N_0}\frac{(G-1)}{G} \approx 2n_{sp}. \tag{I.3.8}$$

It is seen that even in the ideal case (when $N_0=0$) the noise figure of the amplifier can not be lower than 2. In the practice the noise figure of the standard semiconductor optical amplifiers operating at the 1.3μm is around 3-6 and the noise figure of a gain clamped amplifier is ~10.

A.Yariv further generalised the above-described formalism to determine the noise figure in fiber links with periodic amplification and attenuation for an ideal photodetector [30]. A generalised form of eq.I.3.7 for the signal to noise ratio in an arbitrary point of the link is:

$$SNR(z) = \frac{P^2(z)}{2P(z)h\nu\Delta f + 4F(z)P(z)}, \tag{I.3.9}$$

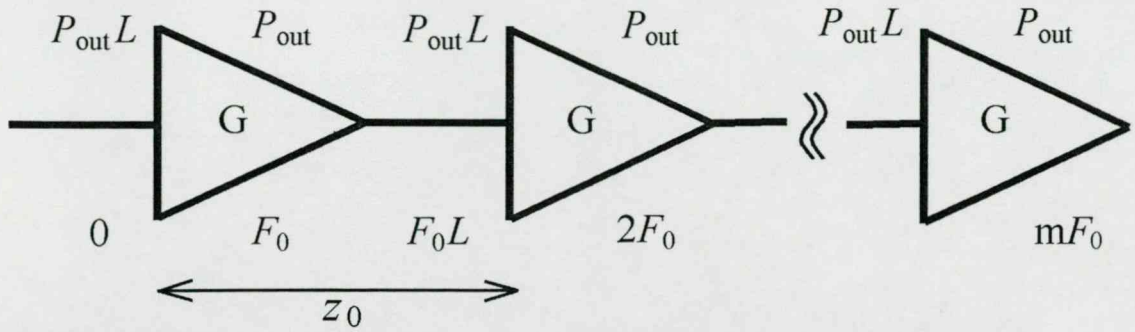

Fig I.3.1: The evolution of the signal power P and the spontaneous emission noise F in a chain containing periodic attenuation and re-amplification. The segments are uniform and the loss is equal to the amplifier gain (L^{-1}=G).

where $P(z)$ is the signal power at point z and $F(z)$ is the total ASE noise power at z originating from all the preceding amplifiers in the line.

Let's consider now equidistantly spaced amplifiers separated by optical fibers of z_0 length. Presume that the amplifiers have a uniform gain exactly compensating for the loss (L) in the subsequent fiber section $G=L^{-1}=exp(-\alpha z_0)$. It is easy to see that the signal power changes periodically and the amplified spontaneous emission power noise is increasing by the increment F_0 after each amplifier (see Fig.I.3.1). Substituting eq.I.3.4 into eq.I.3.9:

$$SNR_m = \frac{P_{out}}{2h\Delta\nu\{1 + 2mn_{sp}[\exp(\alpha z_0) - 1]\}}, \qquad \text{(I.3.10)}$$

is obtained for the signal to noise ratio after the m-t amplifier. From eq.I.3.10 it is obvious that the noise figure of the communication link can be improved by applying more amplifiers (large m) with reduced distance between them (smaller $exp(\alpha z_0)$).

There are several papers devoted to the optimisation of the amplifier gain distribution if the amplifiers are not equidistantly placed though closed form analytic solution still does not exist for such a problem [31,32,33].

It is interesting to consider the case when the amplifier spacing keeps to zero. By substituting $m=Z/z_0$ in eq.I.3.10 (where Z is the total length of the fiber link),

$$SNR(z) = \frac{P_{out}}{2(1 + 2n_{sp}\alpha Z)h\nu\Delta f}. \qquad \text{(I.3.11)}$$

is got at the $z_0 \rightarrow 0$ limit. In this case the whole length of fiber acts as an amplifier exactly compensating for the fiber losses ($\alpha=g^{-1}$). It is the case of so-called distributed

amplification, which represents an ideal limit. This ideal case can be approached in the practice by optical pumping of lightly doped fibers [34] or by utilising the Raman amplification process in the fiber [35]. Significant drawback of such schemes is that they are usually much more sensitive on the environment (temperature fluctuations, vibrations) than passive fibers with lumped amplification.

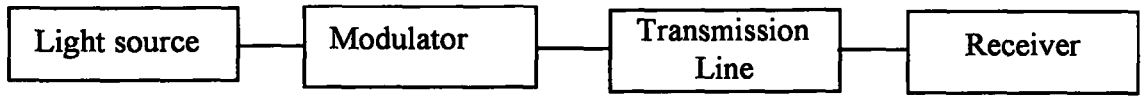

Fig. I.4.1: Schematic diagram of a fiber optical transmission system.

I.4. Data transmission in fiber optical links

In the following section the most important problems associated with information encoding and retrieving in a binary optical transmission line will be discussed with special interest to the systems using semiconductor optical amplifiers.

I.4.1 Data encoding and retrieving

A schematic diagram of a fiber optical transmission system is shown in Fig.I.4.1. Such a system generally contains a light source, a modulator, a transmission line and a receiver. The modulator is responsible for encoding the data to optical signal A transmission line usually contains the optical fiber and re-amplification nodes compensating for the fiber and distribution losses.

Now, let us focus on the transmission of binary data. There are two possible representations of a binary data sequence: the return to zero (RZ) and the non-return to zero (NRZ) representation. In RZ representation each pulse representing a bit 1 is shorter than the bit slot. In NRZ representation the duration of the signal pulses is exactly the same as the bit slot and its amplitude does not drop to zero between successive bit 1-s. The electric field associated with the optical carrier can be written as:

$$E_s(t) = A_s(t)[\cos(\omega_0 t) + \phi_s(t)]. \qquad \text{(I.4.1)}$$

To encode the binary information three basic properties of light can be varied: amplitude, phase, frequency. The corresponding modulation formats are called amplitude-shift keying (ASK), phase-shift keying (PSK) and frequency-shift keying (FSK). The modulation can be introduced by an external device or in some cases by direct modulation of the diode laser source.

Amplitude-shift keying is commonly realised by a Mach-Zender type modulator. In such designs, the refractive index of an electro-optic material (usually $LiNbO_3$) is changed in one of the arms by an external voltage. By properly varying the driving

voltage, the optical signal interferes constructively or destructively leading to amplitude modulation. Mach-Zender type intensity modulators are commercially available up to 40GHz modulation frequency. The typical extinction ratio of such devices is better than 20dB. It is worth noting that amplitude modulation can also be realised by direct modulation of the driving current of a diode laser. In such a case fiber dispersion could seriously limit the system performance because of the introduced strong nonlinear chirp.

In the case of PSK modulation format the information is encoded by varying the phase of the optical signal by usually π between bit ones and zeros. An interesting aspect of phase modulation is that the signal power remains constant. The implementation of PSK modulation is rather easy by modulating the voltage on an electro-optic crystal. Unfortunately the PSK format requires that the phase of the carrier remains stable for a long period of time so that the phase information can be extracted. That stringent requirement can be reduced significantly by the so-called differential phase-shift keying format (DPSK). Here the information is coded by the phase difference between two neighbouring bit slots. In this case the extraction of the binary information can be realised by the combination of a photodetector and a Mach-Zender interferometer having one bit slot optical path difference between the two arms.

In the case of frequency shift keying (FSK) the ω_0 carrier frequency is shifted to $\omega_0+\Delta\omega$ in ones and $\omega_0-\Delta\omega$ in zeros. The FSK format can also be considered as a kind of PSK with increasing or decreasing phase shift in the bit slot. It is quite rarely used in the practice. One possible realisation of frequency-shift keying is to modulate the driving current of the semiconductor laser used as a light source. That not only changes the laser power but shift the frequency as well. The typical values for the frequency shifts are 0.1-1GHz/mA.

At the receiver the optical signal converted again to electrical one. The receiver unit contains two major blocks. One is responsible for the optical to electrical signal conversion, and the other is for the electrical signal to data conversion. The later is called the data recovery. The data recovery block contains a decision circuit and a clock recovery. The decision circuit decides whether a bit 1 or a bit 0 is received. The clock recovery circuit ensures that the data retrieval is synchronised to the optical signal. In most of the cases active control is necessary since the propagation time slowly varies (at

the ms scale) mainly due to the temperature fluctuation induced refraction index changes in the fiber. The most common way to solve the problem is to extract the $1/T_{bitslot}$ frequency component from the optical signal and use that for synchronisation. In NRZ representation the $1/T_{bitslot}$ frequency component is not present. Here usually the frequency corresponding to half of the bit rate is extracted form the optical signal and than doubled.

Finally the most important measure of the data transmission quality have to be introduced. It is called the bit error rate (BER) and defines as:

$$BER = \frac{1}{2}[P(0/1) + P(1/0)].$$

Where the same probability for receiving bit 1 and bit 0 is presumed and P(0/1), P(1/0) is the probability of detecting 0 when bit 1 is received and detecting 1 instead of bit zero, respectively. A transmission is generally called error free if the BER<10^{-9}. Obviously the bit error rate depends on how the decision threshold is set and how well the data retrieval is synchronised to the optical signal. If the probability density function of *P(1/0)* and *P(0/1)* is presumed to be gaussian then by the optimal setting of the decision threshold the bit error rate can be calculated as:

$$BER = \frac{1}{2} erfc\left(\frac{Q}{\sqrt{2}}\right), \tag{I.4.2}$$

where:

$$erfc(x) = \frac{2}{\sqrt{\pi}} \int_x^{\infty} \exp(-y^2) dy \tag{I.4.3}$$

and Q is called the Q factor and defined as:

$$Q = \frac{I_1 - I_0}{\sigma_1 + \sigma_0}. \tag{I.4.4}$$

Here I_1 and I_0 are the detected average photocurrent in ones and zeros and σ_1 and σ_0 are the root mean square of the current fluctuations in ones and in zeros, respectively. The transmission is error free (BER<10^{-9}), if $Q>6$. It is worth to emphasise that the Q factor is strongly dependent on the synchronisation of the data retrieval with the optical signal.

I.4.2 SOA based data transmission

In the previous section we have studied the limitations imposed by the growth up of spontaneous emission induced noise propagating together with the signal. Here the advantages and disadvantages of different kind of modulation formats are considered with special attention to the semiconductor optical amplifier (SOA) based transmission lines.

Amplitude-shift keying is probably the most straightforward modulation format resulting in a relatively simple receiver design. However it arises the problem of in-space noise management. In an EDFA the gain recovery time is much longer than the bit slot. Therefore the amplifier is saturated rather by the average power than by the individual pulses. So the noise between the signal pulses will be amplified with the same gain as the signal. For a SOA the situation is completely different. The gain recovery time is comparable with the bit slot and the amplifier is saturated by the individual pulses. That means that in a long set of zeros or even between two subsequent pulses in RZ representation, the noise will be amplified with larger gain than the signal. Hence the growth up of in-space noise is inevitable. Traditionally, the in-space noise is managed by keeping the signal pulses in the weak saturation region and even allowing slight decrease of the signal power over the distance. Theoretical considerations show that the ideal gain map for equidistantly spaced SOAs is where the small signal gain of the amplifier equals to the reciprocal of the fiber losses ($G_0=L^{-1}$). Or in a generalised case the optimum gain distribution is such that the amplifier gain in dB is the arithmetic mean between the loss in dB of the fiber segments before and after the amplifier [36].

In phase-shift keying (PSK) transmission mode the problem of in-space noise does not arise because the radiation is quasi-CW in the line. Here the main limitation is imposed by the phase noise. Schematic diagram of the generation process of the phase noise is shown in Fig I.4.2. The phase noise originates from two sources: a) direct disturbance of the signal field by the ASE, b) transformation of carrier density fluctuations to phase noise. Since the linewidth enhancement factor of semiconductor optical amplifiers are rather large the latter one is the dominant factor. The carrier density fluctuation may arise from non-radiative carrier recombination, from the spontaneous emission, which is not coupled into the output and from the beating of the ASE with the signal field in the

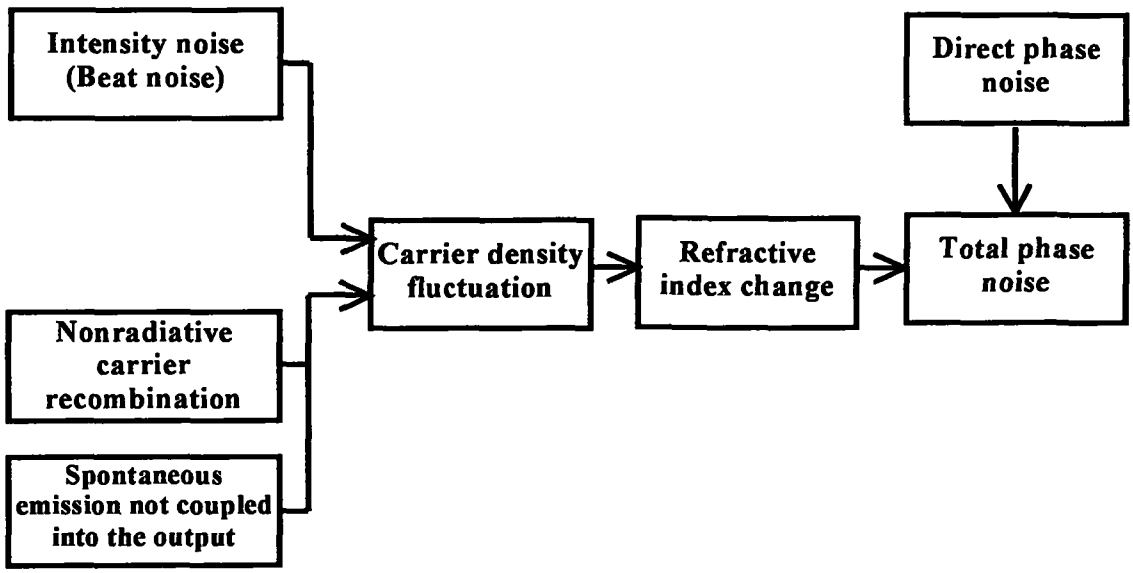

Fig I.4.2: The generation process of the phase noise from semiconductor optical amplifiers

amplifier. The latter one is the most important [37]. It is interesting to note that the carrier density fluctuation induced components of the noise have a cut-off frequency determined by the carrier lifetime.

I.5 Latest experimental results obtained for transmission lines with in-line semiconductor optical amplifiers:

Single chanel transmission:

.	Organisation/ Bit rate & transmission format	Year:	Distance:	Type:	Ref:
1.	FZ Telekom, Darmstadt 10Gb/s RZ ASK	1996	300 km (5*50km)	test-bed	[38]
2.	Philips Optoelectronics Center 10Gb/s RZ ASK	1996	420 km (12*38km)	test-bed	[39]
3.	UPGRADE / ACTS 10Gb/s RZ ASK	1997	210 km (6*SOA)	field trial Kassel-Hannover	[40] [41]
4.	FSU-Jena 10Gb/s RZ ASK	1997	550 km (17*33km)	fiber loop	[42]
5.	UPGRADE / ACTS 10Gb/s+4*2.5Gb/s RZ ASK	1998	460 km (13*SOA) 10Gb/s + 350 km (10*SOA) 2.5Gb/s	field trial Madrid-Lisbon (810 km)	[43]
6.	FSU-Jena 10Gb/s DPSK-DD	1998	500 km (20*25km)	fiber loop	[44]
7.	FSU-Jena 10Gb/s RZ ASK	1998	1500 km (40*37km)	fiber loop	[45]
8.	**FSU-Jena (with SA)** 5Gb/s RZ ASK	1999	30,000 km (1200*25km)	fiber loop	[46, [47]
9.	**FSU-Jena (with SA)** 10Gb/s RZ ASK	2000	5,000 km (200*25km)	fiber loop	[48]

Wavelength Division Multiplexing (WDM):

	Organisation/ Bit rate & transmission format	Year:	Distance:	Type:	Ref:
10.	TU Eindhoven 4x10Gb/s, RZ ASK	1998	80 km (2*40km) 200 km predicted	test-bed	[49]
11	Lucent Technologies 32x2.5 Gb/s, NRZ ASK	1999	125 km (3*42km)	test-bed	[50]
12.	Lucent Technologies 8x20 Gb/s, NRZ ASK	1999	160 km (4*40km)	test-bed	[51]
13.	Lucent Technologies 32x2.5 Gb/s, NRZ ASK	2000	315 km	test-bed	[52]

Table:I.5.1 Overview of the recent results obtained in SOA based transmission experiments

As the last section of the introduction an overview of the latest experimental results obtained by using SOA as in-line amplifiers in transmission lines are given (Table I.5.1). In SOA based, high bit rate, long distance transmission experiments almost exclusively the ASK transmission format is used. The fundamental parameters influencing the system

performance are the low saturation energy, high linewidth enhancement factor and amplitude patterning originating from the bit rate comparable gain recovery time. However the most important limitation of all is the growth up of in-space ASE noise. Conventionally, the problem is reduced by careful management of the power evolution in the transmission line and by the use of in-line bandpass filters. As it will be shown in the following chapters this problem can be completely eliminated by the implementation of in-line saturable absorbers. Such a system has very different operational characteristics and the system performance is limited by the factors previously doomed to secondary importance. Recently there are several reports on WDM transmission with SOA. Here the main limitation is imposed by the interchannel crosstalk caused by cross gain modulation.

II. Modulation instability in SOA based transmission lines

II.1 Theoretical predictions

It was shown in the previous chapter that the performance of SOA based systems are limited by the bit rate comparable gain recovery time, the low saturation energy and the strong dependence of the refraction index on the carrier density (large linewidth enhancement factor). Since in the amplitude-shift keying transmission mode (ASK) the most important limitation is the growth up of ASE noise in zeros originating from the bit rate comparable gain recovery time, it seems advantageous to apply some different type of transmission format resulting in a quasi-CW signal. Onishchukov et. al. applied differential binary phase-shift keying - direct detection (DBPSK-DD) transmission to enhance the performance of SOA based transmission lines in [44]. With such a setup error free transmission of 10Gb/s signal was demonstrated up to 500km at the 1.3μm communication window in a re-circulating fiber loop arrangement. Though in that publication the most important cause of performance degradation was identified as the phase noise from SOA, there is an additional effect, which could impose serious limitations to such lightwave communication systems. Namely: modulation instability due to the interplay of the in-line optical bandpass filter and the SOA nonlinearity.

Modulation instability (MI) of continuos waves (CW) due to GVD and Kerr-nonlinearity is a well known fundamental phenomenon occurring in optical fibers. The interplay of the anomalous group velocity dispersion and the Kerr-nonlinearity leads to instability of a steady state CW solution and it may result in the formation of periodic pulse trains [53,54,55,56].

Here the existence of a novel type of modulation instability phenomenon originating from the interplay between the SOA nonlinearity and the in-line optical bandpass filter will be demonstrated both theoretically and experimentally. In a SOA based transmission line such an instability can amplify any initially small periodical amplitude disturbance with an appropriate period ω_m to a level, where it seriously deteriorates the system performance. If the system contains in-line bandpass filters, a

small periodic amplitude disturbance is always present in a phase-modulated train due to the periodic change of the carrier frequency. The introduced periodic modulation has got twice the frequency than that of the phase modulated signal [57]. Another source of periodic amplitude disturbances could be a linear effect called self-amplitude modulation (SAM). This originates from the slightly different group velocity of the different frequency components in the phase modulated signal [58].

A simplified empirical explanation for the semiconductor optical amplifier induced modulation instability is the following. If there is an amplitude peak in the signal it depletes the steady state carrier concentration. Because of the introduced phase modulation the carrier wavelength is shifted and the changed carrier wavelength results in a different filter loss. If the loss increases the signal will be stable, but if the loss decreases, the modulation will be further enhanced.

Theoretical treatment of the SOA and bandpass filter action associated modulation instability is based on the following propagation equation:

$$i\frac{\partial Q}{\partial z} = -2\beta_2\omega_s\frac{\partial Q}{\partial t} + \left(\frac{\beta_1}{2} + i\beta_2\right)\frac{\partial^2 Q}{\partial t^2} - \chi|Q|^2 Q + i\delta_e Q - \rho(\alpha+i)Q\int_{-\infty}^{t}|Q|^2\exp\left(-\frac{t-t'}{\tau_c}\right)dt' \quad \text{(II.1.1)}$$

Where $\beta_1=k''(\lambda_0)$ is the fiber group velocity dispersion (GVD) coefficient; $\chi=2\pi n_2/(\lambda_0 A_{eff})$ is the fiber nonlinearity, n_2 is the Kerr-coefficient, A_{eff} is the effective mode cross section and λ_0 is the carrier wavelength.

$\beta_2=2ln(2)/(z_a\Delta\omega_f^2)$ characterises the effective filter bandwidth, where z_a is the fiber span and $\Delta\omega_f$ is the FWHM of the applied Gaussian shaped bandpass filter. $\delta_e=g_0/2z_a-\gamma-\beta_2\omega_S^2$ is the net gain coefficient, where g_0 denotes the gain coefficient of the amplifier, γ is the fiber loss and $\omega_S=-2\pi c(\lambda_F-\lambda_0)/\lambda_0^2$ is the detuning of the filter position (λ_F) from the carrier wavelength (λ_0).

$\rho = a_0^2/(2z_a E_{sat})$ is the saturated amplification coefficient and E_{sat} is the saturation energy, $a_0=2\gamma z_a/[1-\exp(-2\gamma z_a)]$ is the correction accounting for periodic gain and attenuation between the amplifiers in the average field description.

α is the linewidth enhancement factor and τ_c is the recovery time of the amplifier. The CW solution of eq.II.1.1 is:

$$Q^{(0)}(z,t) = Q_0 \exp[i(\Gamma z - \omega t)], \tag{II.1.2}$$

where:

$$\Gamma = \frac{\beta_1 \omega^2}{2} + (\chi + \rho\alpha\tau_c)Q_0^2 \tag{II.1.3}$$

and with the energy balance:

$$\frac{h_0}{2z_a} = \gamma + \beta_2(\omega - \omega_s)^2 + \rho\tau_c Q_0^2. \tag{II.1.4}$$

A stability analysis of the CW solution against small amplitude perturbations has been carried out. By inserting $Q(z,t) = (Q_0 + \varepsilon(z,t))\exp(i\Gamma z - \omega t)$ into eq.II.1.1 and linearising in the terms containing ε(z,t) one obtains:

$$\begin{aligned} &i\frac{\partial\varepsilon}{\partial z} + 2\beta_2\omega_S\frac{\partial\varepsilon}{\partial t} - \left(\frac{\beta_1}{2} + i\beta_2\right)\frac{\partial^2\varepsilon}{\partial t^2} + \chi Q_0^2(\varepsilon + \varepsilon^*) = \\ &= -\rho(\alpha + i)Q_0^2\int_{-\infty}^{t}(\varepsilon + \varepsilon^*)\exp\left[-\frac{t-t'}{t_r}\right]dt'. \end{aligned} \tag{II.1.7}$$

By separating the real and the imaginary parts as ε=v+iω and transforming the equations to the spectral domain we get a first order system of differential equations. The increment λ of the corresponding spectral components $\tilde{v}(z,\omega_M), \tilde{\omega}(z,\omega_M) \sim \exp(\lambda z)$ can be obtained from the following characteristic polinom:

$$(\lambda + \beta_2\omega_M^2)^2 + \frac{2\rho Q_0^2 t_r}{1 - i\omega_M t_r}(\lambda + \beta_2\omega_M^2) + a\left(a - 2\chi Q_0^2 - \frac{2\rho\alpha Q_0^2 t_r}{1 - i\omega_M t_r}\right) = 0, \tag{II.1.8}$$

where $a = -\beta_1\omega_M^2/2 + 2i\beta_2\omega_S\omega_M$ and ω_M is the modulation frequency of the perturbation. The characteristic polinom is generally satisfied by two different value of λ. The physically significant solution was chosen to be the one with the larger real part. Obviously the CW signal is unstable against the perturbation ω_M if Re[λ]>0. Since our primary concern was to demonstrate the existence of unstable behaviour due to the interaction of the bandpass filter and of the SOA, the terms in eq.II.1.8 responsible for the conventional modulation instability were set initially to zero (χ=0,β_1=0). The analysis shows that SOA all alone can not cause an unstable behaviour because $\rho>0$. If the bandpass filter is included, unstable domains are appearing in the ω_S-ω_M parameter space. However, for zero filter detuning (ω_s=0) the solution is always stable. In Fig II.1.1 the MI

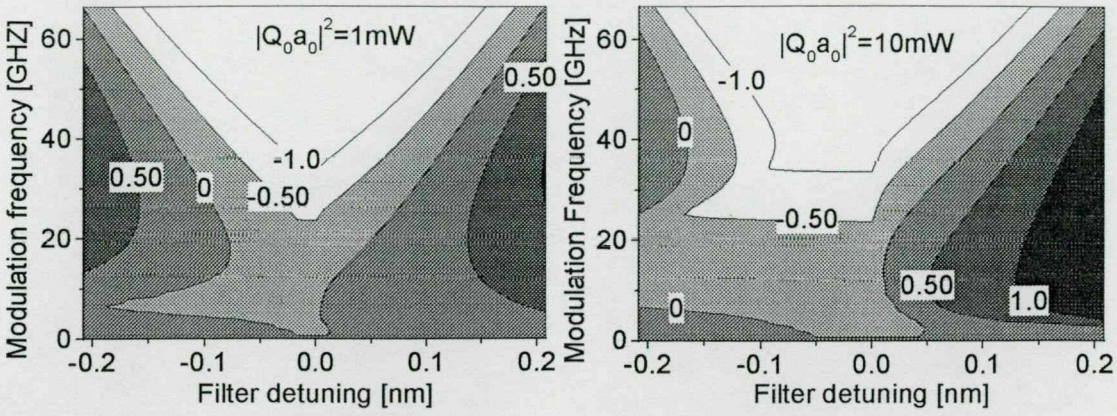

Fig.II.1.1: The modulation instability (MI) gain as a function of filter detuning and modulation frequency at different fiber input powers. The filter bandwidth is 0.7nm, the saturated amplification coefficient is ρ=0.026km^{-1}pJ^{-1}and the fiber Kerr nonlinearity and the GVD are neglected.

gain as a function of the filter detuning and the modulation frequency is shown. Note that the stable area is asymmetrical.

Fig.II.1.2 shows the MI gain if both the Kerr nonlinearity in the fiber and GVD are taken into account. In the anomalous GVD regime for large input powers conventional MI dominates. At the normal GVD regime and at zero GVD wavelength the MI gain is reduced and mainly evoked by the bandpass filter and the SOA.

Finally it is worth to mention that eq.II.1.1 can be substantially simplified if Q can be expressed as for a modulated CW:

$$Q(z,t) = \sum_j c_j(z)\exp(-ij\omega_M t) \tag{II.1.9}$$

By substituting eq.II.1.9 to eq.II.1.1 one obtains:

$$i\frac{dc_m}{dz} = \left(i\delta - \frac{\beta_1}{2}(m\omega_M)^2 - i\beta_2(m\omega_M - \omega_S)^2\right)c_m + \sum_{\substack{j,k,l \\ m=j-k+l}}\left(\chi + \frac{\rho(\alpha+i)\tau_r}{1-i(m-j)\omega_M\tau_r}\right)c_j c_k^* c_l . \tag{II.1.10}$$

From here it is easy to see that the process can be understood as a kind of four wave mixing where the SOA changes the fiber nonlinearity.

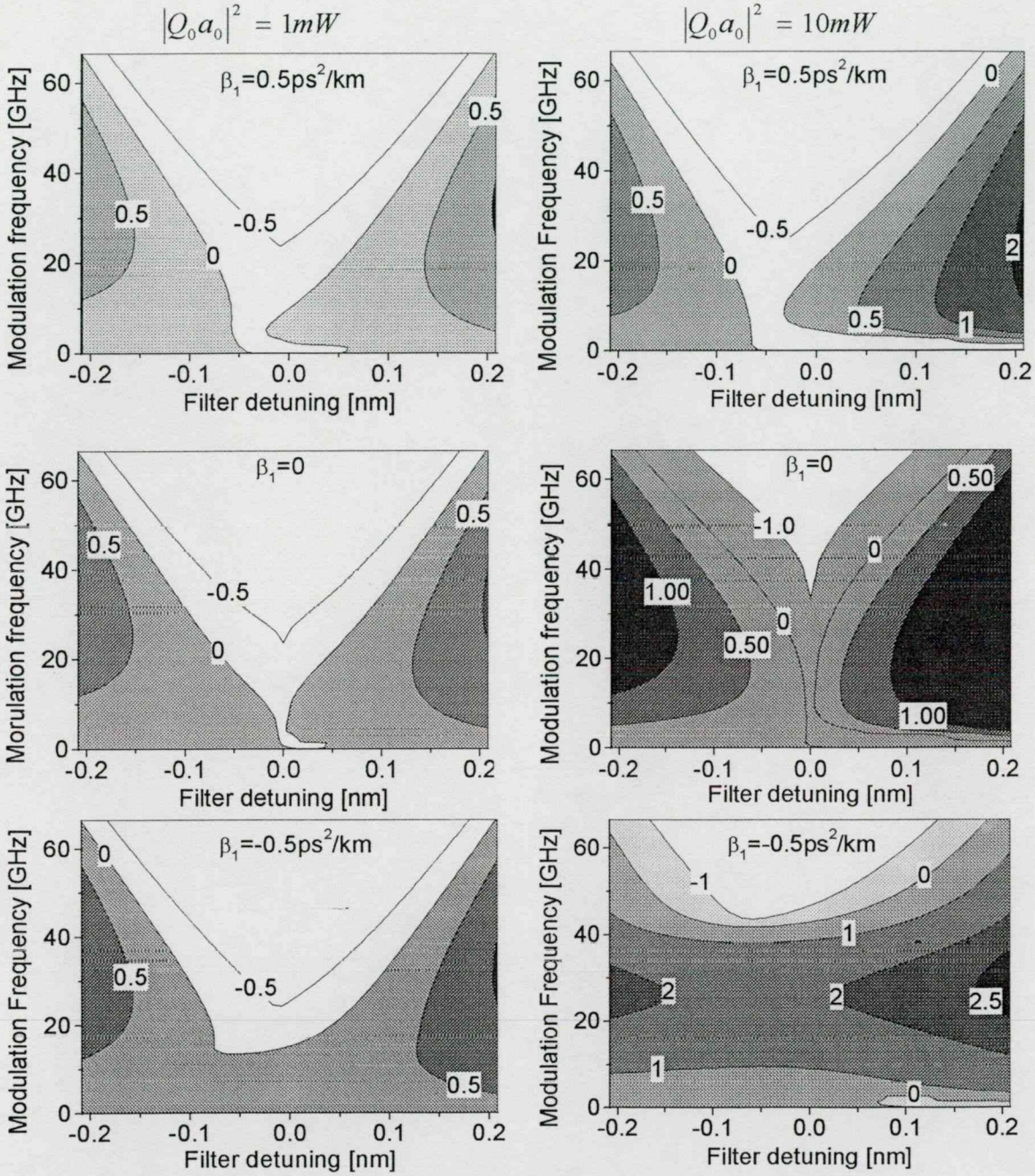

Fig.II.1.2: The modulation instability gain as a function of filter detuning and of modulation frequency for two different fiber input powers in the case of normal (β_1=0.5ps^2/km), zero (β_1=0) and anomalous (β_1=-0.5ps^2/km) GVD. The FWHM bandwidth of the in-line bandpass filter is 0.7nm , the Kerr coefficient of the fiber is χ=3.1W^{-1} km^{-1}, the saturated amplification coefficient is ρ=0.026km^{-1}pJ^{-1}.

New Scientific Results

II.2 Experimental demonstration of the SOA-filter interaction induced modulation instability

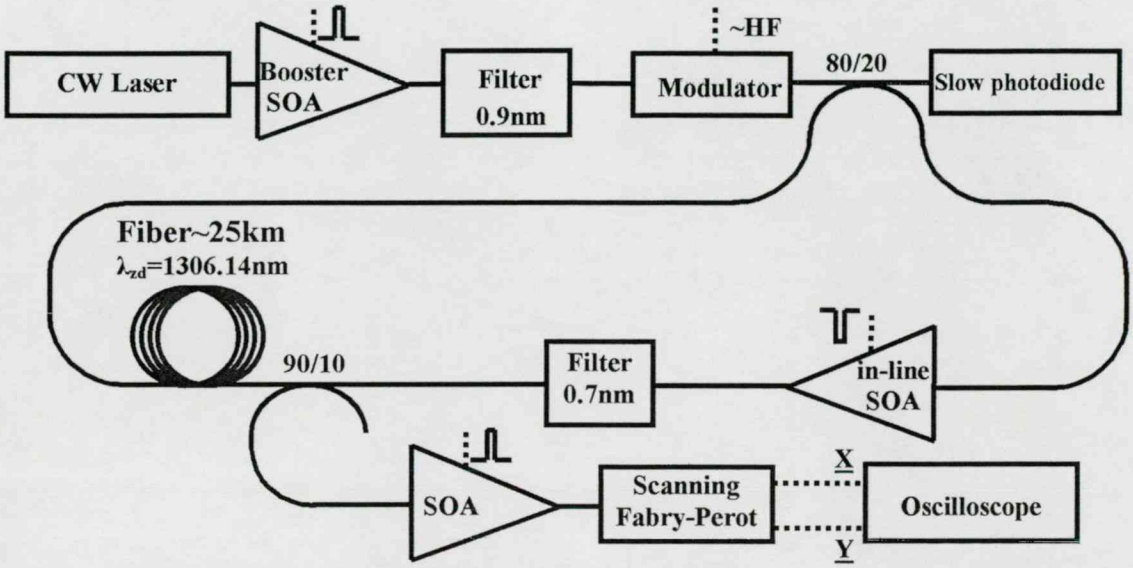

Fig. II.2.1) A schematic layout of the re-circulating fiber-loop setup.

The behaviour of a fiber optical transmission line can be simulated in a re-circulating fiber loop setup. As a first step a burst of the laser radiation is injected to the fiber loop by appropriate gating of the booster amplifier. In the loop the optical signal circulates and in each roundtrip some portion of the radiation is coupled out to the signal diagnostics. By gating the diagnostics the parameters of the optical signal can be determined in each roundtrip. Thus the distance (temporal) evolution of the radiation can be recorded. The gating of the data acquisition can be realised by an additional SOA used as an optical switch or by internal gating option of the instrument. After the radiation reached the desired distance the loop is cleared by switching off of the in-line amplifier. The schematic layout of such an arrangement is shown in Fig.II.2.1. The CW light source was a Radians Innova TUN-1300ML tunable laser. The laser radiation was amplified by a Philips CQF882/0 MQW SOA and the ASE of the booster amplifier was blocked by a tunable 0.9nm filter. In the first experiments, the CW signal was modulated with an UTP 9603 phase modulator. In this way higher modulation frequency (~20GHz) was

accessible since a given frequency phase modulation transfers to a double frequency amplitude modulation due to the filter. It was found that the modulation instability effect is the strongest in the available power range, if the frequency of the introduced amplitude modulation is ~10GHz. Later, instead of the phase modulation, a weak amplitude fluctuation was directly introduced by a Sumitomo Osaka Cement Co. T-MZI 3-10 Mach-Zehnder type intensity modulator. In this way it was much easier to study the initial build up stage of the phenomenon. The pre-modulated train was injected to the fiber loop through an 80%/20% coupler. The fiber loop contained 25km standard single mode telecommunication fiber, a Uniphase CQF882/0MQW SOA as an in-line amplifier and a tunable 0.7nm bandpass filter. The re-circulating fiber loop arrangement was controlled by a Quantum Components M9310 four channel pulse generator.

In the present experiment a slow photodiode monitored the evolution of the average power in the loop and a Burleigh® FSP-9000 scanning Fabry-Perot interferometer was used to monitor the signal spectra. The signal of the scanning Fabry-Perot device was recorded in a Tektronix 620B 500MHz digital oscilloscope.

The modulation instability gain was investigated for different initial modulation amplitude, stationary power and in-line filter detuning both in the anomalous and in the normal GVD regions. In both regions the instability gain was found significant only if the filter is detuned to the red side of the carrier wavelength. Fig.II.2.2. shows the typical evolution of the modulation sidelobes over the distance if the laser is tuned to the weak normal GVD region and to the weak anomalous GVD region. In both regions the modulation instability shows similar characteristics. The enhanced modulation sidelobes could initiate larger MI gain for the neighbouring modulation sidelobes and it leads finally to a spectral distribution of equally spaced spectral components with an envelope similar to the transmission function of the in-line bandpass filter. It is worth to mention that though the average power in the loop was almost constant the amplitude of the sidelobes was still decreasing at large distances because of the accumulation of broad band background radiation.

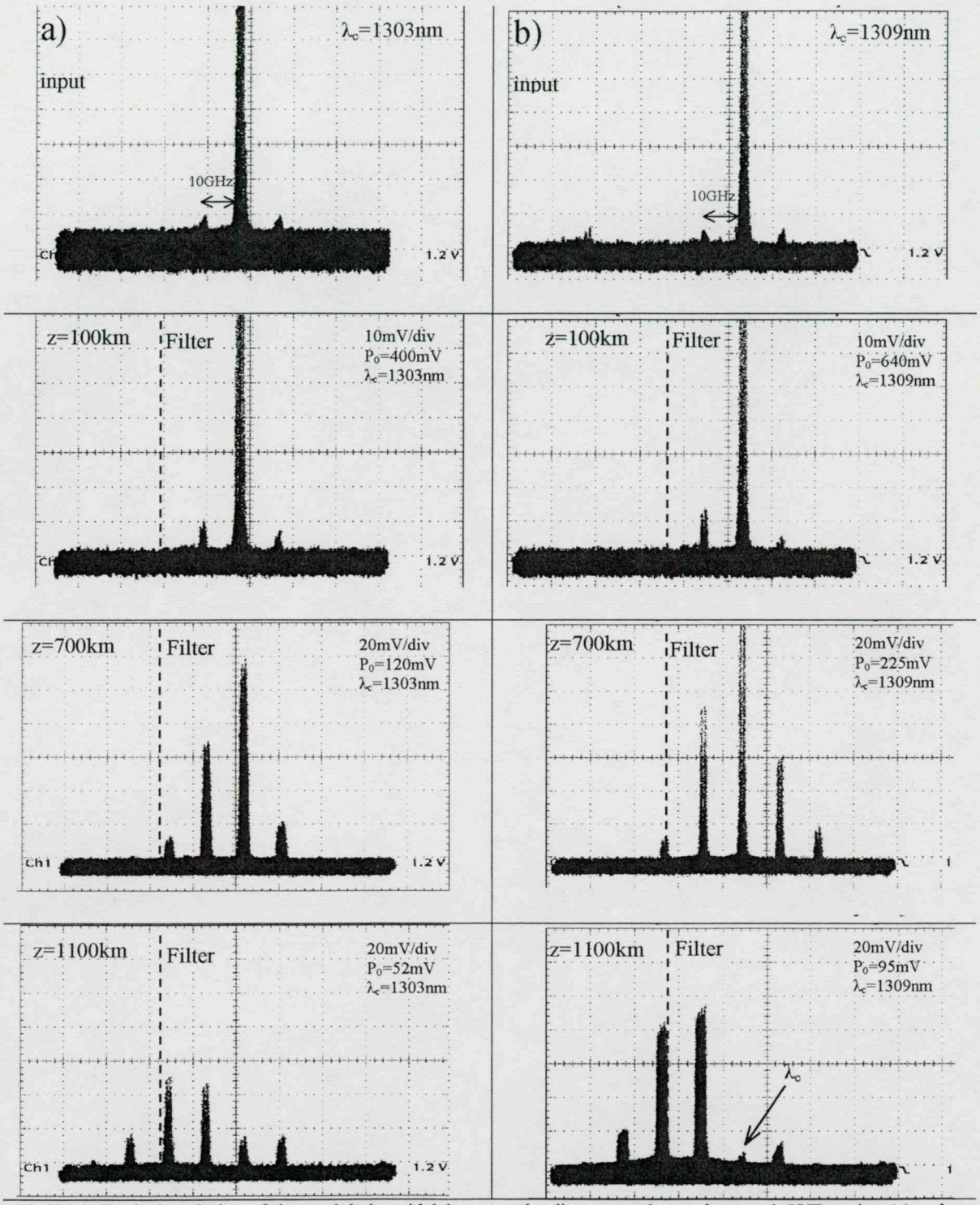

Fig.II.2.2: Typical evolution of the modulation sidelobes over the distance at the weak normal GVD region (a) and at the weak anomalous GVD region (b). The in-line filter is tuned to the red side of the carrier wavelength as it is marked with dashed lines. The depth and the frequency of the initial amplitude modulation are 20% and 10GHz, respectively. The filter bandwidth is 0.7nm and the detuning is ~25GHz (~0.15nm). The vertical resolution of the oscilloscope, the amplitude of the strongest spectral component compared to the background level and the carrier wavelength are marked on the upper right corner of the screenshots. The zero GVD wavelength is 1306.4nm. The driving current of the in-line SOA is 140mA in both cases.

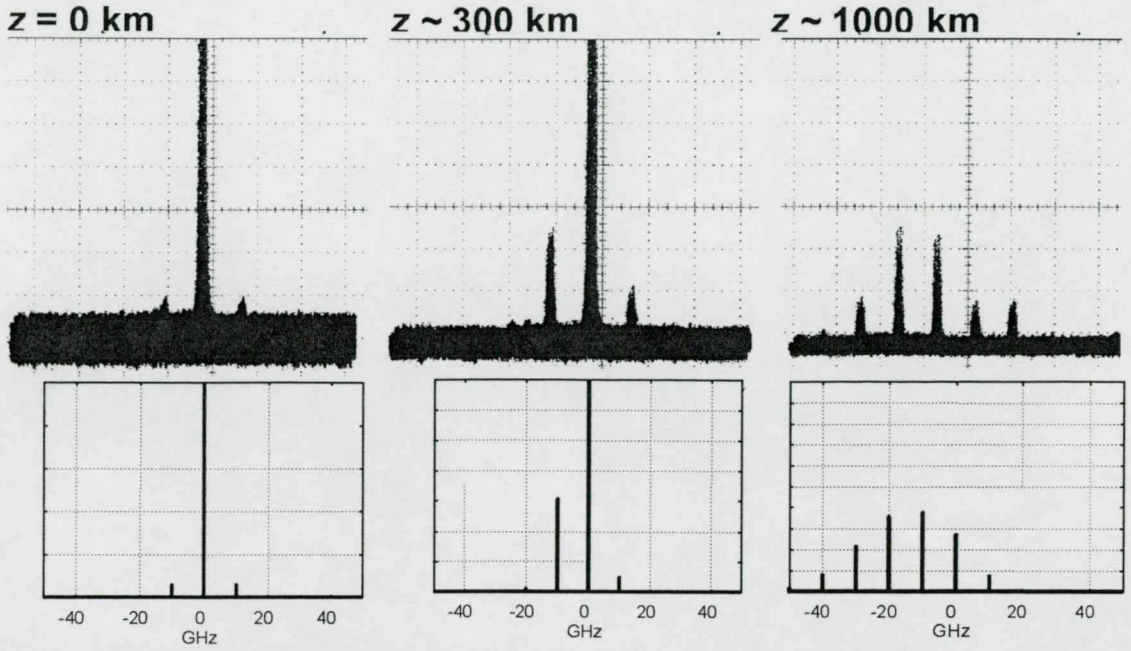

Fig. II.2.3: Comparison between the experimentally observed (top) and the calculated (bottom) evolution of spectral power $|c_m^2|$. The carrier wavelength is λ_c=1303nm (normal GVD) The filter is tuned 20GHz to the red side of the carrier wavelength. The initial amplitude modulation is 30%. Though the amplitude scaling is arbitrary the relative amplitude of the side bands agrees well.

At zero filter detuning no enhancement of the modulation sidelobes was observed within the accuracy of the measurements. If the filter was tuned to the blue side of the carrier frequency, at high stationary power and strong (50%) initial amplitude modulation some weak enhancement of the blue sidelobes was observed in the anomalous GVD region. However the effect was found to be too weak to impose additional limitation to a real world transmission line.

The experimental findings were compared to the numerical solution of eq.II.1.9. In Fig.II.2.3 the result of such calculation is compared to an experimentally observed evolution of the spectrum on the propagation distance. Though the scaling is arbitrary, the relations between the relative amplitude of the side bands agree quite well.

The most important finding of this section:

The existence of a novel type of modulation instability phenomena originating from the interplay of the SOA nonlinearity and the in-line bandpass filter was demonstrated in a re-circulating fiber loop setup. The experimental findings are in a good agreement with the theoretical predictions.

III. The feasibility of using saturable absorbers to improve the performance of Semiconductor Optical Amplifier based ASK RZ transmission

III.1 Basic concept

In ASK transmission mode it is necessary to keep the noise between the pulses low. As it was mentioned in the previous chapters, in SOA based systems the gain recovery time is comparable to the transmitted bit rate and the amplifier is saturated by the individual pulses rather than by the average signal power. Since the noise in space is amplified by the unsaturated gain and the signal gain is lower than that, the growth up of in-space noise is inevitable. The basic idea behind the saturable absorber (SA) based noise suppression is that the SA is introducing high losses for the low power noise and has got a lower loss for the signal. To demonstrate the principle the energy dependent transmission function of an amplifier and a transmission function of an amplifier-saturable absorber chain are going to be compared.

The pulse duration is presumed to be much shorter than the recovery time of the device and both the absorber and the amplifier is going to be characterised by eq.I.2.6. By dividing both sides with the input energy we get the expression for the energy gain:

$$G = \frac{\varepsilon_{sat}}{E_{in}} \ln\left\{1 + \left[\exp\left(\frac{E_{in}}{\varepsilon_{sat}}\right) - 1\right] Go\right\}. \qquad \text{(III.1.1)}$$

Where all notations are as in eq.I.2.6 and Go is the small signal gain. For saturable absorbers the quantity G and Go is generally singed as T, To and called the transmission and the small signal transmission, accordingly. The gain of an amplifier-saturable absorber chain can be calculated as:

$$G_{SOA-SA} = T(G(E_{in})E_{in})\,\mathrm{G(E_{in})}. \qquad \text{(III.1.2)}$$

By writing out eq.III.1.2 we get for the transmission function of the combined device:

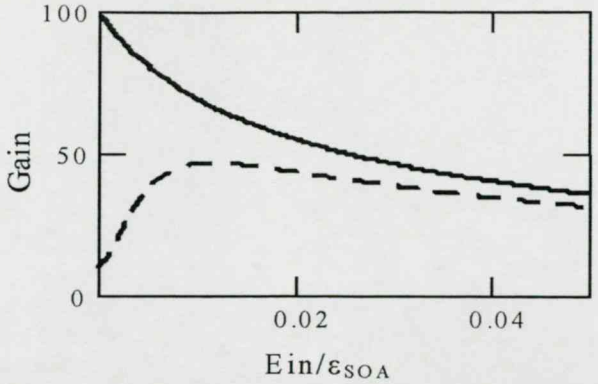

Fig. III.1.1: The solid line is the energy dependent gain of the single amplifier and the dashed line is the gain function of an amplifier –saturable absorber chain. G_0=100,T_0=0.1,$\varepsilon_{SA}/\varepsilon_{SOA}$=.2.

$$G_{SOA-SA} = \ln\left[1 + To\left(1 + Go\exp\left(\frac{E_{in}}{\varepsilon_{soa}}\right) - Go\right)^{\frac{\varepsilon_{soa}}{\varepsilon_{sa}}} - To\right]\frac{\varepsilon_{sa}}{E_{in}}. \qquad \text{(III.1.3)}$$

Where ε_{soa} is the saturation energy of the amplifier and ε_{sa} is that of the absorber. This expression is only valid if the recovery time of the amplifier and the absorber is much shorter than the interval between the subsequent pulses ($\tau_{recov} << T_{bit}$) so that the device gain can fully recover before the next pulse.

In Fig.III.1.1 the gain of a single amplifier and an amplifier saturable-absorber chain is compared. The main difference is that in the case of the standalone amplifier initial low energy noise spikes have got higher gain than that of the signal pulse and after several re-amplification it grows up a to be comparable with the signal. On the other hand the amplifier-saturable absorber chain (A-SA) has a low gain for the low energy disturbances and for the quasi-CW ASE noise as well.

III.2 Bit rate dependent transmission function

For the more realistic treatment of the problem it is necessary to consider the case where the bit period of the signal is comparable to the recovery time of the amplifier and the small signal gain does not recover fully between the subsequent pulses. In this section the transmission function of the combined semiconductor optical amplifier-saturable absorber (SOA-SA) module will be introduced for regular pulse trains with different pulse repetition rates. For that purpose the rate equation model is used, which was applied by Agrawal and Olson to semiconductor optical amplifiers. Let us presume that the pulse

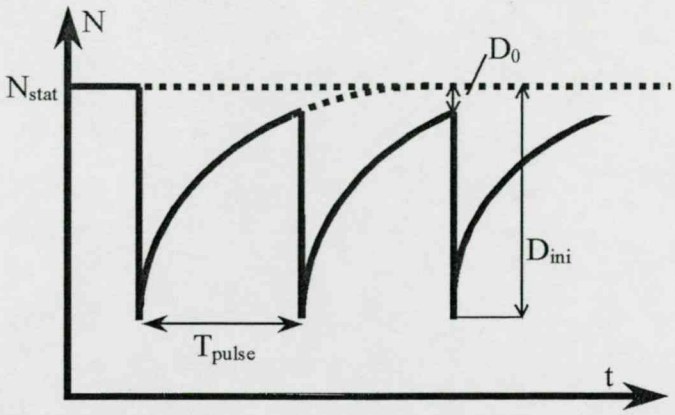

Fig.III.2.1: Schematics diagram for the temporal evolution of the carrier density in a medium interacting with a regular pulse train.

duration is much shorter than the recovery time of the amplifier and the carrier density is quasi instantaneously depleted by the pulse. The pulse train consists of E_{in} energy pulses following each other with T_{pulse} time period The value of the carrier density before the medium interacts with the pulse train is N_{stat}. A quantity Δ will be called the population inversion and defines as the difference of the actual carrier density from the carrier density necessary for transparency: $\Delta = N - N_0$. The static population inversion is defined as $\Delta_{stat}=N_{stat}-N_0$. The population inversion can be also written as:

$$\Delta=D+\Delta_{stat.} \qquad \text{(III.2.1)}$$

Where D is the deviation of the population inversion from its static value. The gain is defined as:

$$G = \exp(\Delta\sigma l). \qquad \text{(III.2.2)}$$

Where σ is the cross section and l is the length of the device. Using eq.III.2.1 and eq.III.2.2 we get for the small signal gain:

$$G_0 = G_{stat} \exp(D_0\sigma l). \qquad \text{(III.2.3)}$$

Where G_{stat} is the static small signal gain, defined as $G_{stat}=exp(\Delta_{stat}\sigma l)$. D_0 is the value of D right before the pulse interacts with the media (see illustration on Fig III.2.1).

From eq.III.2.3 D can be expressed as:

$$D = \frac{1}{\sigma l}\ln\left(\frac{G}{G_{stat}}\right). \qquad \text{(III.2.4)}$$

If the duration of the optical pulse is much shorter than the recovery time and the coefficient for the internal loss is negligible compared to the gain coefficient ($\alpha_{int} << g$) the gain can be expressed as:

$$G = \ln\left[1 + \left(\exp(\frac{E_{in}}{\varepsilon_{sat}}) - 1\right)G_0\right]. \qquad \text{(III.2.5)}$$

After the n-th pulse interacted with the medium, using eq.III.2.4 and eq.III.2.5 we get for D:

$$Dini_n = \frac{1}{\sigma l}\ln\left[\ln\left[1 + \left(\exp\left(\frac{E_{in}}{\varepsilon_{sat}}\right) - 1\right)G0_{n-1}\right]\frac{G_{stat}}{\varepsilon_{sat}}\right]. \qquad \text{(III.2.6)}$$

Presume that between the pulses the influence of the amplified spontaneous emission is negligible and the recovery of the carrier concentration is governed by the following equation:

$$\frac{d}{dt}N = \frac{I}{qV} - \frac{N}{\tau_c}. \qquad \text{(III.2.7)}$$

Where the notations are the same as in eq.I.2.3. By solving the differential equation and keeping in mind that $N_{stat}=I\tau_c/(qV)$, we get that:

$$D(t) = Dini\exp\left(-\frac{t}{\tau_c}\right). \qquad \text{(III.2.8)}$$

Where t is the elapsed time after the pulse interacted with the medium.

By substituting eq.III.2.8 into eq.III.2.6 we get for the value of D before the medium interacts with the next pulse (Do) that:

$$Do_n = \frac{1}{\sigma l}\ln\left[\ln\left[1 + \left(\exp\left(\frac{E_{in}}{\varepsilon_{sat}}\right) - 1\right)Go_{n-1}\right]\frac{Gstat}{\varepsilon_{sat}}\right]\exp\left(-\frac{T_{pulse}}{\tau_c}\right). \qquad \text{(III.2.9)}$$

Where T_{pulse} is the time interval between the pulses. From there using eq.III.2.3 we get an iterative formula for the small signal gain of the n+1-th pulse:

$$Go_{n+1} = Gstat\exp\left[\ln\left[\ln\left[1 + \left(\exp\left(\frac{E_{in}}{\varepsilon_{sat}}\right) - 1\right)Go_n\right]\frac{Gstat\,\varepsilon_{sat}}{E_{in}}\right]\exp\left(-\frac{T_{pulse}}{\tau_c}\right)\right]. \qquad \text{(III.2.10)}$$

It is easy to see that Go is converging to a certain value in a regular pulse train this value is called the small signal gain for the pulse train and defines as: $Go_{train} = \lim_{n\to\infty} Go_n$. As

a rule of a thumb the number of iteration necessary for a certain accuracy is proportional to T_{pulse}/τ_c. In the practical cases, when T_{pulse} is comparable or larger than τ_c, only few iterations are needed to get the value of Go_{train} within 1% accuracy.

If the small signal gain for the train (Go_{train}) is substituted into eq.III.2.5 the energy gain of the pulses participating in a regular train can be calculated.

To get the transmission function of the combined module the calculations have to be repeated for the saturable absorber. To describe the behaviour of a combined amplifier-saturable absorber module it is advantageous to introduce the following parameters:

- The ratio of the saturation energy of the absorber to that of the amplifier $\varepsilon=\varepsilon_{SA}/\varepsilon_{SOA}$,
- The ratio of the input energy to the saturation energy of the amplifier $E=E_{in}/\varepsilon_{SOA}$,
- The ratio of the pulse period to the recovery time of the amplifier $t_p=T_{pulse}/\tau_{amp}$,
- The ratio of the absorber's recovery time to that of the amplifier $\tau=\tau_{SA}/\tau_{amp}$
- The static small signal gain of the amplifier G_{stat} and the static small signal transmission of the absorber T_{stat}.

The parameters ε, τ, G_{stat}, T_{stat} are purely determined by the combined device and E, t_p rather belong to the pulse train. For that reason wherever it does not cause confusion the combined transmission function of the chain is going to be abbreviated as $TG(E,t_p)$.

A Mathcad routine for calculating the energy gain of a single amplifier (or saturable absorber) and a routine to calculate the energy gain of a combined device are given in Appendix I.

The most important result in this section:

- In this section a quasy analitic formula was introduced to describe the energy gain of periodic pulse trains interacting with a SOA or with a SA.

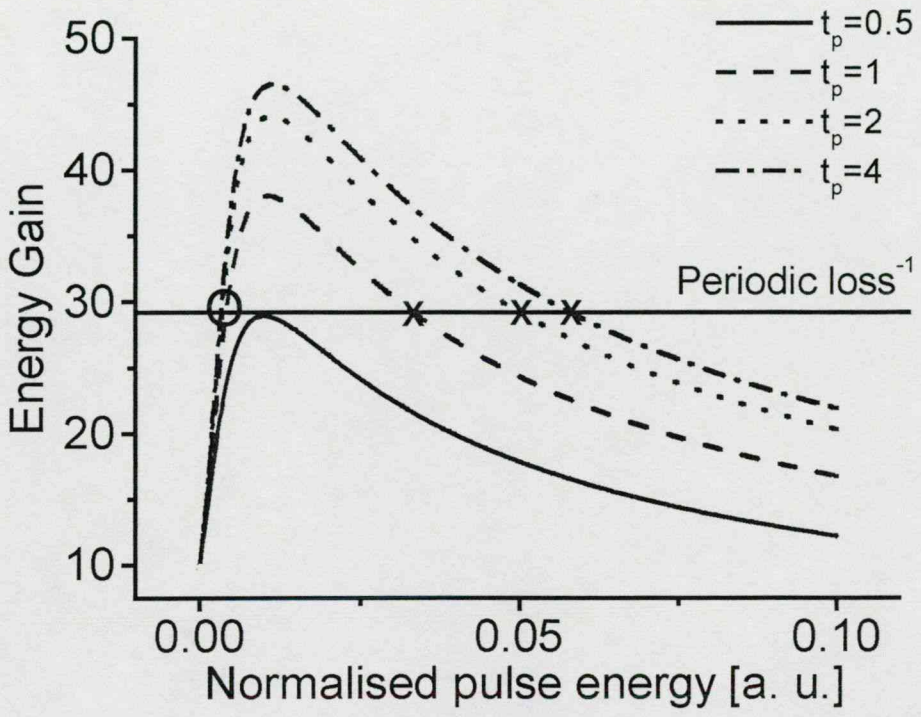

Fig. III.3.1: The dependence of the energy gain on the input energy in a combined amplifier-saturable absorber chain for different pulse period regular trains. The inverse of the periodic loss is marked with a horizontal line. The pulse suppression thresholds are marked with O and the stationary energies with X. The device parameters are: G_{stat}=100; T_{stat}=0.1; ε=0.2; τ=0.1;t_p=0.5, 1, 2, 4 for the solid, dash, dot, dash-dot line, respectively.

III.3 Amplitude patterning

In this section a closer look is going to be taken on the system behaviour if several re-amplification stages are cascaded as it is usually necessary in real world transmission lines. One section of such a transmission line consists of a re-amplification stage and the optical fiber. For the calculations identical re-amplification stages with uniform losses between them are presumed. This presumption also complies very well with the nature of our experiments carried out in the fiber loop setup. The basic characteristics of such a cascade can be understood with the help of Fig.III.3.1.

Fig.III.3.1 shows the input energy dependent transmission of a combined amplifier-saturable absorber stage for different pulse period regular trains. The inverse of the periodically introduced fiber loss is also marked. As it is shown at low input energies

the fiber losses are larger than the device gain and after several cascaded network sections the signal decays. If the input energy of the signal exceeds a certain threshold, what we call the pulse suppression threshold, the gain of the device will be larger than the losses in the fiber. The energy of the signal pulse will be increased from cascade to cascade until the stability point is reached. That is what we call the stationary energy of the pulse train. The stationary energy satisfies the following equation:

$$L\,TG(E_{stat}, t_p) = 1. \qquad \text{(III.3.1)}$$

Where L is the fiber loop loss and $TG(E,t_p)$ is the transmission function of the combined device. If the recovery time of the device is comparable with the pulse period of the regular train, the recovery of the population inversion is incomplete. That leads to different stationary energies for a different pulse period train. If real data is transmitted the time interval between the pulses is non-uniform. Consequently, the energy of the pulses in the data train will not be uniform as well. That phenomenon is called amplitude patterning.

The amplitude patterning can lead to a complete decay of certain signal components, limits the detection threshold and results in other unwanted effects, like temporal walk off (see next chapter). Here the bit rate dependent transmission function is extended to determine the stationary energy levels for an arbitrary pulse train and the most important limitations imposed by amplitude patterning is discussed with the help of numerical simulations.

As a reminder, a regular pulse train contains constant E_{in} energy pulses following each other by T_{pulse} time intervals. Since the pulse distance and the pulse energy is uniform the small signal gain of the device is going to reach a stationary value after the n-t pulse. This stationary value was determined by the iterative formula of eq.III.2.10 and then the energy of the amplified signal pulse was calculated by using eq.III.2.5. Let us now presume a pulse train consisting of m pulses, each with E_i energy following each other by constant T_{bit} time intervals. Since $E_i=0$ is allowed any bit stream belonging to $B=1/T_{bit}$ transmission rate can be described in this way. Let us consider first the amplifier section of the combined device. The amplification of the i-th pulse is determined by the pulse energy and the population inversion (i.e. the small signal gain) of the device. The small signal gain for each pulse (Go_{i-1}) is determined by the influence of the previous

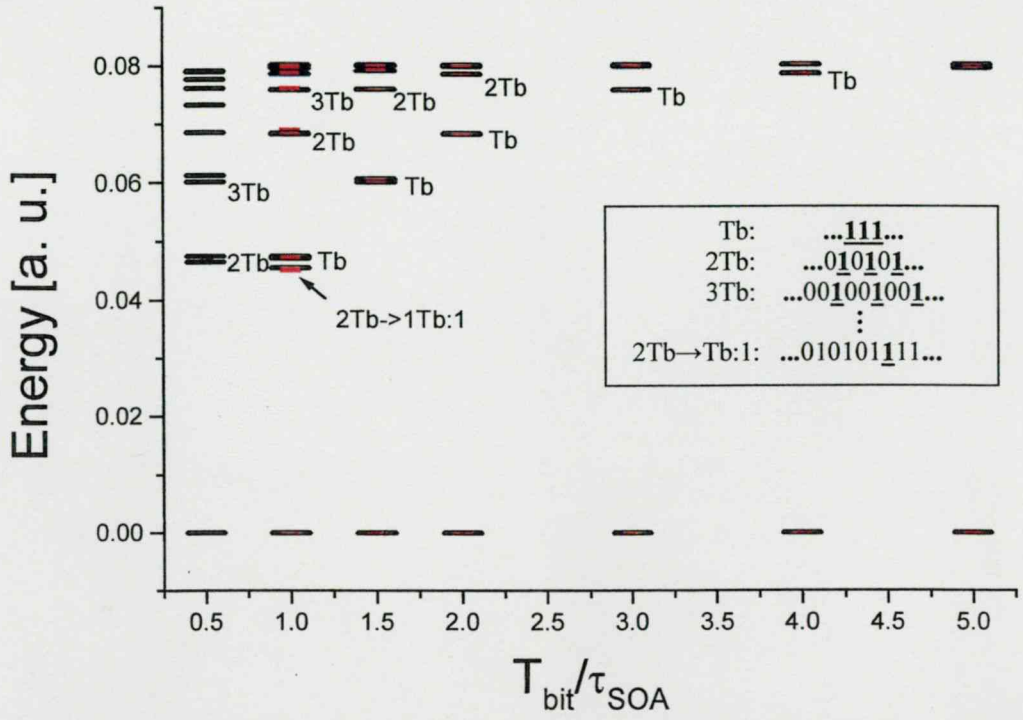

Fig. III.3.2 The stationary levels for a bit stream containing a composition of regular trains with the bit distance of $8T_{bit}$,$7T_{bit}$,$6T_{bit}$…$1T_{bit}$ (black lines) and for a 2^7-1 PRBS train (red lines) at different ratios of the bit slot to the amplifier recovery time(T_{bit}/τ_{SOA}). The device parameters are: ε=0.2, T_{stat}=0.3, G_{stat}=100, E=0.05 and τ=0.1. The losses between the re-amplification stages were set to L=0.03. The level "nTb" corresponds to the stationary energy of a regular train with the bit distance of $n*T_{bit}$ (i.e. (n-1)zero bits followed by a bit one.) 2Tb->Tb:1 is the first bit of the regular train with Tb bit distance after a regular train with the bit distance of 2Tb (see inset).

pulse on the amplifier. If the first pulse of the train is presumed to see the static small signal gain of the system ($Go_0=G_{stat}$), the output energy of the i-th pulse of the interacting train can be calculated with the following set of equations:

$$Eout_i = \varepsilon_{sat} \ln\left[1 + \left(\exp\left(\frac{E_i}{\varepsilon_{sat}}\right) - 1\right) Go_{i-1}\right],$$

(III.3.2a-b)

$$G_i = Gstat \exp\left[\ln\left[\ln\left[1 + \left(\exp\left(\frac{E_i}{\varepsilon_{sat}}\right) - 1\right) Go_{i-1}\right] \frac{Go_{stat}\,\varepsilon_{sat}}{E_i}\right] \exp\left(-\frac{T_{bit}}{\tau_c}\right)\right].$$

The same procedure has to be repeated for the absorber section. The system loss is included by multiplying the output energy by a factor L before the simulation of the next re-amplification stage. The corresponding Mathcad routine is incorporated in the Appendix. It was found that after few re-amplification stages the system reaches a

stationary state. The pulse energy at the stationary state is not depending on the input pulse energy and in a random data train will take up quantised values. To study this phenomenon simulations were carried out using a bit stream containing a composition of regular trains with the pulse distance of $8T_{bit}$, $7T_{bit}$, $6T_{bit}...T_{bit}$ and with a 2^7-1 bit long pseudo random bit sequence (2^7-1 PRBS). The input pulse train was presumed to be imperfectly modulated and the energy of the "zero pulses" was presumed to be hundred times less than the pulses in ones (*E1/E0=100*). Fig.III.3.2 shows the stationary levels for the bit streams. For the parameters used in Fig.III.3.2 the initial weak pulses in zeros are completely suppressed. Since the recovery time of the SA section was chosen to be much shorter than that of the amplifier section the number of levels is mainly depending on the ratio of the bit slot to the recovery time of the amplifier section. If the bit period is five times larger than the recovery time, the pulse energy of each bit is the same within the numerical limit. As the bit period is reduced the energy levels of the different frequency components of the pulse train are splitting up. In that stage the lowest level corresponds to the highest frequency regular train. At even shorter bit slots (larger transmission rates) the coupling between the pulses are getting stronger and transient levels are appearing. These levels does not belong to a given repetition rate regular train of the signal but rather to the transition from one repetition rate to another one. (see Fig.III.3.2 level 2Tb->1Tb:1). As the bit distance is further reduced some of the signal pulses are lost (like level 1Tb at $Tbit/\tau_{SOA}=0.5$). The numerical simulations show that if the system is not capable to propagate a certain pulse period train, it converts it to a larger pulse period one by dropping out some of the pulses and than the propagation of the modified train is stabilised. This phenomenon was also observed experimentally. The calculations with 2^7-1 PRBS train show a very similar level structure to the results of the calculations carried out with the synthesis of different frequency regular pulse trains.

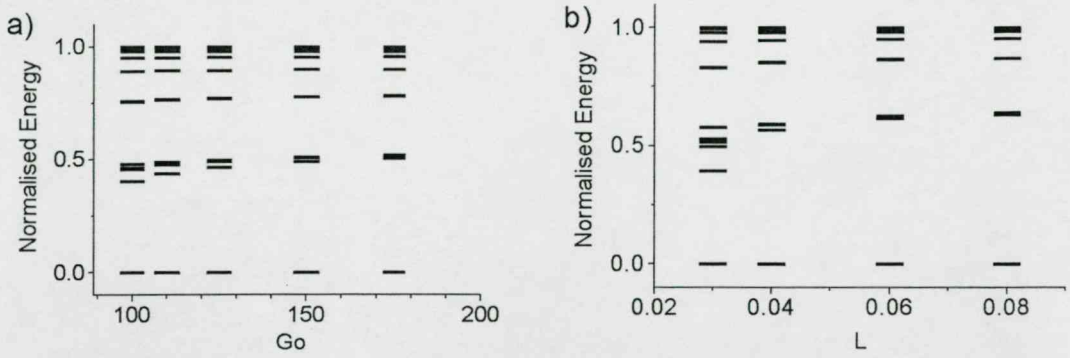

Fig.III.3.3: a) The influence of the small signal gain on the stationary energy levels, b) the influence of the loop loss on the stationary energy levels. The energies are normalised to the low frequency stationary energy, the device parameters are ε=0.2,τ=0.1, T_{stat}=0.3, t_b=0.75 for a), t_b=1, for b), (if not varied than G_{stat}=100 and L=0.03).

Since the recovery time of the device is a hardly variable parameter, it is important to know if the amplitude patterning can be minimised by optimising other system parameters. In the laboratory experiments probably the two easiest to optimise parameters are the periodically introduced loss and the small signal gain of the device. Obviously, if the amplifier is working at a stronger saturation, the difference between the stationary levels can be reduced. The saturation of the amplifier can be influenced by the small signal gain and by the fiber losses as well. Unfortunately stronger saturation results in a deterioration of the noise suppression capabilities of the system. Fig.III.3.3 shows how the fiber loss and the small signal gain influence the stationary levels of a PRBS 2^7-1 train. At very low small signal gain (or at high fiber loss) the patterning is strong and there are several transient levels as well. Here the system operation is limited by the drop out of pulses. By increasing the small signal gain (reducing the fiber loss) the number of observable levels is reducing. In the present model the limitation is imposed in strong saturation by the growth up of the imperfectly suppressed pulses in zeros. In Fig.III.3.4 the energy gain-input energy curve of the system is calculated for several values of the static small signal gain. It is interesting to note how dramatically the pulse suppression threshold is reducing if the small signal gain of the amplifier was increased. In a real world system additionally, the in-space noise growth imposes serious limitation to the system performance.

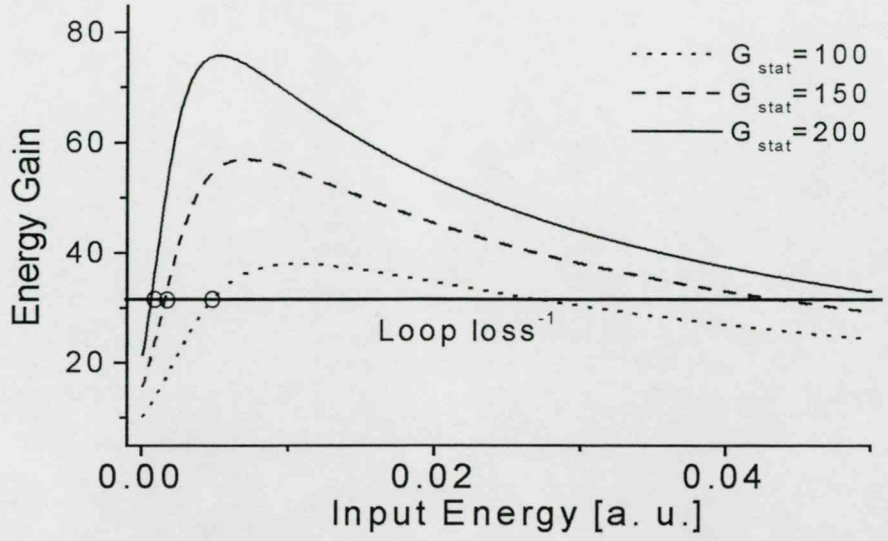

Fig.III.3.4: The energy gain dependence on the input energy of a combined amplifier-saturable absorber chain for different static small signal gains of the amplifier. The noise suppression thresholds are marked with circles. The device parameters are: G_{stat}=100; T_{stat}=0.1; ε=0.2; τ=0.1;t_p=1.

The most important findings of the simulations are:

- In a cascaded SA-SOA based transmission line the pulses are dying out if the initial pulse energy is lower than the pulse suppression threshold.
- If the input energy exceeds the pulse suppression threshold the pulses are reaching a stationary energy during the subsequent re-amplifications and the stationary energy is independent from the input energy.
- By injecting irregular pulse trains to the system discrete pulse levels are appearing. The number of observable levels is much less than the number of the possible bit combinations.
- If the system is unable to propagate a given pulse sequence some pulses are dropped and the propagation of the modified sequence is stabilised.

IV. Experimental investigation of the performance of combined SOA-SA based transmission lines

IV.1 Combining a traditional semiconductor optical amplifier with a saturable absorber

IV.1.1 Experimental set up

For our experiments an integrated SA-SOA module was provided by the Heinrich-Hertz-Institut, Berlin. The device was manufactured from a commercially available Fabry-Perot laser diode chip. In a thin surface layer the non-radiative recombination rate of the carriers was increased by ion implantation through one of the chip facets. Since in that region the carrier concentration remains always under the transparency point the

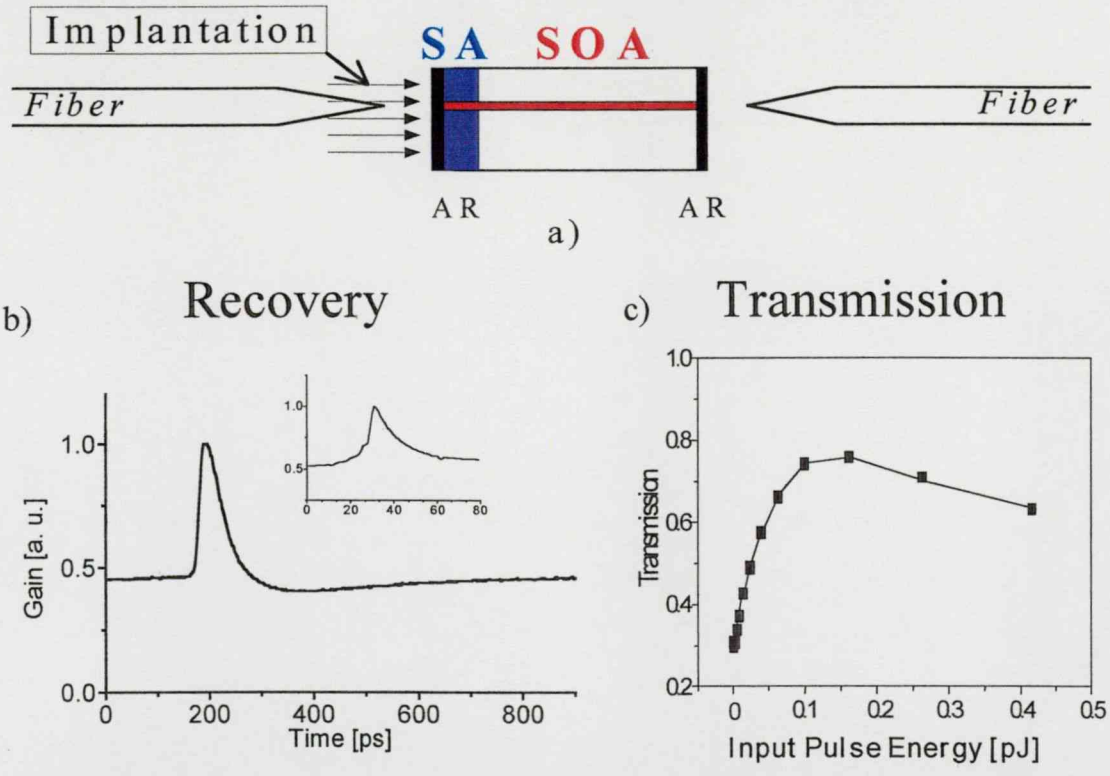

Fig.IV.1.1 a) The schematic structure of the combined SA-SOA module used in the experiments. b) The recovery dynamics of the module. The duration of the pump and the probe pulse were 20ps and 1.5ps respectively. Inset: a pump probe measurement carried out using 1.5ps pulses both as a pump and as a probe for the better resolution of the saturable absorber dynamics. The bleaching and the recovery time of the absorber is ~3dB and the ~30 ps respectively. c) The energy dependent transmission of the module measured with a 10GHz train of 1.5ps pulses. The pulses were injected at the amplifier side of the module, the driving current was 100mA in all cases.

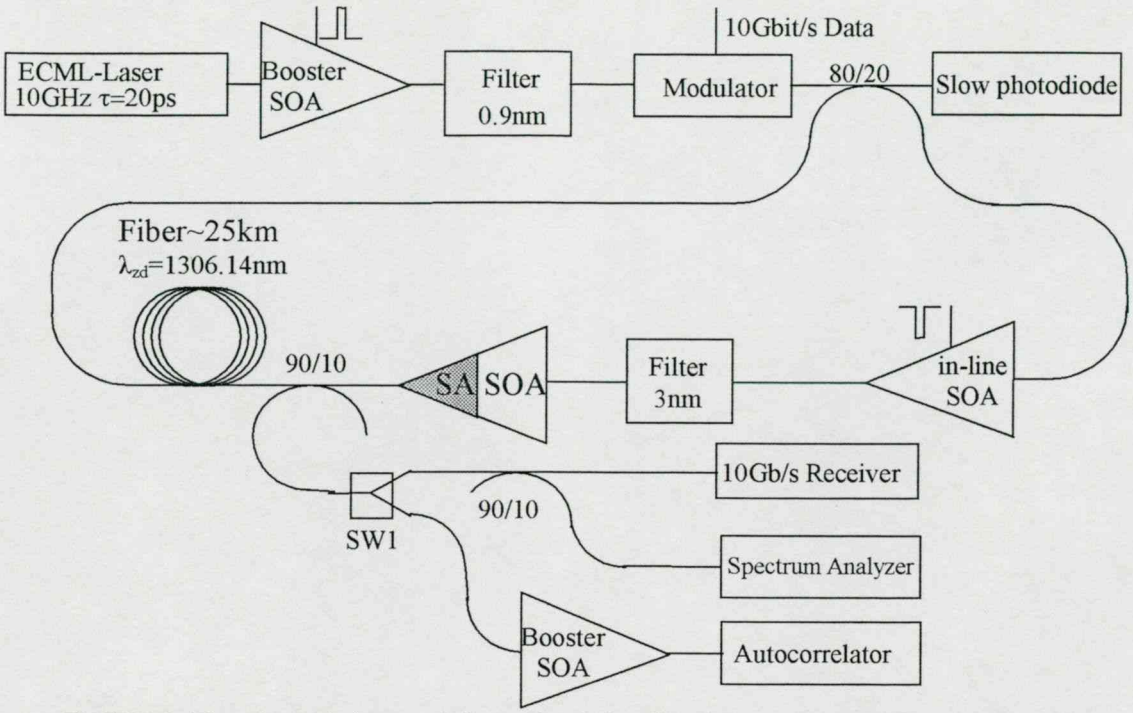

Fig IV.1.2: The schematic layout of the re-circulating fiber loop setup used in the experiments

layer acts as a saturable absorber. Later, the facets were anti-reflection coated to eliminate resonance feedback (Fig. IV.1.1.a). Similar devices have been efficiently used in passive and hybrid mode-locking, all-optical clock recovery and in optical gates [59,60].

Due to the single chip design of the SOA-SA module it was not possible to measure the parameters of both sections separately. Pump-probe measurements were carried out to reveal the temporal characteristics of the combined module. Those experiments will be discussed in detail later in this chapter. The measurements give an estimate value for the maximum transmission bleaching and the recovery time of the absorber section to be ~3dB and ~30ps, respectively. The recovery time of the amplifier section is estimated to be ~270ps (Fig. IV.1.1b). The dependence of the overall transmission of the combined module on the input pulse energy was also measured. For the measurement a 10GHz regular train of 1.5ps pulses were used. Initially, the transmission of the device is increasing with the average power due to the bleaching out of the saturable absorber. At a high average power the transmission of the device is limited by the saturation of the

amplifier section (Fig.IV.1.1c). (Note the good agreement with theory (Fig.III.3.1)). Due to high unsaturated losses (~13dB) of the SA layer the overall fiber-to-fiber gain of the SOA-SA module always remains somewhat lower than unity.

To model experimentally the pulse propagation in a long haul SOA-SA based transmission line a re-circulating fiber loop set up was used. Its schematic layout is shown on Fig.IV.1.2. Generally as a pulse source a Radians Innova TUN-1300ML actively mode locked tunable laser providing 10GHz ~20ps pulses was used. The laser pulses were amplified by a Philips CQF882/0 MQW SOA and the ASE was blocked by a tunable 0.9nm filter. The transmitted bit patterns were generated by an Anritsu Pulse Pattern Generator MP1701A and converted to RZ optical signal format by a Sumitomo Osaka Cement Co. T-MZI 3-10 Mach-Zehnder intensity modulator. It is worth noting here that the pulse trains belonging to lower transmission rates were also produced from a 10GHz regular pulse train. The pulse train is than injected to the fiber loop usually consisting of 25km single mode telecommunication fiber and the re-amplification block. The dispersion characteristic of the fiber was carefully measured and the zero-dispersion point was found to be at λ=1306.14nm and the dispersion slope was: S=0.078 ps km/nm^2.

The eye diagrams were recorded by an HP83480A communication analyser containing an HP83483A (20GHz) and an HP83484A (50GHz) drawer. The optical receiver was a 13GHz HP11982A type Lightwave Converter. Even at lower transmission rates the data acquisition was triggered by a home-made 10GHz clock recovery device based on a high-Q cavity filter. For the recording of the spectra an HP70951B Optical Spectrum Analyser was used. The pulse duration was measured by a APE GmbH Pulse Check® multi-shot background-free autocorrelator.

The re-amplification block consisted of the combined SOA-SA module, an in-line optical bandpass filter and an additional SOA. The best performance was achieved if a 3nm filter were placed between the in-line amplifier and the SOA-SA module decoupling the ASE of the two devices. As an in-line amplifier a 500μm long Philips CQF882/0 MQW SOA was used.

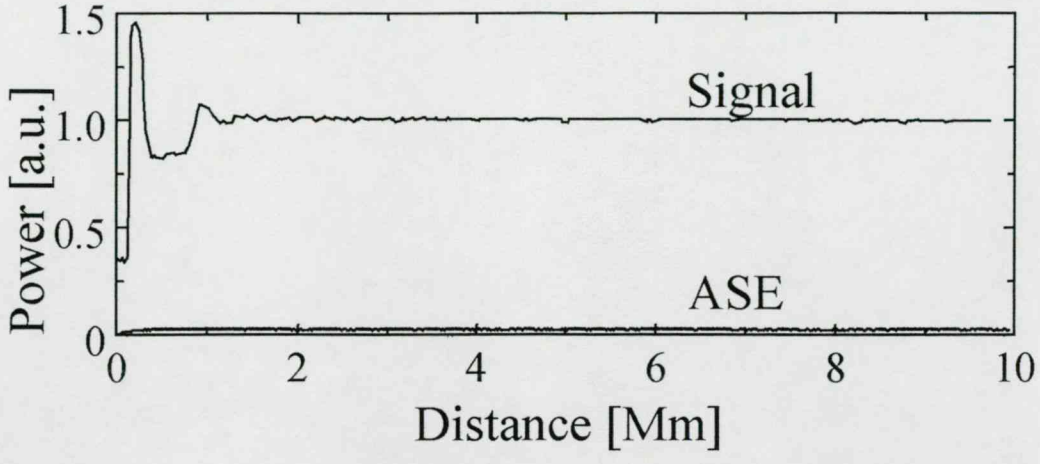

Fig. IV.1.3 The evolution of the average power for a 2.5GHz pulse train and the ASE.

IV.1.2 Investigations with regular pulse trains

The average power evolution in the fiber loop (Fig.IV.1.4) shows a complete suppression of the ASE growth and a stabilisation of the pulse power after the first 1000 km. The stationary power proved to be independent from the input pulse power above a certain threshold value. Below that threshold the average power was reduced due to the loss of some pulses during the initial transient regime. The small signal gain margin of the in-line amplifier between the growth of in-space ASE and the decay of the pulse train was ~1dB for 2.5 Gbit/s transmission. It is much larger than that in the system without SA [45], where the in-line SOA gain needed to be set with an accuracy of ~0.1 dB in order to reach just 1500 km transmission distance.

The distance evolution of the pulse duration was measured for different input pulses. A 75ps pulse train was produced by the modulation of the radiation of the laser operating in CW mode and 17ps pulses were generated by operating the laser in mode-locking mode. When either 75 ps or 17 ps pulses were injected into the system in a 2.5 GHz regular pulse train the system was found to reach the very same stationary pulse duration of ~15ps (Fig.IV.1.4).

It was found that the system reaches a stationary signal spectrum practically independently from the input wavelength of the signal. To avoid distortions of the injected bit sequence, the input wavelength should not differ from the position of the in-line filter by more than the filter bandwidth. The stationary spectra of the pulses were

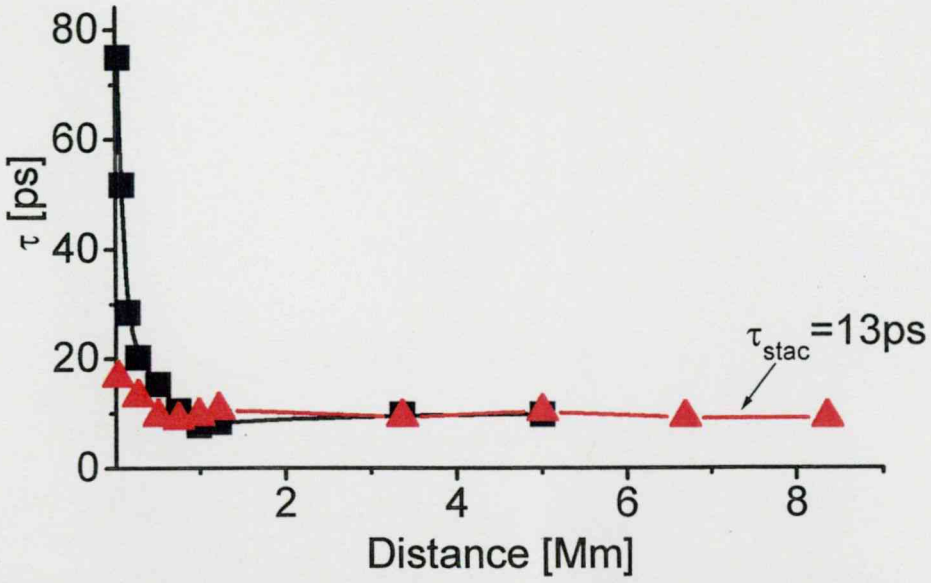

Fig.IV.1.4) The distance evolution of the pulse duration in a 2.5GHz train. The black line with squares is for a pulse train of 75 ps pulses. The red line with triangles is for the initial pulse duration of 17ps.

determined mainly by the interplay of the slow SPM caused red-shift in the amplifier and the spectral narrowing in the in-line filter. The blue shift in the SA section and the self-phase modulation in the fiber were weak. The formation of the stationary spectrum for a 2.5 GHz regular pulse train is shown in Fig IV.1.5a. The system tolerated the tuning of the in-line filter between ~1304.5nm and ~1306.4 nm. The shape of the stationary spectrum was strongly depending on the position of the in-line filter. In Fig.IV.1.5b some typical spectral shapes are shown for both ends of the in-line filter tuning range. It is worth to note that the peak of the stationary spectrum is always situated in the region of weak normal fiber dispersion or at the zero dispersion wavelength. As it is shown in Fig.IV.1.5c the stationary spectra were bit rate dependent. Due to the higher pulse peak power, lower bit rate pulse trains are suffering a stronger red shift. For regular 1.25GHz, 2.5 GHz and 5 GHz pulse trains strong suppression of both the in-space and the in-mark noise was observed (see inset Fig.IV.1.5c.). The effective in-space noise suppression can be explained with the SA effect all by itself. But to explain such a good suppression of the in-mark noise requires further argument. It is also interesting that the best performance was achieved with a 3nm in-line filter and not with a narrow, ~1nm one.

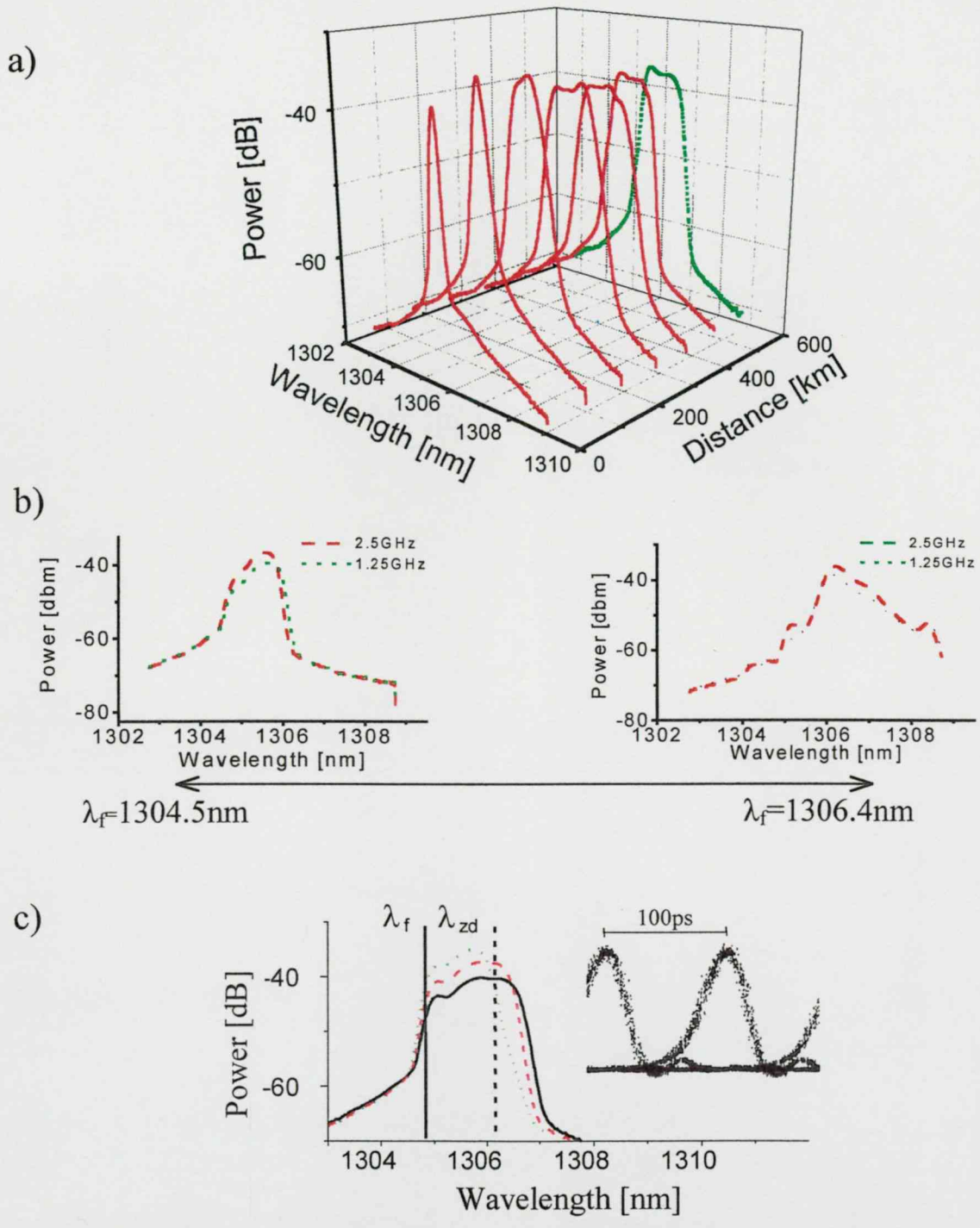

Fig.IV.1.5: a) The evolution of the pulse spectrum in a 2.5GHz regular train over the first 500 km. The stationary spectrum is shown with green dotted line at the end of the distance axes. The position of the in-line filter was 1305.2nm.
b) Typical stationary spectra at both ends of the in-line filter tuning range. c) The stationary spectra of a 1.25GHz, 2.5GHz, 5GHz regular pulse train marked (solid, dashed and doted lines, respectively). Note that the spectrum analyzer is sensitive for the average power of the train and not to the pulse energy. The vertical solid line shows the position of the filter (λ_f=1304.8nm) the dashed line stands for the zero dispersion wavelength, (λ_{zd}=1306.14nm). Inset: the eye diagram of a 2.5 GHz regular pulse train is shown at 10000km, the Q factor is 23.

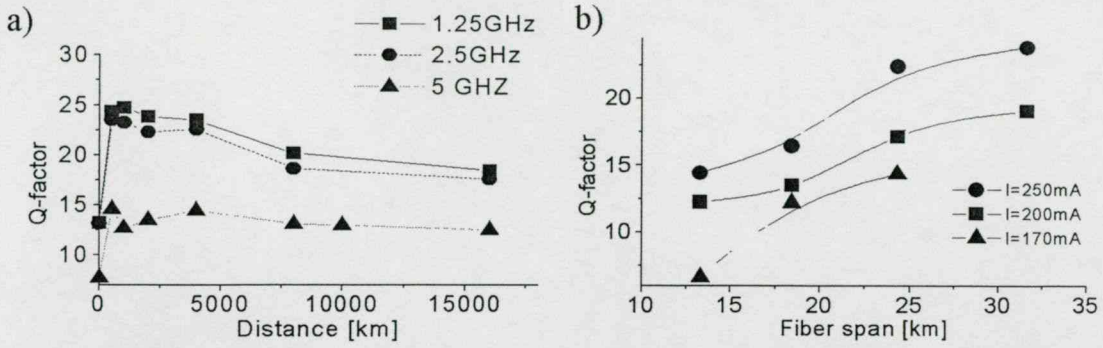

Fig.IV.1.6: a) The Q-factor evolution over distance for regular pulse trains with different pulse repetition frequency. The fiber span is 25km. b) The dependence of the Q-factor after 360 roundtrips on the fiber span for different amplifier currents. During the measurement the input power of the re-amplifier chain was kept constant wit an attenuator at the end of the fiber loop

As it is shown in Fig.IV.1.5c, if a 3nm filter is applied, the stationary spectrum is formed usually with ~ 1-1.5 nm width. The noise of the amplifier is quite broad and after the in-line filter the noise spectrum coincides with the transmission function of the filter. In the case, when a 3nm in-line filter is applied, the peak of the ASE spectrum could be as far as 1nm from the signal spectrum peak. Because of the fiber dispersion, the ASE separates temporally from the signal pulse. Since the low loss time window due to the SA and SOA saturation dynamics is connected to the signal, the ASE is suppressed similarly as in the case of synchronous AM in-line modulation. This effect predicts less efficient noise suppression for higher bit rates since there the lower pulse power leads to a less pronounced red shift. It is also easy to see that if the in-line filter is too narrow and the signal spectra can not separate from the noise spectra significantly, such an in-mark noise suppression mechanism will not work. Indeed, in the experiments strong in-mark noise accumulation was seen if a 1nm bandpass filter was applied instead of the 3nm one, whereas the in-space noise was not effected. The Q-factor of the signal was found largely dependent on the bit rate but only very moderate deterioration with the distance was observed (Fig.IV.1.6a). The dependence of the Q-factor on the length of the fiber span was also measured after a given number of re-amplification while the amplifier parameters and the signal power at the end of the fiber spool were kept constant by an additional variable optical attenuator. As the fiber length between the re-amplification blocks was increased, the Q-factor has improved because of the larger temporal

separation of the ASE and the signal due to the introduced larger fiber dispersion (Fig.IV.1.6b).

IV.1.2 The transmission of random bit sequences.

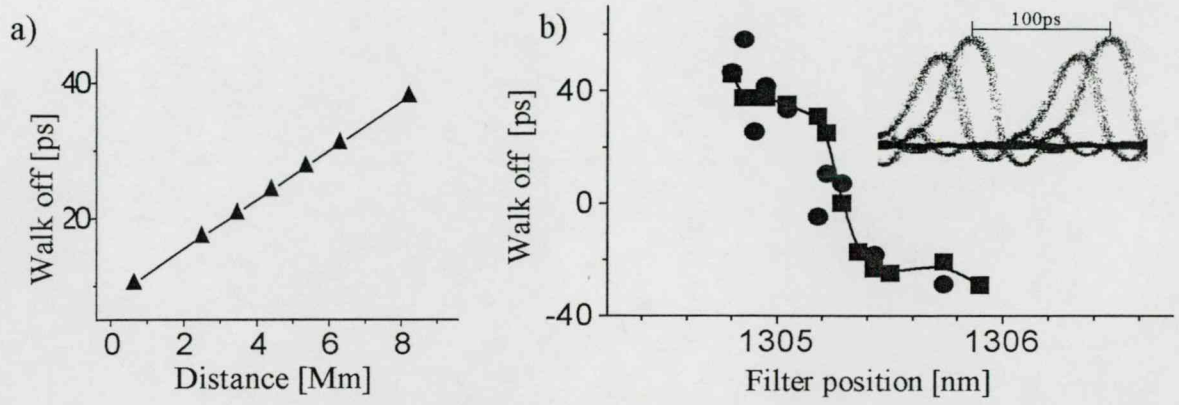

Fig.IV.1.7: The temporal walk off in a 2.5Gb/s 2^7-1 PRBS pulse train : a) Distance dependence b)The dependence on the in-line filter position at 10000km. The measured and the calculated values are marked with squares and circles, respectively. Inset: an eye diagram at 10000km (negative walk off).

If a PRBS signal was transmitted quantised amplitude levels were observed in the eye diagram. The amplitude variation is due to the bit rate comparable gain recovery time of the SOA. The experimental findings quantitatively confirm the results of the numerical simulations discussed in the previous chapter. There were two observable levels for 2.5 Gbit/s operation and three levels at 5 Gbit/s. Additionally, a temporal walk-off between the different energy pulses was observed in the experiments. The walk off is linearly proportional to the distance (Fig.IV.1.7a) in the stationary regime and usually stronger at high bit rates. The dependence of the walk off on the filter position was measured for a 2.5 Gbit/s PRBS pulse train while the average power was kept constant by an in-line attenuator at the end of the fiber span. The current of the in-line amplifier and the SA-SOA module were 114 mA and 100 mA, respectively. The walk off is defined as positive if the stronger pulse is the leading one (Fig.IV.1 7b).

The walk off originates from two effects: a) The interplay of the fiber dispersion and the bit pattern dependent stationary signal spectrum. b) The bit pattern dependent pulse energy also results in temporal walk off due to the saturation-induced pulse reshaping in the SA section and in the amplifiers. To confirm that the two effects mentioned above are

responsible for the walk off, it was calculated at several in-line filter positions from other measured pulse parameters by the following formula:

$$\tau_{woff} = \frac{S}{2} l \left(\frac{\int_{-\infty}^{\infty} A_{01}(\lambda)(\lambda - \lambda_{zd})^2 d\lambda}{\int_{-\infty}^{\infty} A_{01}(\lambda) d\lambda} - \frac{\int_{-\infty}^{\infty} A_{11}(\lambda)(\lambda - \lambda_{zd})^2 d\lambda}{\int_{-\infty}^{\infty} A_{11}(\lambda) d\lambda} \right) + CN(P_{01} - P_{11}). \qquad \text{(IV.1.1)}$$

Where S=0.078 ps·km/nm^2, l =10 000km, λ_{zd}=1306.14nm, $A_{01}(\lambda)$, $A_{11}(\lambda)$, are the dispersion slope, the propagation length, the zero dispersion wavelength, and the shape of the stationary spectra at a given position of the in-line filter having a 1.25GHz ("01") and a 2.5GHz ("11") pulse sequence. The first part of the formula describes the power delay between the two different pulse sequences due to fiber dispersion. The calculated dispersion assisted walk off is larger than the measured one and it can not explain the negative walk off obtained, if the filter position was close to the zero dispersion wavelength. Saturation induced effects are usually resulting in a positive walk off, the only exception occurs if the saturation effects are dominant in the SA and the pulse peak power remains under a threshold, which is in our case ~10 times the saturation power of SA [61]. This effect was linearly approximated by the second part of the formula, where C is a fit parameter and N=400 the number of roundtrips. The power was calculated from the signal amplitude in the eye diagram and the pulse duration measured by an autocorrelator. By adding this almost constant term, a good agreement was found with

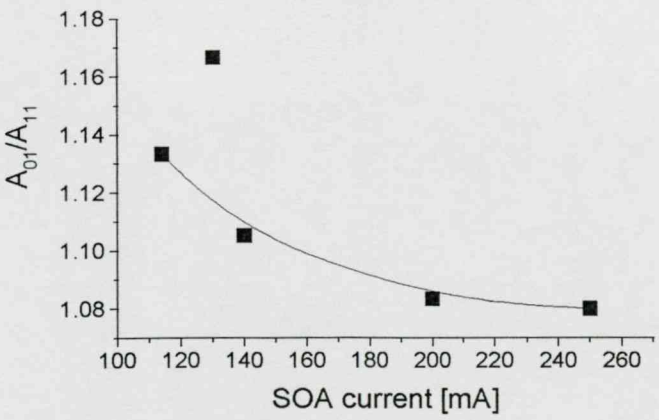

Fig.IV.1.8: The ratio of the pulse energies in a 1.25GHz to that of in a 2.5GHz train.

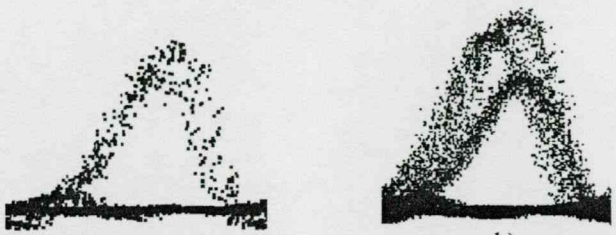

a) b)

Fig.IV.1.9: a) Eye diagram of a 2.5 Gb/s 2^7-1 PRBS pulse train at 60000km. b) Eye diagram of a 5 Gb/s 2^7-1 PRBS pulse train at 30000km

the directly measured walk off (Fig.IV.1 7b). It is worth mentioning that to ensure that the amplitude of the eye diagram is purely proportional to the pulse energy the bandwidth of the receiver was limited by a 7GHz lowpass electrical filter.

IV.1.3. System optimization, transmission results

It was found to be advantageous to operate the amplifiers at high current. As it is shown in Fig.IV.1.8 by changing the amplifier current from 110 mA to 250 mA and increasing the loop loss at the end of the fiber span to maintain the same power, the patterning effect was significantly reduced. The main reason for the performance improvement was the reduction of the amplifier recovery time (see eq.I.2.8). Further increase of the amplifier current resulted in the appearance of in-mark noise. The fact that on high currents the introduced attenuation was about 8dB (equal to the losses in another ~24 km of standard telecommunication fiber) shows the possibility of essentially larger amplifier spacing. Though it worth noting that since the temporal walk-off is the result of two opposite sign terms and only one of them is depending on fiber dispersion, the control of temporal walk-off may become increasingly difficult at longer fiber spans.

Since patterning was not that pronounced at 2.5 Gbit/s, satisfactory operation was found in a wide current range there. By tuning the filter to the zero walk off position error free transmission of 2^7-1 PRBS signal were obtained up to 60000 km (2400 re-amplification stages) at 2.5 Gbit/s (Fig.IV.1.9a). The in-line amplifier current and the current of the SOA-SA device were 170 mA and 100 mA, respectively. 5 Gbit/s operation was found to be possible only at higher currents. Fig.IV.1.9b shows the eye

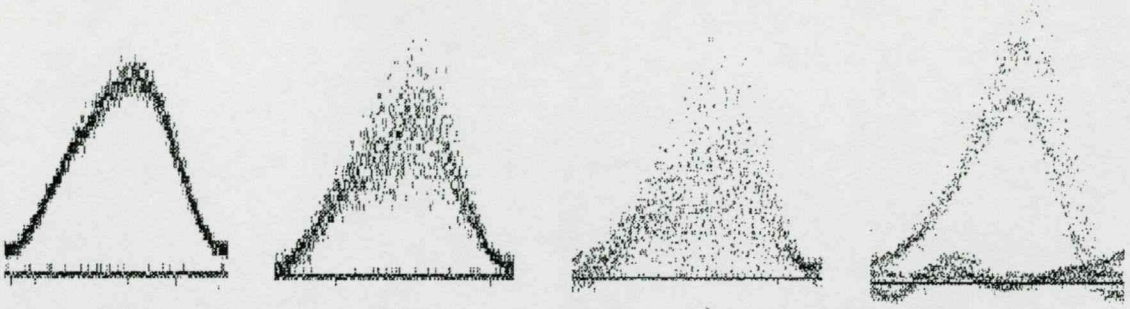

Fig.IV.1.10: The distance evolution of a 10GHz 10^{31}-1 PRBS train. The eye-diagrams are recorded at: a) 25km, b) 100km c)200km d)1500km

diagram of a 5 Gbit/s 2^7-1 PRBS signal after 30000 km (1200 cascaded amplifiers) while the in-line amplifier current was kept constant at 200 mA. This time walk off could play a major role in the deterioration of the signal at large distances.

With traditional semiconductor optical amplifiers no satisfactory system performance was obtained at 10Gb/s. If sufficient gain was provided for the 10GHz component of the signal, the available SA was not able to suppress the ASE noise in space. In Fig.IV.1.10 the distance evolution of a 10GHz 10^{31}-1 PRBS train is shown at the in-space noise suppression limit. Initially the eye diagram is gradually closing and after the high frequency components of the signal train are dropped out it opens up again. Because of this "self adjusting" characteristics in the experiments the number of ones in the transmitted signal always had to be carefully compared with that in the injected train.

The most important findings of the section are:

- It was experimentally demonstrated that in a combined SOA-SA based transmission line the pulse parameters (spectrum, pulse duration, pulse energy) are determined by the system and independent from the input pulse parameters. The acceptance range for the input pulses were found to be broad.
- It was shown that the in-space noise in such system can be effectively suppressed. In the experiments effective suppression of the in-mark noise is observed as well. An explanation for such behaviour was given. It was experimentally shown that the in-mark noise suppression mechanism works better at larger fiber spans.

- By transmitting pseudo random bit sequences it was found that the pulse energy of the transmitted pulses are strongly depending on the bit pattern. The experimental findings quantitatively confirmed the theoretical predictions.
- A temporal walk off between the different components of a random bit sequence was found. The origin of the walk off was explained.
- By the optimisation of the operating parameters error free 5Gb/s data transmission over 30000km was achieved.

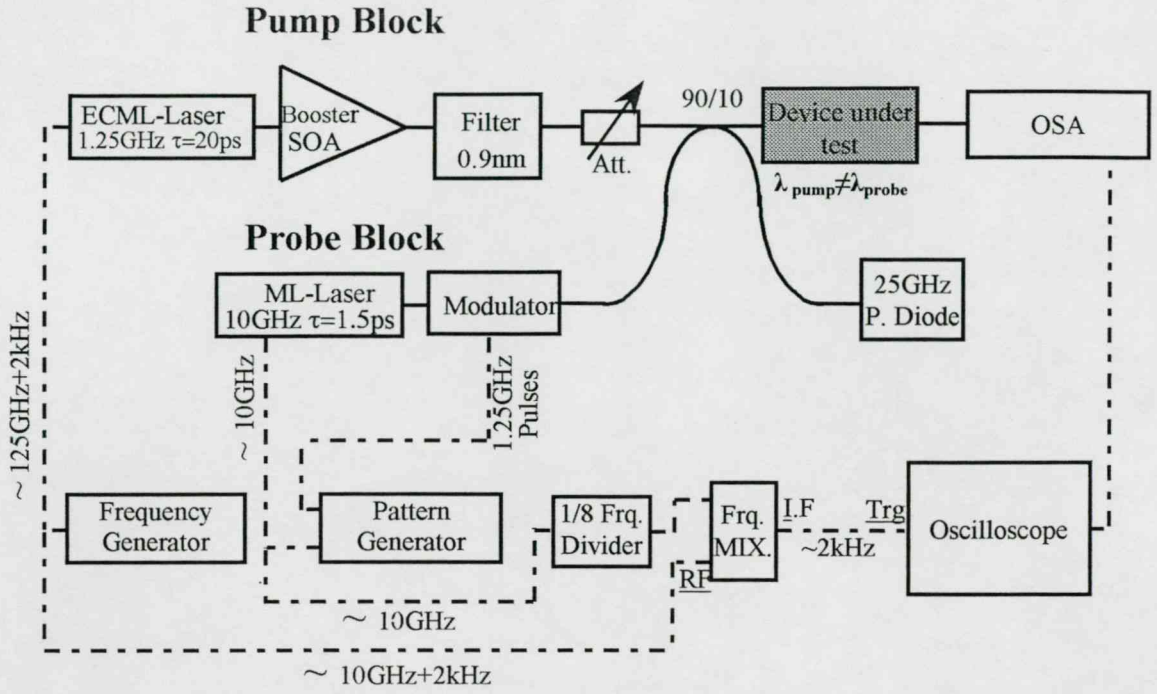

Fig.IV.2.1: Schematic diagram of the pump-probe measurement setup. The optical connections are marked with solid black lines and the electrical connections with dashed lines.

IV.2 Experiments with gain clamped semiconductor optical amplifier

The employment of gain-clamped semiconductor optical amplifiers (GC-SOA) is generally assumed to be one of the possible solutions to overcome amplitude patterning. In the following section the recovery characteristics of such a device are studied with pump-probe measurements and error free data transmission with the combination of our saturable absorber module and a GC-SOA is demonstrated over 5000km at 10Gb/s transmission rate.

IV.2.1 Gain recovery dynamics of GC-SOA

Fig.IV.2.1 shows a schematic diagram of the pump-probe measurement set up. The probe pulse was generated by an Advanced Optics GmBH TMLL 1300/70-10/1-25M tunable actively mode locked laser. The device provides ~1.5ps pulses with 10GHz repetition rate. The electrical signal for the mode locking was provided from the amplified sinusoidal clock output of an Anritsu MP1701A Pulse Pattern Generator. The 10GHz regular train was down-converted to a 1.25GHz one by an Sumitomo Osaka

Cement Co. T-MZI 3-10 Mach-Zehnder type intensity modulator driven from the data output of the pattern generator.

The pump pulse was generated by a Radians Innova TUN-1300ML actively mode-locked external cavity tunable laser. This time the laser cavity was re-built to provide a 1.25GHz train of ~20ps pulses. The laser was driven from the amplified output of an HP83711A signal generator. The frequency of the signal was chosen to be 1.25GHz+2kHz. The laser pulse was then amplified by a PHILIPS CQF822/0 SOA. The ASE of the booster amplifier was de-coupled by a 0.9nm tunable Fabry-Perot filter. At the end of the pump block a variable attenuator was applied to control the pump power. The wavelength of the probe pulses was always chosen to be at least 5nm away from the pump wavelength. By using a 90%/10% coupler the pump and the probe signals were led into the device under test. The maximum available pump pulse energy before the device was around 1pJ and a typical value for the probe pulse energy was 0.3fJ. After the test device the pump and probe signals were spectrally separated in our HP 70951B Optical Spectrum Analyser and an electrical signal proportional to the probe signal was sent to an HP54603B 60MHz oscilloscope. The trigger signal for the measurement was synthesised from the clock signal of the pattern generator and the signal of the HP signal generator by a high frequency mixer.

The measurement is based on the beating of two similar frequency pulse trains with each other. It is easy to see that if the frequency of the probe pulse is less than that of the pump, the delay of the probe is going to gradually increase from pulse period to pulse period. The change of the pump-probe delay for two subsequent pump pulses is $\Delta t = \Delta f / (f_{pump}(f_{pump} - \Delta f))$, where f_{pump} is the pump pulse repetition frequency and Δf is the difference between the pump pulse and the probe pulse frequency. In our measurements the value of Δt was 2fs. The maximum temporal delay is set by the pulse repetition frequency: $T_{maxdelay} = 1/f_{pump}$, in this experiment it was 800ps. And the time needed for a complete delay scan is $1/\Delta f$, which was 500μs in our set up. It is interesting to note that, by choosing a low value for Δf, the theoretically possible temporal resolution and the requirements for the data acquisition speed can be reduced simultaneously. Though in the present experiment the temporal resolution was limited predominantly by the probe pulse duration.

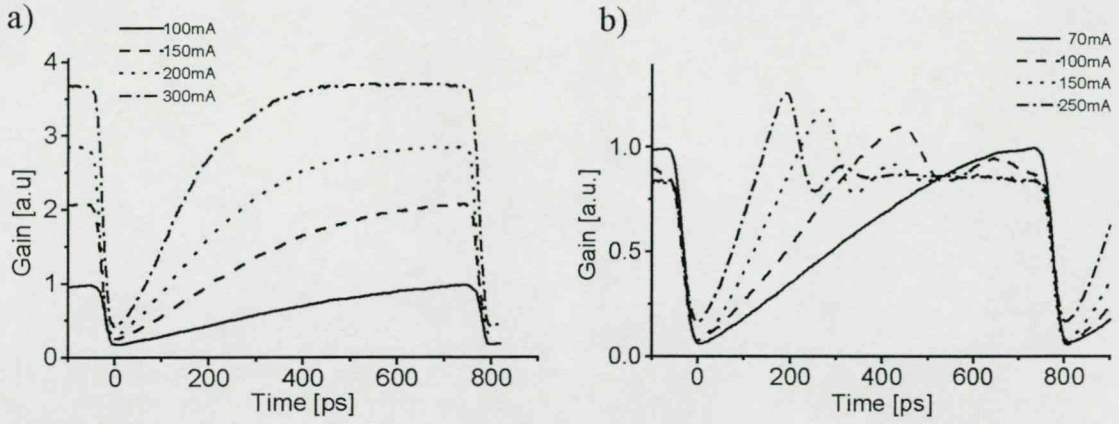

Fig. IV.2.2: a) The recovery of the gain in a PHILIPS CQF882/0 #371 SOA for different driving currents. b) The gain recovery dynamics of a PHILIPS #8126 gain-clamped SOA at different operating currents. Note the oscillation in the signal gain due to the transient oscillation of the lasing. The lasing wavelength is 1286nm. In both cases the chip temperature is 20C°, the pump wavelength is 1300nm, the probe wavelength is 1308nm. The pump pulse energy is 0.6pJ and the probe pulse energy is 0.3fJ.

In Fig.IV.2.2 the typical gain recovery characteristic of a traditional SOA and of a gain clamped amplifier are shown. For both amplifiers the higher the current, the faster the gain recovery dynamics is. However, there are two major differences between the dynamics of the traditional SOA and the gain clamped one. For a traditional SOA the higher driving current results in higher small signal gain. This is not the case for the GC-SOA. At low currents it acts like a regular amplifier but as soon as the carrier concentration reaches the lasing threshold, the characteristic changes. Since the carrier concentration is fixed by the lasing, the static small signal gain is fixed as well. The other major difference is the transient oscillation of the device gain. It originates from the relaxation oscillations of the laser resonator [62,63]. It was found that the time needed to reach the first oscillation peak after saturation (rise up time) is tunable with the driving current, the input pulse power and with the device temperature (Fig.IV.2.3). Such a relaxation dynamics is not always harmful and even can be utilised.

If the operating parameters of the gain clamped device are chosen appropriately, the high frequency component of the signal could coincide with the first peak of the relaxation oscillation. This way it is even possible to compensate for the patterning introduced by an additional conventional SOA in a system. The idea was tested in

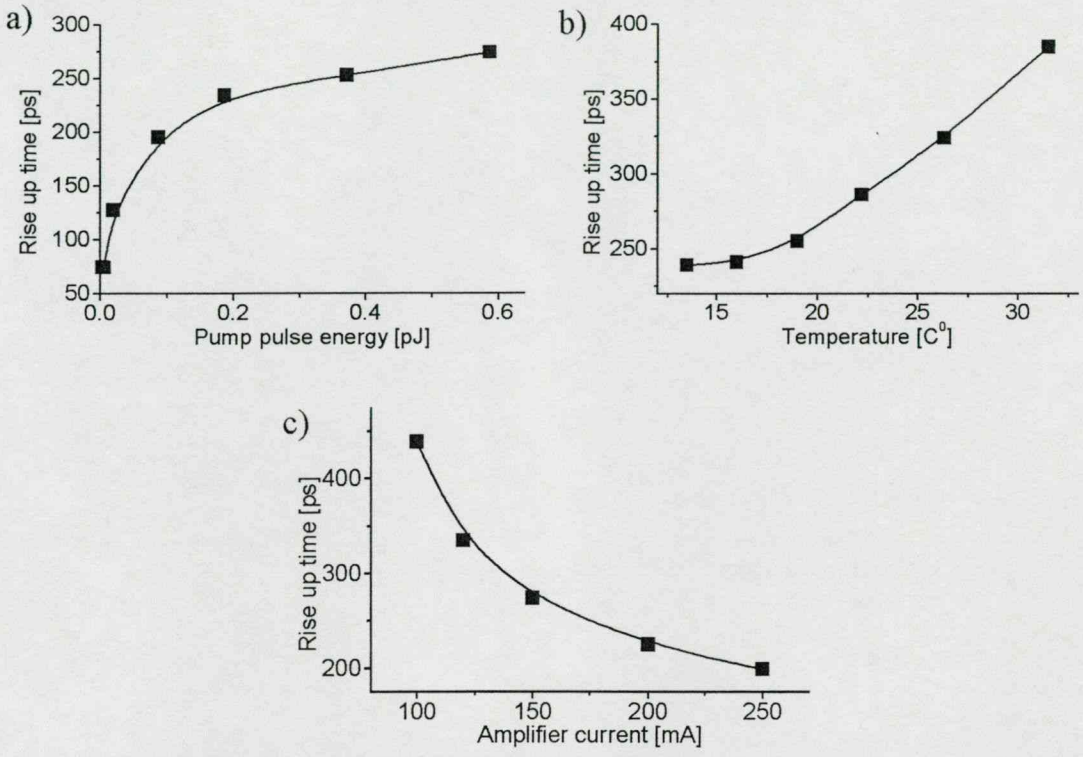

Fig.IV.2.3:The dependence of the rise up time on the input pulse energy a),device temperature b), driving current c). If not varied the amplifier current was 150mA, the device temperature was 22C° and the input pulse energy was .6pJ. The rise up time is defined, as the time needed to reach the first oscillation peak from the depleted state.

transmission experiments. Replacing the regular SOA by a GC-SOA in our fiber loop set up it was found, that with the proper tuning of the amplifier current the patterning introduced by the conventional SOA section in the combined SOA-SA module can be compensated.

In Fig.IV.2.4 the stationary energy levels of a 10GHz 11110101 bit pattern are shown for the GC-SOA based system. At low current, under the lasing threshold the device acts as a regular SOA and the higher frequency component of the signal has a lower energy (Fig.IV.2.4a). If the current is increased the first peak of the relaxation oscillation moves forward. On the situation depicted in Fig.IV.2.4b the 10GHz component is at the leading edge of the first oscillation and the 5GHz component is on the trailing edge. In Fig.IV.2.4c a very strong inverse patterning is shown. It corresponds to the situation, when the high frequency component is around the first peak of the relaxation oscillation and the 5GHz component is at the dip. In Fig.IV.2.4d the high

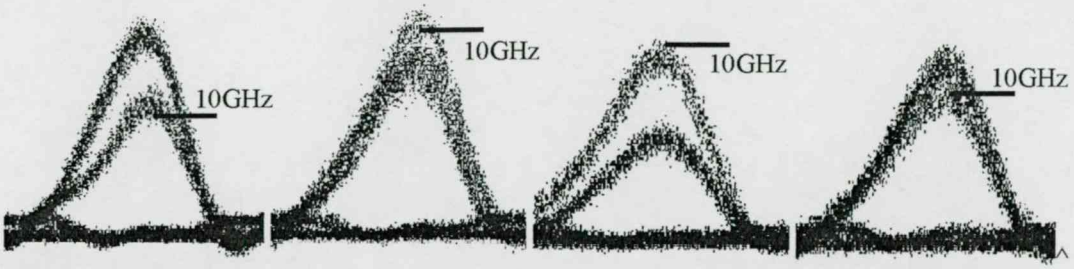

Fig.IV.2.4: The eye diagrams of a 10Gb/s 111011101010 train after 8 roundtrips (200km). The amplifier currents were a) 70mA, b) 90mA, c) 110mA, c) 200mA. The average input power was kept constant during the measurement. The absolute value of the input pulse energies were about ~0.05 pJ. The 10GHz component of the signal is marked with a line.

frequency component comes after the first peak and the excess gain in the gain clamped amplifier is not enough to compensate for the behaviour of the regular SOA. All together it is clearly demonstrated that a gain clamped semiconductor amplifier can be used as a programmable patterning device and even strong inverse patterning can be achieved.

IV.2.2 Transmission results with GC-SOA

In transmission experiments using GC-SOA with properly adjusted current and temperature we succeeded to obtain almost the same steady state energy for all signal components of a PRBS signal while still blocking the growth of in-space noise. As shown in Fig.IV.2.5a both temporal walk off and patterning could be minimised by carefully adjusting the amplifier parameters and the position of the in-line bandpass-filter. For 10 Gb/s 2^{31}-1 PRBS RZ signal error free transmission over 5000 km (200 cascaded amplifiers) has been obtained. It is more than three times the distance previously reported for SOA based systems operating at 10 Gb/s [45]. It has to be noted that the 10 Gb/s system appears to be much more sensitive for the temporal walk off between the different energy pulses, than the conventional SOA based set-up at lower bit rates. There the walk off primarily results in a detection window reduction. In a GC-SOA system both the temporal position and the energy of the subsequent signal pulses are relevant for the compensation of the patterning effect and the temporal walkoff ultimately leads to a threshold-like transmission deterioration. Because there is no patterning for a regular

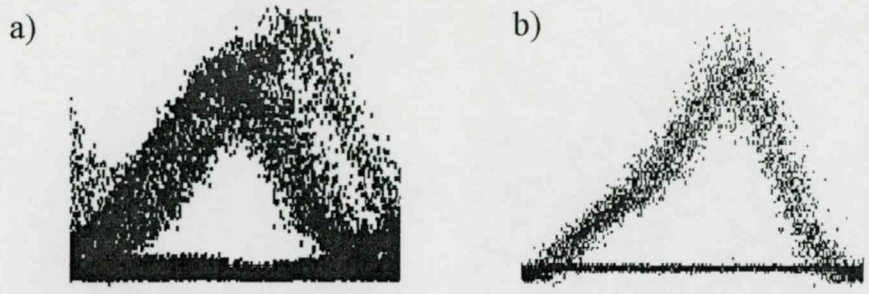

Fig.IV.2.5: Propagation results with the combined system of a GC-SOA and a SA-SOA module. a) Eye diagram of a 10Gb/s 10^{31}-1 PRBS train at 5000km. b) The eye diagram of a 10GHz regular pulse train at 20000km.

pulse train, error free transmission of a 10 GHz train was achieved over 20 000 km (cascade of 800 amplifiers) (Fig.IV.2.5b). The long transmission distances obtained for a 10 Gb/s signal together with our previous results show a large potential of combined SA-SOA based systems. These results have confirmed that the performance of such systems is mainly limited by the slow gain recovery of the SOA. Though the integration of a GC-SOA and a SA into a single chip seems to be difficult because one has to prevent the strong emitted CW radiation to be absorbed by SA, the application of such amplifiers could be still advantageous. This is because of the faster gain recovery and the potential of patterning compensation. Optical pumping at transparency or quantum dot designs look also very promising to achieve long transmission distances.

The applicability of the present method in the 1.5 μm communication window is quite straightforward – only dispersion compensation would be necessary-, but the feasibility of saturable absorber based multiwavelength regenerators is to be examined in the future.

The most important findings of the section are:

- The gain recovery dynamics of a standard SOA and a GC-SOA were compared by pump-probe measurements.

- It was found that the dynamics of the relaxion oscillation of the carrier density in GC-SOA can be strongly influenced with the device current, temperature and with the pulse energy of the depleting pulse.
- It was shown that a GC-SOA could be used as a programmable patterning device and the patterning introduced by regular SOAs can be compensated.
- With the combination of our SA module and a GC-SOA error free 10Gb/s data transmission was achieved over 5000km.

V. Active spatial filtering

In the previous chapters of this work it has been shown that, saturable absorbers can enhance the performance of fiber optical networks. In this section it will be demonstrated that not only the temporal properties of short optical pulses but also the spatial intensity distribution of laser beams can be improved through nonlinear optical interactions.

V.1 The importance of good quality pulses in high intensity laser experiments

The major figure of merit of high-intensity laser systems is how efficiently they can temporally and spatially concentrate the energy carried by the pulse. Short-wavelength lasers have better theoretical capability for such temporal and spatial compression. From the practical point of view the importance of the focusability for a short-wavelength system is more pronounced because of the inverse square dependence of the focusable intensity on the wavelength [64,65]. That is why short-wavelength short-pulse excimer laser systems are now able to produce very high ($I \sim 10^{19}$ W/cm^2) focused intensities with medium peak power [66-68] and can be used to study high-intensity phenomena like harmonic generation in laser plasma [69-74]. The better theoretical capability for focusing of short-wavelength lasers can only be utilised, if the optimum beam quality is maintained. This is however the more complicated the shorter the wavelength is.

Short-pulse excimer laser systems are generally dual-wavelength lasers, where the generation and the final amplification of the pulse is done at two different wavelengths. For KrF lasers the short pulses are normally generated at twice [67,75] or three times [66,68] of the desired wavelength of 248nm, which necessitates frequency doubling or tripling stage before UV amplification.

In such systems the main sources of eventual distortion of the phase front of the output beam are as follows:

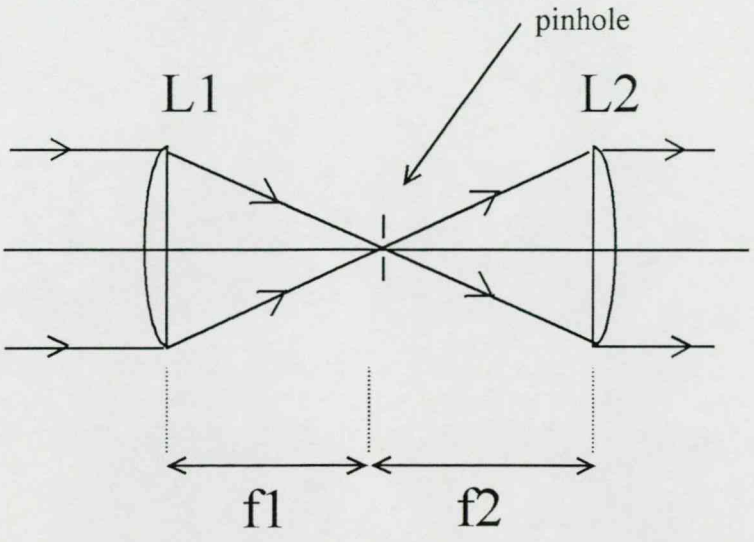

Fig.V.1.1 Schematic layout of the conventional pinhole based spatial filter.

-phase distortion and intensity-modulation of the beam at the fundamental wavelength, -phase distortions and the spatial intensity fluctuations accumulated during UV amplification.

The latter one can be minimised by the use of high-quality optical components and by operating the excimer amplifier in the so-called off-axis mode [65,76-78]. Consequently, the diffraction limited beam quality and well-determined intensity distribution for the frequency-converted beam is of a great importance. Considering that phase distortions and intensity modulations are maintained or even magnified in conventional frequency-conversion schemes, the requirements for the beam quality at the fundamental wavelength are even more pronounced. Since the late 1960s, several effective methods for homogenising the intensity distribution of laser beams were developed. However these methods can hardly be applied in short pulse, high power laser systems. Some of the methods cause temporal broadening of the laser pulse [79], others are very sensitive to the direction of the input beam [80].

Normally, spatial filtering is a widely used technique to improve the directional properties and intensity distribution of the beam by allowing the transmission of only the first spatial-component at the Fourier plane. Generally two lenses (or mirrors) in a confocal arrangement are used for Fourier-transformation and retransformation.

(Fig.V.1.1). In this scheme the selection of the different spatial components is accomplished by a pinhole of appropriate size.

The main problem associated with the pinhole-based arrangement is that the direction of the beam has to be matched to the optical axis of the arrangement with accuracy comparable to the diffraction-limited divergence of the beam. However, this accuracy is generally not allowed by the limited pointing stability of large laser systems, leading to unpredictable transmission of the beam and early damage of the pinhole. The limited pointing stability of large laser systems is generally originated in the limited stability of the optical components, including the oscillator, amplifier chain and target area. The larger the beam size for a given wavelength, the more stringent these requirements are.

The beam filtering method suggested here is based on replacing the pinhole by a nonlinear component. Such a component, due to its intensity (or energy density) dependent transmission automatically selects the more intense central spatial-component, resulting in an output beam of well-determined energy distribution even for input beams of fluctuating directional properties.

V.2 Numerical demonstration of the operating principle

It is known, that a lens converts the complex amplitude distribution of light at the focal plane before the lens (object plane) to its Fourier transform at the opposite side focal plane (Fourier-plane)[80]. The amplitude distribution at the Fourier-plane can be written as:

$$A(x', y') = \frac{k}{2\pi f} \int_{-\infty}^{\infty}\int_{-\infty}^{\infty} a(x, y) \exp\left[\frac{-ik(x'x + y'y)}{f}\right] dx\, dy\,. \qquad (V.2.1)$$

Where A(x',y') is the complex amplitude at the Fourier plane, a(x,y) is the complex amplitude at the object plane (the original amplitude distribution of the laser beam), k is the wave number and f is the focal length.

The problem significantly simplifies if a circular symmetry is presumed. Through transformation of eq.V.2.1 to polar coordinates both at the object plane (x,y) and at the Fourier plane (x',y') we obtain [81]:

$$A(\rho) = \frac{k}{f}\int_0^{\infty} r\, a(r)\, Jo\left[\frac{k}{f}\rho r\right] dr \qquad (V.2.2)$$

Where r and ρ is the radius at the object plane and at the Fourier plane, respectively. Jo(x) it a Bessel function of the first kind.

In the following numerical calculations the image created by the lens at the Fourier-plane was considered by eq.V.2.2. A nonlinear component, having an intensity or energy density dependent transmission is placed at the Fourier plane. Three different transmission functions were considered. The first is a step-function resulting in a mode selection, which is similar to that of a pinhole (Fig.V.2.1a). The second function is the transmission of a slow saturable absorber assuming that the energy density is proportional to the peak intensity of the pulse of a given shape and pulse duration ($J=C\ I_{peak}$) as shown in Fig.V.2.1b. The third function is an idealised conversion-efficiency function of a frequency doubler (Fig.V.2.1c). The corresponding analytic functions are as follows:

$T=0.95$, if $I>I_{threshold}$. (V.2.3)

$T=0$ otherwise.

$$T = \frac{J_{threshold}}{J} \ln\left\{1 + \left[\exp\left[\frac{J}{J_{threshold}}\right] - 1\right] T_0\right\}. \qquad (V.2.4)$$

where $T_0=0.03$

$$\eta = 0.7\ \tanh^2\left(\sqrt{\frac{I}{I_{threshold}}}\right). \qquad (V.2.5)$$

The retransformation is carried out also by eq.V.2.2, where the role of A(r) and a(ρ) are correspondingly changed: a(ρ) and A(r) are the complex amplitudes of the beam at the Fourier-plane and after retransformation, respectively. If frequency conversion is carried out by the nonlinear component at the Fourier-plane than the retransformation has to be done at a different wavenumber (k_2). Since the divergence of the beam is proportional to the wavenumber, significant decrease of the divergence of the output beam is expected,

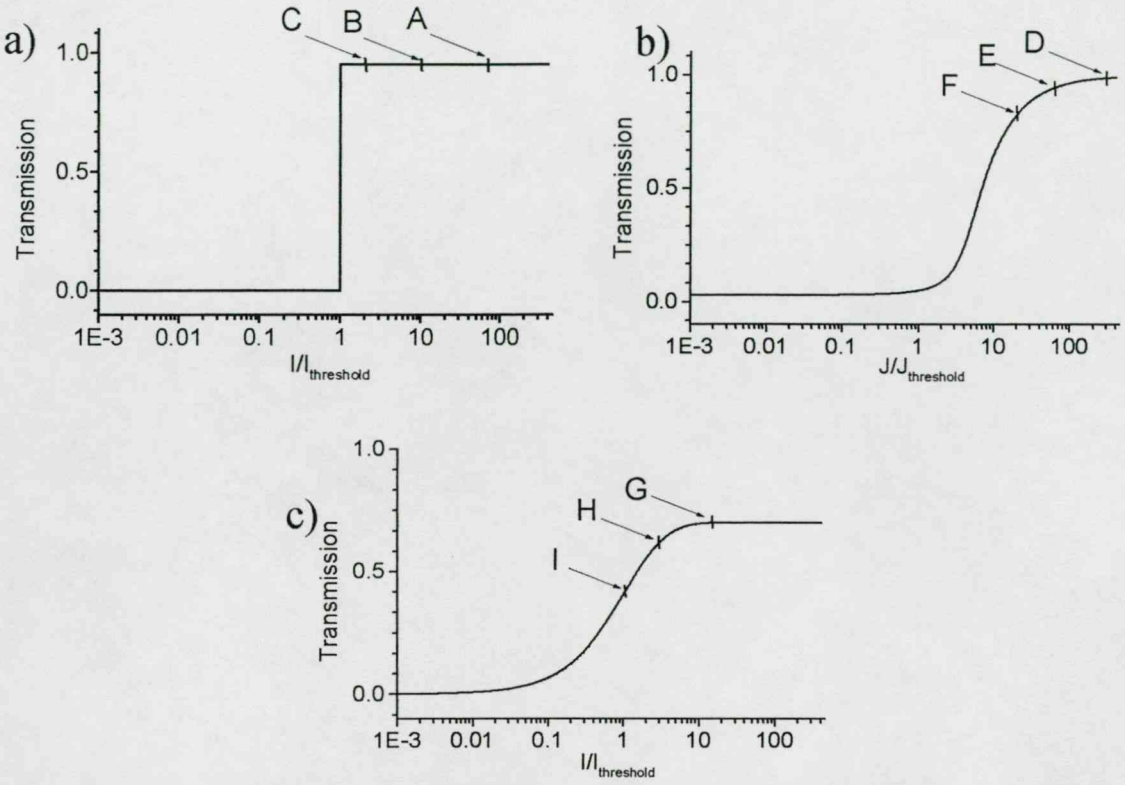

Fig. V.2.1: Transmission functions of the nonlinear components used in the calculations (for details see text) a) step-function, b) saturable absorber and c) frequency doubler.

when a frequency doubler is used as a nonlinear component. This reduction of the divergence of the output beam was also verified experimentally.

The calculations were carried out for a beam of 2.5mm diameter at a wavelength of 500nm. The focal length of L1 and L2 was chosen to 500mm. The intensity distribution of the beam was assumed to have a flat topped profile modulated by a random noise (Fig.V.2.2a). The phase of the input beam was presumed to be the same over the whole profile. For an input beam having such a noisy intensity distribution the calculated sections across the output beams are shown in Fig.V.2.2 b), c) and d) for the three transmission functions indicated in Fig.V.2.1 a), b) and c), respectively. The different output distributions shown by solid, dashed and dotted lines in Fig.V.2.2 are obtained at different peak intensities of the first diffraction-lobe at the Fourier plane. These intensities are marked in Fig.V.2.1 by capital letters. In all cases the peak intensity of the first diffraction-lobe was chosen to be higher than the threshold intensity of the nonlinear component to allow suitable transmission for the central part of the diffraction

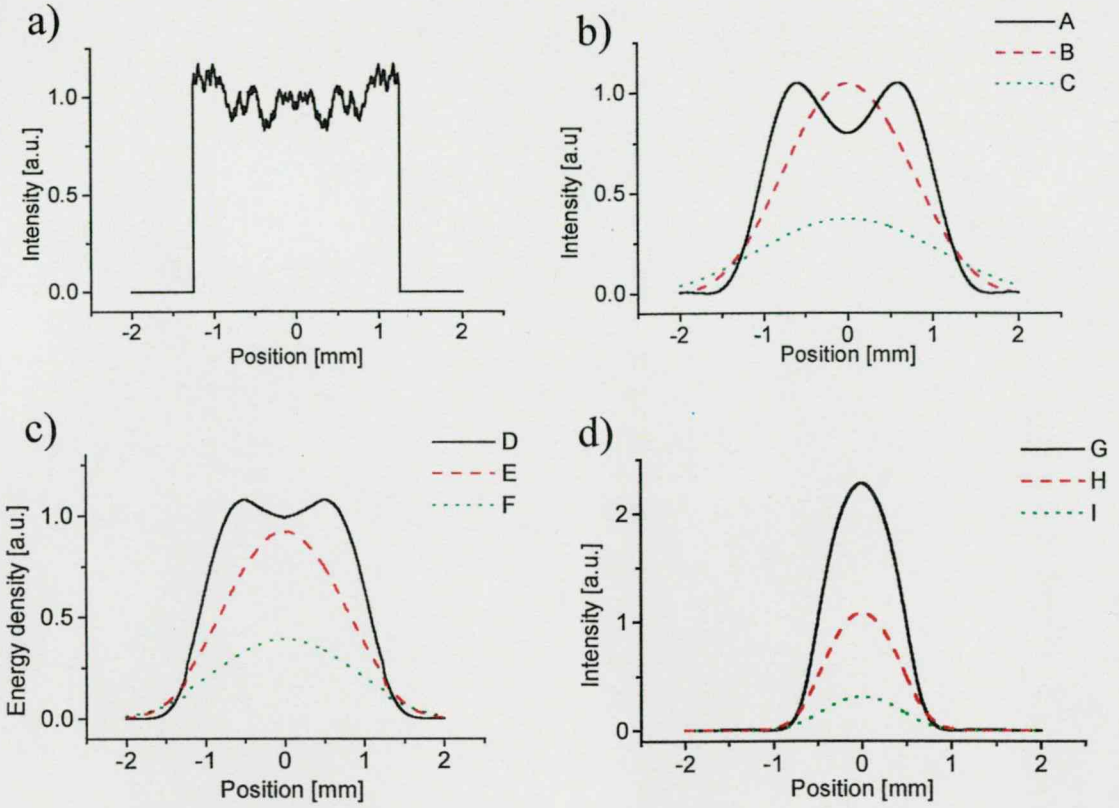

Fig.V.2.2: a) Noisy intensity profile assumed for the input beam. b), c), d), calculated intensity distributions for the output beam, filtered by a step-function-like filter b), a saturable absorber c) and a frequency doubler d). The dotted, solid and dashed curves correspond to different peak intensities of the central diffraction-lobe at the Fourier plane (marked by capital letters in Fig.V.2.1).

pattern. There is a wide intensity range (what we call as "dynamic range") where the first diffraction lobe is transmitted efficiently, while the higher order components suffer low transmission. This results in a well-characterised Gaussian-like distribution for the output beam. It is worth noting that operating the nonlinear component in the above-defined dynamic range the final distribution is practically independent of the transmission function as it is seen by comparing the dotted and dashed curves of Fig.V.2.2 b)-d). On the other hand, when the peak intensity is increased so much that even higher-order components are transmitted with high efficiency, a low-spatial frequency modulation arises in the distribution of the output beam (solid lines of Fig.V.2.2b-c). Since the ratio of the peak intensity of the first and higher order components is more than one order of magnitude for most of the practical beam distributions, the earlier defined dynamic range is large enough for applications. This means that effective beam filtering can be realised

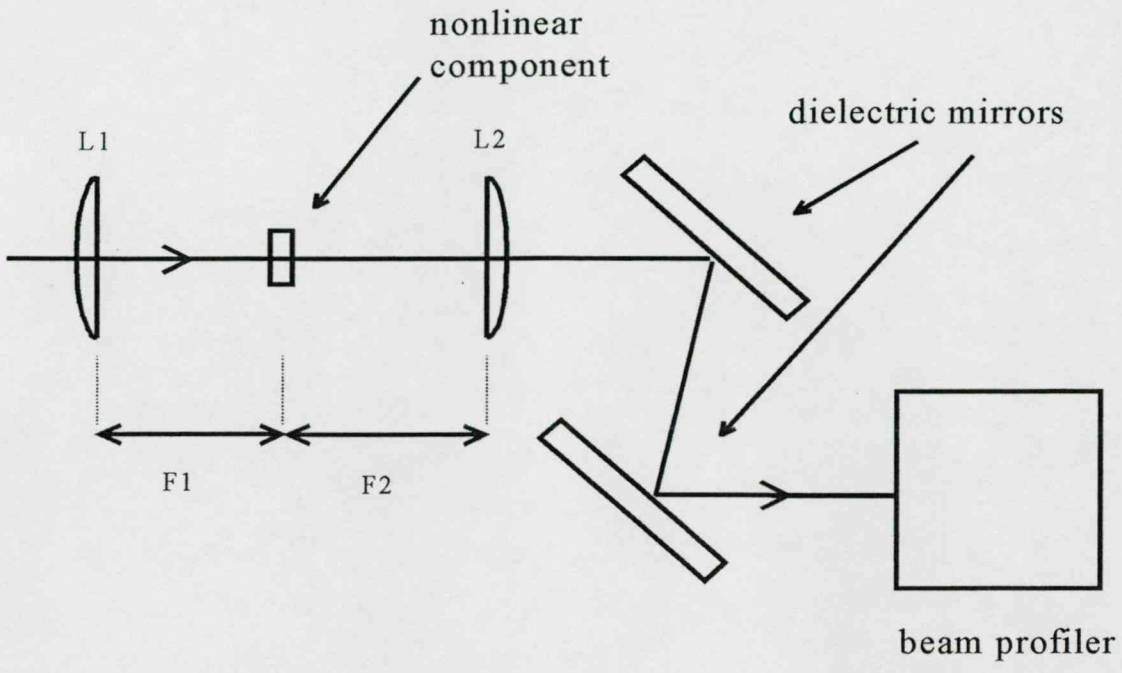

Fig.V.3.1: The experimental arrangement used for the demonstration of nonlinear component based spatial filtering.

even if the intensity of the incoming laser pulses are strongly fluctuating form shot to shot.

V.3. Experimental demonstration of active spatial filtering

The experimental arrangement used for the feasibility test of the nonlinear component-based Fourier filtering is shown in Fig V.3.1. L1 and L2 are fused silica lenses of identical f=500 mm focal length. A 52° cut BBO crystal of 0.5mm thickness was chosen as an active spatial filter. The arrangement was illuminated by a beam emerging from a misaligned Bethune-type dye amplifier [82]. The input beam for the Bethune-cell was obtained from a subpicosecond distributed feedback dye laser oscillator-amplifier arrangement operating at 500nm. The details of the laser system are described in [75,83,84]. The doubled frequency signal emerging at the output of the beam filtering arrangement was separated from the 500 nm fundamental wavelength by two dielectric mirrors having high reflectivity only in the UV range. The typical intensity profile of the beam after the Bethune-cell, just entering the beam filtering system is

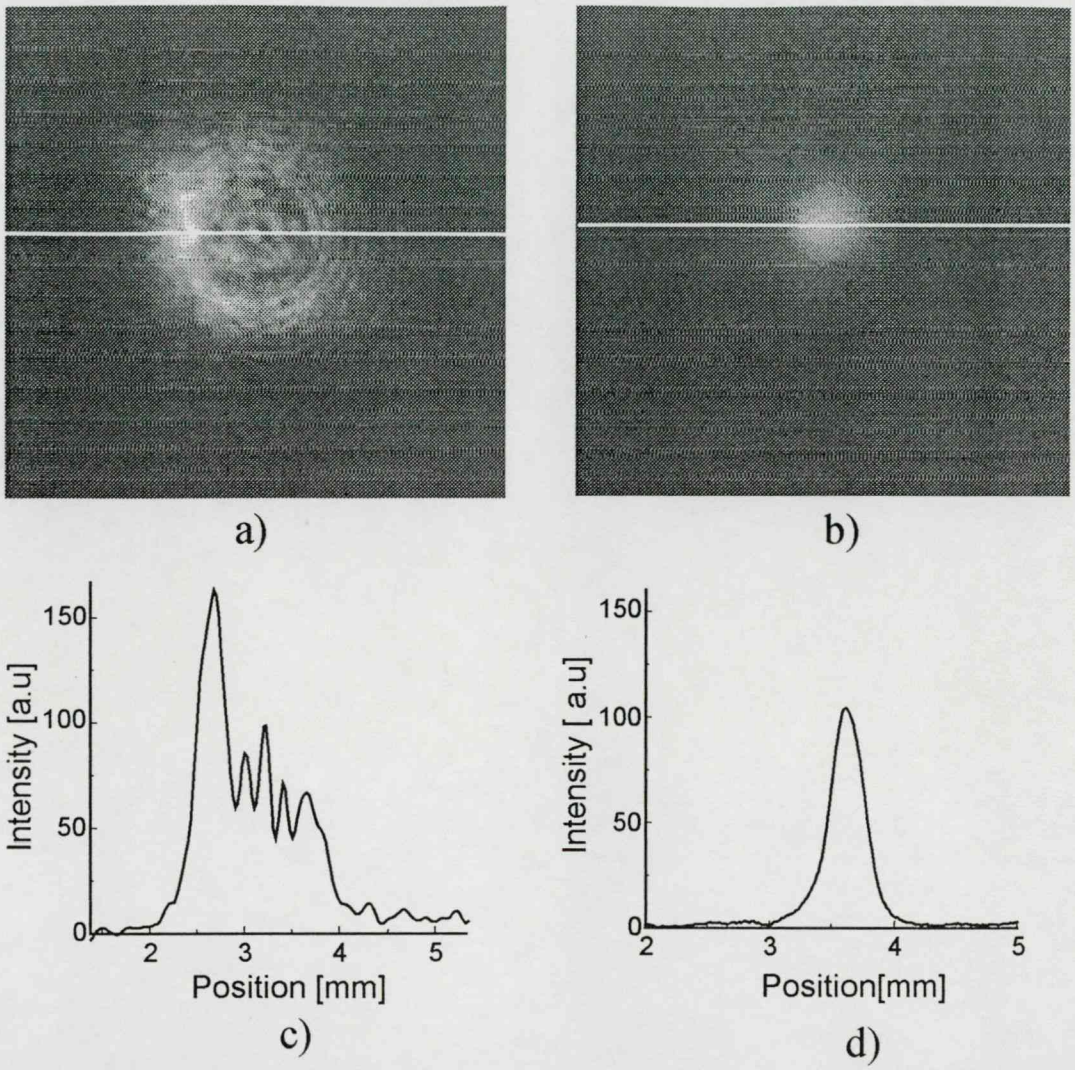

Fig.V.3.2: Measured single-shot distribution of the input beam a) and the filtered output beam b) using a frequency doubler as a nonlinear component, c),d):intensity distribution of the input and output beam along the central horizontal line in a) and b).

shown in Fig.V.3.2a. When the BBO crystal was positioned far from the Fourier plane a distribution of the output beam was very similar to that of the input beam. However, when the crystal was in the vicinity of the Fourier-plane, the size of the output beam shrank, and the intensity distribution became free of modulation, in agreement with the results of the calculations (Fig.V.2.2b). Fig.V.3.2c) and d) show the intensity distributions of the input and the filtered output beams along the central line -indicated as a solid line in Fig.V.3.2a) and b), respectively. The significant improvement in the homogeneity is clearly seen by comparing the corresponding pictures/distributions.

Finally, there is an important fact, which has to be noted in comparison of this

arrangement with the conventional schemes. In conventional frequency conversion or saturable absorber-based optical schemes a focusing lens is normally used to adjust the intensity (or energy density) of low energy beams to the needs of efficient frequency conversion or to the optimum operation of the absorber. In such cases it is accidental whether the nonlinear component is in the focal plane. However, for high-energy beams - where the intensity (or energy density) is normally high enough to efficiently operate a frequency converter or a saturable absorber, focusing is rarely used before the nonlinear component in the standard optical schemes. In such case, where the importance of optimum beam quality is even more pronounced, the primary role of our newly proposed scheme is not to adjust the energy density of the beam, but to realise Fourier-transformation and retransformation. Together with Fourier-transformation the optimum energy density of the beam at the position of the nonlinear component can be adjusted by proper choice of the f-number of the focusing.

In this chapter a novel method to improve the intensity distribution of limited pointing stability laser pulses was presented. The operation of such arrangement was demonstrated both experimentally and by numerical calculations.

VI. Summary

1. *A novel type of modulation instability phenomenon in semiconductor optical amplifier (SOA) based transmission lines was demonstrated experimentally. The effect is originating from the interplay of the SOA nonlinearity and the in-line optical bandpass filter. The experimental results were found to be in a good agreement with the theoretical predictions.*

   The most important limitation for SOA based telecommunication systems operating in amplitude shift keying (ASK) transmission mode is the growth up of ASE in long set of zeros. Thus the application of phase-shift keying (PSK) modulation format may seem to be advantageous, since there the transmitted signal is quasi-CW. In spite of all, in transmission experiments it was found that the performance of such systems is limited to several hundreds of kilometres. Generally, the strong phase noise introduced by the random carrier density fluctuation in the SOA is considered to be the main limitation. It was shown experimentally that modulation instability effects could also lead to a fast growth of amplitude and phase noise, if the in-line optical bandpass filter is detuned from the optimal position. The experimental findings were compared with the theoretical predictions.

2. *It was found that the performance of semiconductor optical amplifier (SOA) based transmission lines operating in the ASK transmission mode can be significantly enhanced by the application of in-line saturable absorbers (SA). The basic characteristics of a transmission line containing combined semiconductor optical amplifier – saturable absorber (SOA-SA) modules were determined by numerical simulations based on a quasi-analytic description of the device gain.*

   In purely SOA based transmission systems using ASK transmission format due to the gain saturation and the bit rate comparable gain recovery time the signal pules are suffering lower gain than the noise between the pulses and in long set of zeros. It finally leads to the accumulation of ASE noise. The effect can be reduced by the application of the appropriate gain map and by in-line bandpass filtering but can not be eliminated. If saturable absorbers are applied in the line, the growth up of in-space

noise can be prevented. Such a combined SOA-SA based transmission line has got completely different system characteristics. It was shown that the below a threshold energy the system suppresses the input pulses, above that threshold a stationary pulse energy is reached. The dependence of the stationary pulse energy on the bit rate and the transmitted bit pattern is studied by numerical simulations

3. *In a re-circulating fiber loop arrangement it was demonstrated, that a stationary state of propagation exists in a combined SOA-SA based transmission line. In that state the pulse parameters are independent of the input pulse parameters.*

   It was shown in a re-circulating fiber loop setup that a combined SOA-SA based transmission line operating in the vicinity of the zero group velocity dispersion wavelength (~1.3μm) reaches a stationary state of propagation. The pulse parameters (spectra, pulse duration, pulse power) are only characteristic to the system and independent from the input pulse parameters in the stationary stage. The acceptance range for the input pulses were found to be broad.

4. *In combined SOA-SA based transmission line a novel, effective mechanism was found for the suppression of in-mark noise.*

   It is easy to understand that saturable absorbtion is an effective tool to address the noise in-space. However a very effective suppression of the noise propagating together with the pulses was also observed in the experiments. It was shown experimentally, that the in-mark noise suppression is more effective for longer-fiber spans and qualitative explanation was given for such a behaviour.

5. *The amplitude and spectral patterning characteristics of combined SOA-SA based transmission lines were studied experimentally. A temporal walk off was found between the different stationary energy pulses in a random data train. The walk off is proportional to the propagation distance at the stationary stage. The mechanism of the walk off was explained.*

   Propagating pseudo random bit sequences (PRBS) in the system discrete energy levels and temporal walk off between the different energy pulses was experienced. The temporal walk off is linearly proportional to the number of roundtrips at the stationary stage of propagation. It is originating from the pulse energy dependent

stationary pulse spectra and from the saturation induced pulse re-shaping effects in the SOA-SA module. The comparison of the calculated walk off with the measured one shows a good agreement. It was found that by the proper tuning of the in-line filter the walk off could be minimised.

6. *The optimum operating conditions for a combined SOA-SA module based system was determined. Error free 5GB/s data transmission was demonstrated over 30000km.*

   Because of the very effective noise suppression mechanisms the information can be transmitted for much larger distances in combined SOA-SA based systems. In such system beside the optical noise the amplitude patterning (originating from the bit rate comparable gain recovery time of the SOA) is one of the most limiting factor. One way to reduce patterning is to reduce the gain recovery time of the SOA. It was shown experimentally that by increasing the amplifier current the recovery time of the SOA and the patterning can be significantly reduced. In a combined system there is a trade off between noise and patterning. Operating the system at the optimal conditions error free transmission of 5Gb/s signal was demonstrated over 30000km.

7. *It was shown experimentally that gain clamped amplifiers can be used as a patterning compensation device.*

   In a gain clamped SOA the active medium is surrounded by distributed Bragg reflectors (DRB) introducing wavelength sensitive feedback to the amplifying medium. The device lases at the corresponding wavelength as soon as the roundtrip gain (material gain plus mirror losses) equals to unity. Thus the optical gain for a signal coming at a different wavelength is also clamped as long as the output signal power is not comparable to the power of the lasing mode. It was shown by pump-probe measurements that the amplitude and the frequency of the relaxation oscillations of the clamping laser are tunable with the driving current, temperature, and input pulse power. It was demonstrated in a re-circulating fiber loop setup that by proper tuning of the temporal position of the oscillation peaks the patterning introduced by a traditional SOA can be compensated.

8. *In a combined system of a SOA-SA module and a GC- SOA error free transmission of 10Gb/s signal over 5000km was demonstrated.*

By compensating the patterning characteristics of our combined SOA-SA module with a GC-SOA error free transmission of 10Gb/s signal was obtained over 5000km.

9. *A novel arrangement for spatial filtering of limited pointing stability laser pulses was suggested.*

It was demonstrated that not only the temporal properties of short optical pulses but also the spatial intensity distribution of laser beams can be improved through nonlinear optical interactions. A novel spatial filtering scheme is proposed which utilises a nonlinear component -instead of the normally used pinhole - for selective transmission of the different spatial-components at the Fourier plane. The arrangement not only improves the spatial properties of laser beams but also enhances the temporal contrast. The operation of such arrangement was experimentally and numerically demonstrated.

Appendix

1. The core of the Mathcad 6.0 project file for calculating the stationary energy of a regular pulse train:

The energy gain for the n-t pulse in a regular pulse train interacting with an amplifier or saturable absorber:

n	(integer)	a sufficiently large number to reach the stationary case.
G_{stat}	(real)	the small signal gain for a single pulse.
E	(real)	the uniform pulse energy of the pulses participating in the train.
t	(real)	the pulse period.
ε	(real)	the saturation energy of the device.
τ_r	(real)	the recovery time of the device.

$$TR(Gstat, E, \varepsilon, t, \tau r, n) := \left| \begin{array}{l} to \leftarrow Gstat \\ E \leftarrow \frac{E}{\varepsilon} \\ \text{for } i \in 1..n \\ \quad to \leftarrow \exp\left[\ln\left[\frac{\ln(1 + (\exp(E) - 1)\cdot to)}{(E)} \right] \cdot \exp\left(-\frac{t}{\tau r} \right) \right] \cdot Gstat \\ T \leftarrow \frac{\ln(1 + (\exp(E) - 1)\cdot to)}{E} \end{array} \right.$$

The stationary energy gain of the combined SOA-SA system:

n	(integer)	a sufficiently large number to reach the stationary case.
Ein	(real)	the input pulse energy.
εsoa	(real)	the saturation energy of the amplifier.
εsa	(real)	the saturation energy of the absorber.
t	(real)	the bit period.
τsoa	(real)	the recovery time of the amplifier.
τsa	(real)	the recovery time of the absorber.
Gstat	(real)	the static small signal gain of the amplifier.
Tstat	(real)	the static small signal transmission of the saturable absorber.

$$Combtr(Ein, t, G, \varepsilon soa, \tau soa, T, \varepsilon sa, \tau sa, n) := \left| \begin{array}{l} GSOA \leftarrow TR(G, Ein, \varepsilon soa, t, \tau soa, n) \\ TSA \leftarrow TR(T, GSOA \cdot Ein, \varepsilon sa, t, \tau sa, n) \\ TSA \cdot GSOA \end{array} \right.$$

2. The core of the Mathcad 6.0 project file for calculating the stationary energy of an arbitrary pulse train:

The function to calculate the output energy:

E	(real)	the pulse energy.
ε	(real)	the saturation energy.
Gain	(real)	the small signal gain.

$$ER(E,\varepsilon,Gain) := \ln\left[1+\left(\exp\left(\frac{E}{\varepsilon}\right)-1\right)\cdot Gain\right]\cdot\varepsilon$$

The function to calculate the small signal gain for the next pulse:

E	(real)	the pulse energy.
ε	(real)	the saturation energy.
t	(real)	the bit period.
τ_r	(real)	the recovery time.
Go	(real)	the small signal gain seen by the present pulse.
Gstat	(real)	the small signal gain for a single pulse (static small signal gain).

$$GoR(E,\varepsilon,Go,t,\tau r,Gstat) := \exp\left[\ln\left[\frac{\left[\ln\left[1+\left(\exp\left(\frac{E}{\varepsilon}\right)-1\right)\cdot Go\right]\right]}{\left(\frac{E}{\varepsilon}\right)}\right]\cdot\exp\left(-\frac{t}{\tau r}\right)\right]\cdot Gstat$$

The function to calculate the pulse energies in a pulse train containing n equidistantly spaced pulses after the interaction with c network sections:

Ein	(real array)	the array of the input pulse energies
n	(integer)	the number of pulses in the pulse train
εsoa	(real)	the saturation energy of the amplifier
εsa	(real)	the saturation energy of the absorber
t	(real)	the bit period
τsoa	(real)	the recovery time of the amplifier
τsa	(real)	the recovery time of the absorber
Gstat	(real)	the static small signal gain of the amplifier
Tstat	(real)	the static small signal transmission of the saturable absorber
L	(real)	the fiber loss
c	(real)	the number of sections

$$
\begin{aligned}
&RES(EIN, \varepsilon soa, \varepsilon sa, t, \tau soa, \tau sa, Gstac, Tstac, n, L, c) := \\
&\quad \text{for } k \in 1..c \\
&\quad\quad G_0 \leftarrow Gstac \\
&\quad\quad T_0 \leftarrow Tstac \\
&\quad\quad \text{for } i \in 1..n \\
&\quad\quad\quad EA_i \leftarrow ER(EIN_i, \varepsilon soa, G_{i-1}) \\
&\quad\quad\quad G_i \leftarrow GoR(EIN_i, \varepsilon soa, G_{i-1}, t, \tau soa, Gstac) \\
&\quad\quad\quad EIN_i \leftarrow ER(EA_i, \varepsilon sa, T_{i-1}) \\
&\quad\quad\quad T_i \leftarrow GoR(EA_i, \varepsilon sa, T_{i-1}, t, \tau sa, Tstac) \\
&\quad\quad EIN \leftarrow L \cdot EIN + 10^{-14} \\
&\quad EIN
\end{aligned}
$$

References

[1] K. C Kao and G. A Hockman, Proc IEE **113**, 1151 (1966)
[2] F.P. Kapron, D. B. Keck, and R. D. Maurer, Appl. Phys. Lett., **17**, 423 (1970)
[3] T. Miya, Y. Terunuma, T. Hosaka and T. Miyoshita, Electron. Lett., **15**, 106 (1979)
[4] M. Born and E. Wolf, Principles of Optics
[5] Goldvin P. Agrawal, Fiber Optics Communication Systems
[6] Goldvin P. Agrawal and Niloy K. Dutta, Semiconductor Lasers
[7] Peter Vasil'ev, Ultrafast diode lasers
[8] C.E. Zal, J.S. Osinski,C. Caneau, S. G. Menocal, L. A. Reith, J. Salzman, F. K. Shokoohi and T.P. Lee, Electron. Lett., **23**, 990 (1987)
[9] I. Cha, M. Kitamura, H.Honmou and I. Mito, Electron. Lett., **25**, 1241 (1989)
[10] E.Gini, E. Gamper, W. Vogt and H. Melchior, ECOC'99, Nice, France, **1**, 174 (1999)
[11] G. P. Agrawal and N. A Olsson, J. Quantum Electron., **25**, 2297 (1989)
[12] L. M. Frantz and J. S. Nodvik, J. Appl Phys., **34**, 2346 (1963)
[13] W.Rudolph and H. Weber, Opt. Commun., **34**, 491 (1980)
[14] M.M. Tilleman and J.H. Jacob, Appl. Phys. Lett., **50**, 121 (1986)
[15] P.Vasil'ev, Optical and Quantum Electronics, **24**, 801 (1992)
[16] F. Stern, J. Appl. Phys.,**47**, 5382
[17] R.W. Dixon and W. B. Joyce, J. Quantum Electron. **QE-15**, 470 (1979)
[18] Y. Tang, Y. Lu, J. Chen and D. Li, J. Opt. Commmun., **20**, 88 (1999)
[19] Virtual Photonics Inc., Photonics Transmission Design Suite 1.2, Photonics Module Reference Manual (1999)
[20] M. J. O'Mahony, J. Lightwave Technol. **6**, 531 (1988)
[21] F. Girardin, G. Guekos and A. Hobavlis, Photon. Technol. Lett., **10**, 784 (1998)
[22] C. J. Simon, P. Doussière, P. Lamouler, I. Valiente and F. Riou, Electron.Lett., **30**, 49 (1994)
[23] AC045: ACTS-UPGRADE, Report on gain-clamped semiconductor amplifier for digital applications
[24] S.L. Danielsen, P. B. Hansen, D. Wolfson, B. Mikkelesen, K. E. Stubkjaer, J. Y. Emery, F. Pommereau and M. Renaud, OFC'98, San Jose ,USA, 41 (1998)
[25] G. Soulage, P. Doussière, A. Jourdan and J. Sotom, ECOC'94, Florence, Italy, 451 (1994)
[26] D.Wolfson, S. L. Danielsen, C. Joergensen, B. Mikkelsen and K.E. Stubkjaer Photon. Technol. Lett., **10**, 1241 (1998)
[27] G. Morthier and J. Sun, Photon. Technol. Lett., **10**, 282 (1998)
[28] N.A. Olson, J. Lightwawe Technol. **7**, 1071 (1989)
[29] R. Loudon, J. Quantum Electron., **QE-21**, 766 (1985)
[30] A. Yariv, Opt. Lett., **15**, 1064 (1990)
[31] S. Wannenmacher, G. Bauer, J. Lightwave Technol., **16**, 512 (1998)
[32] A. Mecozzi, Photon. Tehnol. Lett., **10**, 1033 (1998)
[33] M. Settembre, F. Matera, V. Hägele, I. Gabitov, A. W. Mattheus and S. K. Turitsyn, J. Lightwave Technol., **15**, 962. (1997)

[34] A. Altcunt, L. Noel, W. A. Pender, A. S. Sidiqui, T. Widdowson, A. D. Ellis, M. A. Newhouse, A. J. Antos, G. Kar and P. W. Chu, Electron. Lett., **32**, 233 (1996)
[35] H. Suzuki, J. Kani, H. Masuda, N. Takachio, K. Iwatsuki, Y. Tada and M. Sumida, ECOC'99, Nice, France, PD2-3 (1999)
[36] M. Settembre, F. Mateara, M. Tamburrini, A. Mecozzi, J.J.E. Reid, P. I. Kuindersma and H. Haustein, ECOC'98, Madrid, Spain, 349 (1998)
[37] K. Kikuchi, C. Zah and T. Lee, J. Quantum Electron., **QE-27**, 416 (1991)
[38] V.Hägele, F.Küppers, A.Mattheus, European Conference on Networks and Optical communications NOC'96, Heidelberg, 320 (1996).
[39] P.I. Kuindersma, G.P.J.M. Cuijpers, J.G.L. Jennen, J.J.E Reid, L.F.Tiemeijer, H. deWaardt and A.J.Boot, ECOC'96, Oslo,ThD.2.1 (1996).
[40] J.J.E. Reid, Technical Digest of Optical Amplifiers and their Applications, paper TuB1-1, 82 (1997)
[41] J.J.E. Reid, S. Walczyk, G.N. van den Hoven, G.P.J.M. Cuijpers and P.I. Kuindersma, ECOC'97, Edinburgh, U.K, **1**, 79 (1997)
[42] A. Shipulin, G. Onishchukov, P. Riedel, D. Michaelis, U. Peshel, and F. Lederer, Electron. Lett., **33**, 507 (1997).
[43] J.J.E. Reid, L. Cucala, M. Ferreira, M. Settembre, H. Haunstein and R.C.J. Smets, ECOC'98, Madrid, Spain, WdD01/567, (1998)
[44] G. Onishchukov, V. Lokhnygin, A. Shipulin and M. Gölles, OAA'99, Nara, Japan, ThD4-1//151 (1999)
[45] G. Onishchukov, V. Lokhnygin, A. Shipulin, P. Riedel, Electron. Lett., **34**, 1597 (1998).
[46] Onishchukov, **Z. Bakonyi**, C. Knöll, M. Gölles, F. Lederer R. Ludwig ECOC'99,Nice, France, **2**, 260 (1999)
[47] **Z. Bakonyi**, G. Onishchukov, C. Knöll, M. Gölles, F. Lederer and R. Ludwig Photon. Technol. Lett., **12**, 570 (2000)
[48] **Z. Bakonyi**, G. Onishchukov, C. Knöll, M. Gölles and F. Lederer: Electron. Lett. **36**, 1790 (2000)
[49] J.G.L.Jennen, ECOC'98, Madrid, Spain, **1**, 235 (1998).
[50] Y.Sun, A.K.Srivastava, S.Banerjee, J.W.Sulhoff, R.Pan, K.Kantor, R.M. Jopson and A.R:Chaplyvy, OAA'99, Nara, Japan, PdP6 (1999).
[51] L.H.Spiekman, J.M.Wiesenfeld, A.H.Gnauck, L.D:Garrett, G.N. van den Hoven, T. van Dongen, M.J.H.Sander-Jochem and J.J.M.Binsma, ECOC'99, Nice, France, paper PD2 (1999).
[52] C.Wolf, A.K.Srivastava, S.Banerjee, Y.Sun, J.W.Sulhoff and K.Kantor, OFC'2000, Baltimor, USA, WM32 (2000).
[53] A. Hasegawa and W.F Brinkman, J. Quantum Electron.,**QE-16**, 694 (1980)
[54] A. Hasegawa, Opt. Lett., **9**, 288 (1984)
[55] K. Tai, A.Hasegawa and A. Tomita, Phys. Rev. Lett., **56**, 135 (1986)
[56] G. P. Agrawal, Nonlinear Fiber Optics
[57] A. Shipulin, G. Onshchukov, V. Lokhnydin, M.Gölles, S. Daramanyan and F. Lederer, OAA'99, Nara, Japan, ThD3-1/147 (1999)
[58] M. Desaix, D. Anderson and M. Lisak, Opt. Lett., **15**, 1285 (1990)
[59] R. Ludwig, W. Pieper, A. Ehrhardt, E. Jahn, N. Agrawal, H. J. Ehrke, L. Küller and H.G. Weber, Electron. Lett., **32**, 327 (1996).

[60] I. Ogura, Y. Hashimoto, H. Kurita, T. Shimizu and H. Yokoyama, Photon. Technol. Lett., **10**, 603(1998).
[61] W. Rudolph and H. Weber, Optics Comm., **34**, 491 (1980)
[62] A. E. Sigman, Lasers
[63] A.Yariv, Optical electronics
[64] I.A. McIntyre and C.K. Rhodes, J. Appl. Phys., **69** R1 (1991)
[65] S. Szatmári, Appl. Phys. B **58**, 211 (1994)
[66] T.S Luk, A.McPherson, G. Gibson, K. Boyer and C. K. Rhodes, Opt. Lett.,**14**, 1113 (1989).
[67] S. Szatmári, G. Almási, M. Feuerhake and P. Simon, Appl. Phys. B **63**, 463 (1999)
[68] M. Watanabe, K. Hata, T. Adachi, R. Nodomi and S. Watanabe, Opt. Lett., **15**, 845 (1990)
[69] I.B. Földes, J.S. Bakos, **Z. Bakonyi**, T. Nagy and S. Szatmári, IEEE J. of selected topics in Quant. Electron., **2**, 776 (1996).
[70] I.B. Földes, J.S. Bakos, **Z. Bakonyi**, T. Nagy and S. Szatmári, Phys. Lett. A, **258**, 312 (1999)
[71] I.B. Földes, J.S. Bakos, N.A. Moustafa, G.Veres, **Z. Bakonyi**, T. Nagy and S. Szatmári, ECLIM'96, Madrid, Spain, 653 (1996)
[72] I.B. Földes, J.S. Bakos, **Z. Bakonyi**, T. Nagy and S. Szatmári, PLASMA'97, Jarnoltówek Poland 155 (1997)
[73] I.B. Földes, J.S. Bakos, **Z. Bakonyi**, T. Nagy and S. Szatmári, ECLIM'98, Formia Italy, TU/P/26 (1988)
[74] I.B. Földes, J.S. Bakos, M.Á. Kedves, G. Kocsis, G. Veres, **Z. Bakonyi**, T. Nagy and S. Szatmári, 6-th International Conference on X-Ray Lasers, Kyoto, Japan, 134 (1998)
[75] S. Szatmári and F.P Schäfer, Opt. Commun., **68**, 196 (1988)
[76] S.Szatmári, G. Almási and P.Simon, Appl. Phys. B, **53**, 82 (1991)
[77] G. Almási, S. Szatmári and P. Simon, Opt. Commun., **88**, 231 (1992)
[78] I.N Ross, G.Almási and S. Szatmári, Opt. Quant. Electron., **27**, 1053 (1995)
[79] Y. Ozaki and K. Takamoto, Appl. Opt., **28**, 106 (1989)
[80] A. Nussbaum and R. A. Philips, Modern optika
[81] J. W. Goodman, Introduction to Fourier Optics
[82] D.S. Bethune, Appl. Opt., **20**, 1897 (1981)
[83] S. Szatmári, Opt. Quant. Electron., **21**, 55 (1989)
[84] S. Szatmári and F.P Schäfer, Appl Phys B, **46**, 305 (1988)

Related publications of the author:

1. M. Gölles, S. Daramanyan, G. Onishchukov, A. Stipulin, **Z.Bakonyi**, V. Lokhnygin and F. Lederer:
   Modulation instability in a transmission system with semiconductor optical amplifiers and in line filters
   Optics Letters, **25,** 293-295 (2000)

2. C. Knöll, M. Gölles, **Z. Bakonyi,** G. Onishchukov and F. Lederer:
   Features of a Semiconductor Optical Amplifier/Saturable Absorber Module in Signal Transmission Lines
   CLEAO/Europe'00 Nice, France, CTuD 0004 (2000)

3. C. Knöll, M. Gölles, **Z. Bakonyi,** G. Onishchukov and F. Lederer:
   Noise suppression with Saturable Absorber in Transmission Lines driven by Semiconductor Optical Amplifier
   accepted for publication in Optics Communications

4. G. Onishchukov, **Z. Bakonyi**, C. Knöll, M. Gölles, F. Lederer and R. Ludwig:
   In-line semiconductor optical amplifiers with saturable absorbers for cascaded transmission systems
   ECOC'99, Nice, France, **2,** 260-261(1999)

5. **Z. Bakonyi**:
   Experimental investigations of 10Git/s transmission in fiber systems with semiconductor optical amplifiers
   DFG-Kolloquium "Optische Übermittlungsverfahren in der Informationstechnik", Dortmund (1999)

6. **Z. Bakonyi**, G. Onishchukov, C. Knöll, M. Gnölles, F. Lederer and R. Ludwig:
   In-line saturable absorber in cascaded SOA based transmission systems
   Photonics Technology Letters **12** 570-572 (2000)

7. **Z. Bakonyi**, G. Onishchukov, C. Knöll, M. Gölles, F. Lederer, R. Ludwig and E. Hilliger:
   Noise suppression in transmission lines using saturable absorbers
   Symposium des INK 1/B1 "Optische Informationstechnik", Eyba (1999)

8. **Z.Bakonyi** G. Onishchukov, C. Knöll and F. Lederer:
   Noise suppression by saturable absorber in transmission systems with semiconductor optical amplifiers
   CLEO'2000, San Francisco, USA , CWK56/329 (2000)

9. **Z. Bakonyi**, G. Onishchukov, C. Knöll, M. Gölles and F. Lederer:
10Gb/s RZ transmission in systems with combined saturable absorber-semiconductor amplifier.
COST 266-267 Wokshop 2000, Berlin, 64-66 (2000)

10. **Z. Bakonyi**, G. Onishchukov, C. Knöll, M. Gölles and F. Lederer:
10 Gb/s RZ transmission over 5000 km with gain-clamped semiconductor optical amplifiers and saturable absorbers
Electronics Letters, **36,** 1790-1791 (2000)

11. S. Szatmári, **Z. Bakonyi** and P. Simon:
Active spatial filtering of laser beams
Optics Communication, **134,** 199-204 (1997)